AD-758 462

ULTRASONIC MASS FLOWMETER FOR ARMY AIRCRAFT ENGINE DIAGNOSTICS

Lawrence C. Lynnworth, et al

Panametrics, Incorporated

Prepared for:

Army Air Mobility Research and Development Laboratory

January 1973

DISTRIBUTED BY:

NTIS

National Technical Information Service
U. S. DEPARTMENT OF COMMERCE
5285 Port Royal Road, Springfield Va. 22151

AD 758462

AD

USAAMRDL TECHNICAL REPORT 72-66

ULTRASONIC MASS FLOWMETER FOR ARMY AIRCRAFT ENGINE DIAGNOSTICS

By

L. C. Lynnworth
N. E. Pedersen
E. H. Carnevale

January 1973

EUSTIS DIRECTORATE
U. S. ARMY AIR MOBILITY RESEARCH AND DEVELOPMENT LABORATORY
FORT EUSTIS, VIRGINIA

CONTRACT DAAJ02-71-C-0061
PANAMETRICS, INC.
WALTHAM, MASSACHUSETTS

Approved for public release; distribution unlimited.

U.S. ARMY MATERIEL COMMAND

DDC
RELEASED
APR 17 1973
B

NATIONAL TECHNICAL INFORMATION SERVICE

DISCLAIMERS

The findings in this report are not to be construed as an official Department of the Army position unless so designated by other authorized documents.

When Government drawings, specifications, or other data are used for any purpose other than in connection with a definitely related Government procurement operation, the United States Government thereby incurs no responsibility nor any obligation whatsoever; and the fact that the Government may have formulated, furnished, or in any way supplied the said drawings, specifications, or other data is not to be regarded by implication or otherwise as in any manner licensing the holder or any other person or corporation, or conveying any rights or permission, to manufacture, use, or sell any patented invention that may in any way be related thereto.

Trade names cited in this report do not constitute an official endorsement or approval of the use of such commercial hardware or software.

DISPOSITION INSTRUCTIONS

Destroy this report when no longer needed. Do not return it to the originator.

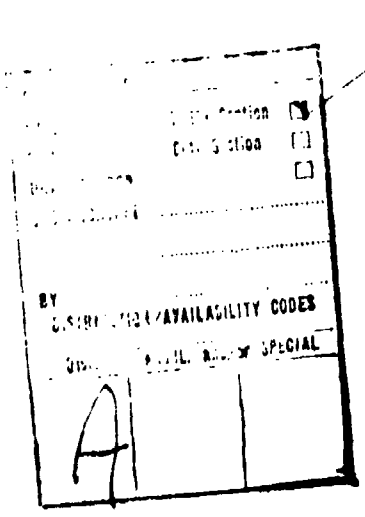

Unclassified

Security Classification

DOCUMENT CONTROL DATA - R & D

(Security classification of title, body of abstract and indexing annotation must be entered when the overall report is classified)

1. ORIGINATING ACTIVITY (Corporate author)	2a. REPORT SECURITY CLASSIFICATION
Panametrics, Inc. 221 Crescent Street Waltham, Massachusetts	Unclassified 2b. GROUP

3. REPORT TITLE

ULTRASONIC MASS FLOWMETER FOR ARMY AIRCRAFT ENGINE DIAGNOSTICS

4. DESCRIPTIVE NOTES (Type of report and inclusive dates)

Final Technical Report, Period covered: June 1971 to August 1972

5. AUTHOR(S) (First name, middle initial, last name)

Lawrence C. Lynnworth
Norman E. Pedersen
Edmund H. Carnevale

6. REPORT DATE	7a. TOTAL NO. OF PAGES	7b. NO. OF REFS
January 1973	115	19

8a. CONTRACT OR GRANT NO.	9a. ORIGINATOR'S REPORT NUMBER(S)
DAAJ02-71-C-0061 b. PROJECT NO. c. Task 1F162203A43405 d.	USAAMRDL Technical Report 72-66 9b. OTHER REPORT NO(S) (Any other numbers that may be assigned this report)

10. DISTRIBUTION STATEMENT

Approved for public release; distribution unlimited.

11. SUPPLEMENTARY NOTES	12. SPONSORING MILITARY ACTIVITY
Details of illustrations in this document may be better studied on microfiche.	Eustis Directorate, U. S. Army Air Mobility Research and Development Laboratory, Fort Eustis, Virginia

13. ABSTRACT

Development began on a new type of ultrasonic mass flowmeter for fuel flow in gas turbine engines. The fuel flowmeter consists of a flow velocimeter, a densitometer, a time intervalometer, and a metering section containing nonintrusive transducers. The velocimeter measures the phase difference between two coherent individually coded 5 MHz waves continuously transmitted obliquely upstream and downstream across a common path, yielding a phase difference proportional to v/c^2, where v = area-averaged flow velocity and c = sound speed. The densitometer consists of a stepped-diameter probe; the difference in echo amplitudes at the wetted end and at the dry step is a function of the acoustic impedance ρc of the fuel, where ρ is the fuel density. The time intervalometer measures the time T between two successive echoes, which time is proportional to 1/c. The mass flow rate $\dot{M}$ is $\dot{M} = (K)(v/c^2)(\rho c)(1/T)$, where K is a constant. The complete system was tested on various liquids at rates up to 5000 lb/hr. It was operated during and recalibrated after 104 hours exposure to a contaminated fluid flowing at ~1900 lb/hr. Response time was 20 ms. The flowmeter can operate in laminar, transitional, and turbulent flow, and it uses a novel method of weighting the profile. It is concluded that the logical development of the basic approach demonstrated in this program should be able to yield $\dot{M}$ accuracy of 1% or better.

DD FORM 1 NOV 1473 REPLACES DD FORM 1473, 1 JAN 64, WHICH IS OBSOLETE FOR ARMY USE.

Unclassified

Security Classification

14. KEY WORDS	LINK A		LINK B		LINK C	
	ROLE	WT	ROLE	WT	ROLE	WT
Flowmeter						
Ultrasonics						
Mass Flowmeter						
Densitometer						
Flow Velocimeter						
Intervalometer						
Flow Profile						
Acoustics						
Instrumentation						

DEPARTMENT OF THE ARMY
U. S. ARMY AIR MOBILITY RESEARCH & DEVELOPMENT LABORATORY
EUSTIS DIRECTORATE
FORT EUSTIS, VIRGINIA 23604

This report has been prepared by Panametrics, Inc, under the terms of Contract DAAJ02-71-C-0061. The effort is a part of a continuing effort to advance the state of the art of sensor technology for Army aircraft engine diagnostics.

The objectives of this effort were to design, fabricate, and test an ultrasonic mass fuel flowmeter. The report consists of a discussion of various approaches that could be used to measure fuel flow using ultrasonics and the identification of the approach that was developed for the final design.

The objectives of the effort were achieved. The inaccuracy of the flowmeter was excessive for diagnostic applications. The accuracy should lend itself to significant improvement by the use of currently available improved electronic components.

The conclusions and recommendations are generally concurred in by this Directorate, inasmuch as it is felt that the accuracy and design of the flowmeter can be improved.

The technical monitor for this contract was Mr. G. William Hogg, Military Operations Technology Division.

TABLE OF CONTENTS

Preceding page blank

LIST OF ILLUSTRATIONS

LIST OF ILLUSTRATIONS (cont' d)

LIST OF ILLUSTRATIONS (cont' d)

LIST OF TABLES

LIST OF TABLES (cont' d)

LIST OF SYMBOLS

a_i	average radius of particles of the i' th kind
A	echo amplitude, volts
Avgas-100	aviation gasoline, 100 octane
B	echo amplitude, volts
c	speed of sound, m/s
C	echo amplitude, volts
C_1, C_2	codes
C_{1d}, C_{2d}	delayed codes
d	thickness of end plate, cm
d(min)	particle diameter for geometrical scattering, μm
D	diameter, cm
dB	decibel
DBM	double balanced mixer
DVM	digital voltmeter
e	2.7182818....
f, f_1, f_2	transmitted frequencies, MHz
f_d	Doppler frequency, MHz
F_v	fractional volume concentration
i	particle type or number
I	integral
j	$\sqrt{-1}$

LIST OF SYMBOLS (cont'd)

k	coefficient of A echo
k'	constant depending on pipe area and units of measurement for M
k''	wave number, $2\pi/\lambda$, cm^{-1}
K	ratio of v_a/v_d
L	path length; as subscript, longitudinal, cm
m	temperature coefficient of density
$\dot{M}$	mass flow rate, lb/hr
$\bar{n}_i$	average number of particles of the i'th kind per cm^3 of fuel
r	radius variable or ratio of impedances
R	pipe radius or reflection coefficient
$\hat{R}$	range
Re	Reynolds number
s^E_{11}, s^E_{12}, etc.	elastic constants
S_1, S_2	Doppler signals
t	time, s
T	temperature, ^oF or ^oC
Ts	temperature coefficient of elastic constant in ppm/^oC
T_v	temperature coefficient of sound velocity in ppm/^oC
v	flow velocity, m/s
v(0)	value of v on axis, m/s

LIST OF SYMBOLS (cont' d)

v_a	value of v averaged over area, m/s
v_d	value of v averaged over diameter, m/s
v^*	friction velocity
V_c	volume of cell, cm^3
V_L	longitudinal velocity, m/s
VCO	voltage controlled oscillator
x	acoustic path or distance, cm
X	interrogation length, cm
y	radial distance, cm
Z_0, Z_1, Z_2	characteristic acoustic impedances, g/cm^2-μs
Z_{IN}	input impedance, g/cm^2-μs
α	attenuation coefficient, dB/cm
β	angle of incidence or refraction, deg
β'	ratio of v/c
Δ	increment
ϵ	error
λ	wavelength, cm
Λ	pipe friction coefficient
ν	kinematic viscosity, centistokes
ρ	density, g/cm^3
σ_i	scattering cross section per particle, cm^2

LIST OF SYMBOLS (cont'd)

σ_{total}	total scatter per cell or per volume element
τ	transit time, μs
$\overline{\tau}$	integration time, s
ω	angular frequency, $2\pi f$, MHz
θ, ϕ, ψ	phase angles or crystal angles, deg
η	viscosity coefficient, centipoise

INTRODUCTION

From both diagnostic and control viewpoints, it is important to know accurately the value of the fuel mass flow rate $\dot{M}$. Since the heating values for typical fuels such as JP-4, JP-5, diesel fuel and Avgas grades from 80 to 145 octane are within about 1% of 19,000 Btu/lb, it is clear that the maximum power that can be extracted from the fuel is proportional to $\dot{M}$.

In engine diagnostic studies, one is interested in measuring engine performance from start-up, at relatively low flow rates of about 50 lb/hr, up to maximum running conditions, where $\dot{M} \approx 2000$ lb/hr in some engines. Thus, a range of ~40:1 is of interest. For diagnostics, response time of 500 ms presently appears to be adequate. Accuracy of better than 1% is desirable at high flow and ~5% at the low end.

In engine control systems, one can control in terms of the temperature of the combusted fuel and/or in terms of $\dot{M}$. The same $\dot{M}$ ranges and accuracy apply as for diagnostics, but response time should be in the 10 to 30 ms range.

While a number of commercially available flowmeters could meet most or all of the above requirements, there are additional requirements imposed by the situations where Army aircraft gas turbine engines are tested and/or used. For example, the fuel composition may be an unknown mixture of two or more fuels. The fuel temperature may range between wide limits. The fuel may be contaminated by different types of particles of various sizes, and by corrosive material. The engine environment includes noise and vibration. The flowmeter measuring cell, transducers and electronics should be small and lightweight, and rugged enough to withstand the expected operating conditions.

The main problem with previous (turbine) flowmeters has been clogging within ten hours under contaminated fuel flow. The present ultrasonic flowmeter employs recessed, nonintrusive transducers and has no rotating parts. Accordingly, it is not subject to clogging and has continued to operate after being contaminant-tested for approximately one hundred hours, i.e., substantially longer than specified in MIL-F-8615.

A logical development of the present breadboard system is expected to meet accuracy and range requirements. Contractual objectives for upper flow range and speed of response have already been exceeded by factors of 2.5 and 25, respectively.

The following sections of this report define the problem of measuring mass flow rate in greater detail, indicate the background, explain the ultrasonic approaches to the problem, and describe the measuring and testing methods and results. Conclusions are based on our analysis, measurements, tests, and results; and recommendations are offered relative to achieving the remaining objectives.

STATEMENT OF THE PROBLEM

The purpose of this program was to develop an ultrasonic mass flowmeter to meet the following objectives:

a. Operate over the temperature range of -65°F to +160°F (-54°C to +71°C).

b. Measure fuel flow over the range of 50 lb/hr to 2000 lb/hr, with an accuracy of 2.5 lb/hr at a flow of 50 lb/hr, and 10 lb/hr at a flow of 2000 lb/hr, with linear variation between this range.

c. Maximum integration time of 0.5 second.

d. The transducer was to have no moving parts.

e. The transducer was not to restrict or obstruct the flow.

f. The transducer was to be sized and configured so as to be capable of being mounted on an Army aircraft gas turbine engine.

In designing an ultrasonic flowmeter, one must translate these objectives into ultrasonic terms. For example, items (a) and (f) translate to transducer materials selection. Barium titanate, in common use below its Curie point of about 120°C, would not necessarily be appropriate because of the higher ambient temperatures encountered at no-flow, after engine turnoff. Of the many other transducer materials available, the final choice may depend on variation of transduction and impedance values versus temperature. As a further example, item (b) translates to ultrasonic measurement of flow velocity, sound speed in the fuel, and density, with calculable error limits.

BACKGROUND

The deficiencies of the mass flow rate sensors currently used to diagnose Army aircraft gas turbine engine performance include:

- Turbine-type sensors erode, degrade, cease to operate due to dirt - lifetime limited.
- High accuracy and high reliability not found in same sensor.
- Sensitive to vibration.
- Calibration depends on fuel type/composition.
- Density correction depends on factors besides density.
- Rotating turbine-type sensor must be maintained inside the fuel pipeline. Repair requires disassembly, downtime.

Recognizing the significance of the above problems, and the need for an approach sufficiently new and advanced so that it could, by design, substantially avoid these problems, a program was initiated in June 1971 to develop an ultrasonic mass flowmeter system.

Historically, the fundamental acoustic principles underlying most present ultrasonic flowmeters are traceable to Doppler (the "Doppler effect") or to Newton, who recognized that the time for sound waves in air to propagate between two points depended on the wind velocity. Worldwide, over one hundred ultrasonic flowmeters presently measure liquid flow, and occasionally gas or particulate flow, in industrial installations. Additional ultrasonic flowmeters are used in biomedical applications, for measuring blood flow or the motion of organs. The Doppler effect is utilized in most biomedical flowmeters, while the transit time difference (upstream minus downstream) is utilized in most industrial flowmeters.

In this program we pursued initially the Doppler effect, or scattering approach, to measure flow velocity, but later changed to a transit time, or phase shift, approach. Reflection principles were also utilized, to measure fuel density.

ULTRASONIC APPROACHES TO THE PROBLEM

As stated on page 2, part of the problem translates to ultrasonic measurements of fuel flow velocity, sound speed in the fluid, and fuel density. Table I lists the specific ultrasonic approaches that were used for these three measurements.

TABLE I. ULTRASONIC APPROACHES USED IN MEASURING FUEL FLOW VELOCITY, SOUND SPEED, AND DENSITY

Fuel Parameter	Measurement Approach
Flow Velocity	Doppler scattering; phase difference on transmission, using phase meter.
Sound Speed	Transit time of transmitted pulse, using intervalometer.
Density	Reflection coefficient at probe/fuel interface, using special probe and circuitry.

To clarify these approaches, we explain briefly the basic ideas underlying acoustic scattering, transmission and reflection measurements. Then we present a more detailed description of the three tasks into which the program was divided: Task I, Theoretical and Analytic Optimization; Task II, Design and Fabrication; and Task III, Tests.

SCATTERING

Doppler flowmeters measure the change in frequency of a wave scattered off moving particles in the fluid. The Doppler shift is proportional to the ratio of particle velocity to sound speed. If the particles are small enough, each acquires the local fluid velocity. If they are uniformly distributed and uniformly insonified, the scattered wave can be processed to yield the average flow velocity. When the scatterers are not uniformly distributed, range-gated Doppler techniques are sometimes employed to obtain the flow profile, from which the average flow velocity may be computed.

The "particles" may be foreign bodies such as contaminants, or bubbles, or they may be regions of fuel having an acoustic impedance slightly different from the neighboring fuel. In Doppler blood flowmeters, the red

corpuscles are the particles which scatter ultrasound having a frequency of about 5 to 10 MHz. However, Doppler scattering has also been observed in pure distilled liquid metals such as sodium-potassium (NaK).

The Doppler approach was selected at the beginning of this program, because at that time it appeared to offer, at least theoretically, the best way of measuring average flow velocity with minimum disturbance of simple pipelines. Calculations of the power scattered at 20 MHz (wavelength approximately 0.05 mm, or 50 μm) from fuel contaminated according to MIL-E-5007C showed that scattering should be adequate even in fuels containing approximately 1% of the specified contaminant. However, tests on uncontaminated liquid did not provide enough scatter to be detected with our equipment.

The theory of scattering of sound in a fluid by obstacles which are rigid or nonrigid (including bubbles) has been well developed for simple shapes such as spheres or cylinders. Without tracing the theory all the way back to Rayleigh, we merely present one of his simple but important theoretical results, for a spherical scatterer whose radius is very small compared to wavelength. This result is that, for so-called Rayleigh scattering, the scattered power is directly proportional to the sixth power of the radius, and inversely proportional to the fourth power of the wavelength.[1, 2]

This Rayleigh scattering result suggests that one could increase the scattered power by increasing the frequency (decreasing the wavelength). However, the sound attenuation coefficient increases as the square of frequency. As a practical compromise on frequency, we calculated that for a path of 5 cm, the maximum frequency would be 30 MHz, with 10 to 20 MHz probably being the most appropriate range to utilize (Appendix I).

We also considered, but did not pursue, the possibilities of increasing acoustic scattering by increasing the size (and number) of scatterers, either by introducing air bubbles or by cavitating the fuel.

At this point in the program, a new theoretical development unfolded, which predicted that the average flow velocity could be determined by a new transmission measurement. This is discussed next.

TRANSMISSION

Transit time or phase shift flowmeters usually measure the difference in transmission time or phase, with oblique propagation upstream and downstream.[3] These observed differences are proportional to the average flow velocity v_a in the acoustic path, divided by the square of the sound speed, c^2. Previous techniques to account for nonuniform flow velocity profile

include iterative methods based on estimates or knowledge of the Reynolds number, and Gaussian quadrature methods which compute the average flow from measurements across four parallel chords. Neither of these earlier approaches, however, sampled all of the fluid.

A novel way of obtaining the average flow velocity was utilized in the present program. An ultrasonic measuring cell was designed such that all the flowing liquid could be interrogated. The interrogation was accomplished by a pair of 5 MHz continuous plane waves which ideally remain substantially undistorted in the flowing liquid. To separate upstream from downstream waves, each wave was phase-coded with a pseudo-random-noise code.

Since the observed differences in transmission time are proportional to $c \pm v$, where $c >> v$, it is clear that a small fractional error in c is equivalent to a large fractional error in v. To minimize this error contribution, the upstream and downstream paths should be as identical as possible. In practice, therefore, it is desirable to use the same pair of transducers for both upstream and downstream measurements. This was done in the present design.

To eliminate the dependence of the output signal on c^2, one can arrange to measure the difference between two frequencies, each frequency being inversely proportional to one of the travel times. This was not done in the present program, because at the time the Doppler approach was abandoned, the two-variable-frequency technique required to continuously measure v independent of c had not yet been conceived. In any event, the present v/c^2 measurement would still be a logical first step.

In passing we may note that, compared to the transmission approach, a potential advantage of the Doppler approach to mass flow metering is that the Doppler shift is proportional to v/c. Multiplying this quotient by the ρc output of the reflection coefficient densitometer yields an output proportional to $\dot{M}$, without the need to measure c explicitly. We may further note that, alternatively, if one can use a densitometer approach that directly yields ρ alone (such as certain resonant structures whose resonant frequency is a function of ρ, independent of c) then a transmission measurement of upstream and downstream frequencies, whose difference is proportional to v, appears most appropriate. Multiplying these latter outputs yields $\dot{M} = \rho v$.

In this program a separate transmission path normal to the fuel flow direction was utilized to measure a time interval τ, which is inversely proportional to c, and independent of v, with a precision of $\pm$ 0.05%.

REFLECTION

The reflection approach to measuring the properties of a medium is based on the principle that a wave incident upon a boundary is partly reflected and partly transmitted, depending on the boundary conditions. Previous applications of the ultrasonic reflection approach include the measurement of viscosity in a liquid using obliquely incident shear waves,[4] and the measurement of sound velocity in solids using either obliquely incident longitudinal wave pulses[5] or normally incident longitudinal continuous waves.[6]

In this program we utilized the reflection of normally incident longitudinal wave pulses to determine fuel density. At normal incidence the reflection coefficient for plane waves depends only on the characteristic acoustic impedances of the adjacent media at the boundary. These media, for example, may be a probe and the fuel. Since the fuel's characteristic impedance equals ρc, if the probe's impedance Z_1 is known, measurements of the reflection coefficient at the boundary, together with a measurement of sound speed c (or time interval τ, where τ is proportional to $1/c$), enable one to determine the fuel density ρ.

TASK DESCRIPTIONS

Having generally introduced the three main ultrasonic approaches used in this program - scattering, transmission, reflection - we present next a brief description of the three tasks into which the program was divided.

Task I - Theoretical and Analytical Optimization Study

In this task we conducted an analysis to determine the optimum parameters of the above mass flowmeter. The principal factors included in the analysis were temperature range, flow range, fractional contaminant content, pipe geometry, noise level as a function of frequency, allowable system response time, and suitability for Army aircraft gas turbine installations.

We also analyzed six piezoelectric transducer designs as candidates for use in the velocimeter. They are listed in Table II.

The normally incident longitudinal wave design was analyzed for the velocimeter, to convert the phase shift, which is proportional to v/c^2, to flow velocity v. This design, using a second transducer and special probe, was also analyzed for the densitometer.

TABLE II. TRANSDUCER APPROACHES	
Wave Type	Method of Introduction
Longitudinal	Phased array
Longitudinal	Axially incident (from end wall)
Longitudinal	Obliquely incident (from solid wedge)
Longitudinal	Obliquely incident (from recessed liquid wedge)
Longitudinal	Normally incident (from side wall)
Shear	Obliquely incident (from solid wedge)

Task II - Design and Fabrication

This task involved designing and fabricating the mass flowmeter system. The mass flowmeter system included three main electronic functions: a velocimeter, a time intervalometer, and a densitometer. Additionally, several transducers and measurement cells were designed and built.

Task III - Tests

In this task we tested the system components to detect and correct deficiencies, to determine optimum values of adjustable operating parameters, and to verify performance. We also conducted room temperature tests on the complete system at flow rates of 50 to 5000 lb/hr. These tests included the use of water, Avgas-100, JP-4 and JP-5 fuels, and a fluid contaminated as specified by MIL-E-5007C. The purpose of these tests was to determine the accuracy of the mass flowmeter system and to determine the effects of the contaminant on the mass flowmeter system.

ULTRASONIC METHODS

Following the format of the previous section on ultrasonic approaches, we describe in this section the ultrasonic methods we used in investigating scattering, transmission and reflection. These methods provided the test data for determining flow velocity, density and mass flow rate. A discussion of Reynolds number and flow profile is presented first, however, since the accuracy of any ultrasonic method of measuring flow velocity will be ultimately limited by this factor.

REYNOLDS NUMBER AND FLOW PROFILE

Reynolds Number is the dimensionless ratio $Re = \rho vD/\eta = vD/\nu$. For common fuels, the temperature dependence of ρ and ν are shown in Figures 1 and 2. To graphically illustrate the change in Re as a function of fuel type, temperature, and flow velocity, the Reynolds number nomogram of Figure 3 was constructed. The extremes of Re occur when v/ν is minimum or maximum, as shown in Table III.

TABLE III. RANGE OF REYNOLDS NUMBERS ENCOUNTERED IN TWO FUELS FOR $\dot{M}$ FROM 50 TO 2000 LB/HR AND TEMPERATURE FROM -65°F TO +160°F, CALCULATED FOR A 1/2-INCH DIAMETER PIPE

Fuel Type	Minimum Re			Maximum Re		
	Re (-)	$\dot{M}$ (lb/hr)	Temp (°F)	Re (-)	$\dot{M}$ (lb/hr)	Temp (°F)
JP-4	127	50	-65	51,200	2000	160
Avgas-100	435	50	-65	71,600	2000	160

Experimentally, the flow velocity distribution v(r) is observed to depend on Re as shown in Figure 4. The turbulent flow data may be represented by an empirical equation of the form[7]

$$v(r)/v(0) = [(R-r)/R]^{1/n} \quad (1)$$

where n varies slightly with Re. n = 6 at Re = 4000, n = 6.6 at Re = 23,000, and n = 7 at 110,000. The ratio of mean-to-maximum velocity is

$$v_a/v(0) = 2n^2/(n+1)(2n+1) \quad (2)$$

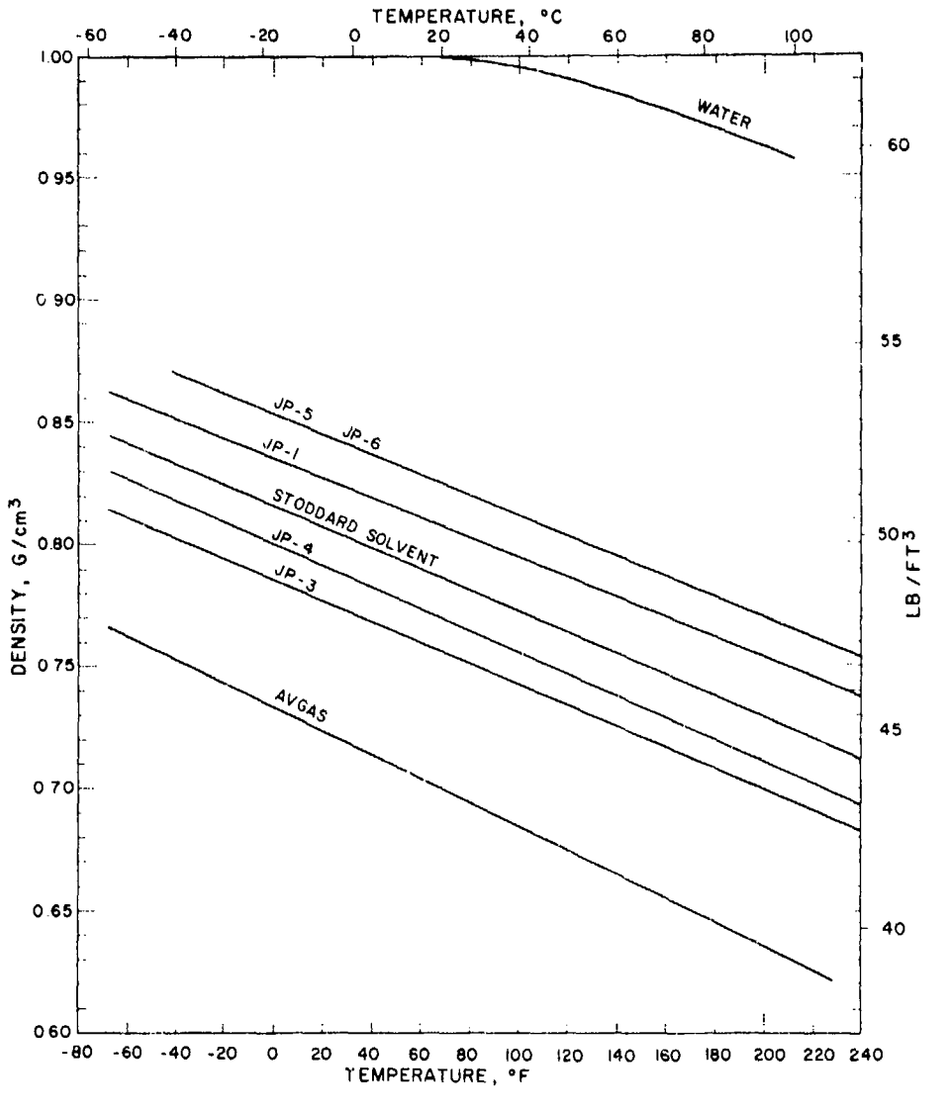

Figure 1. Density Versus Temperature.

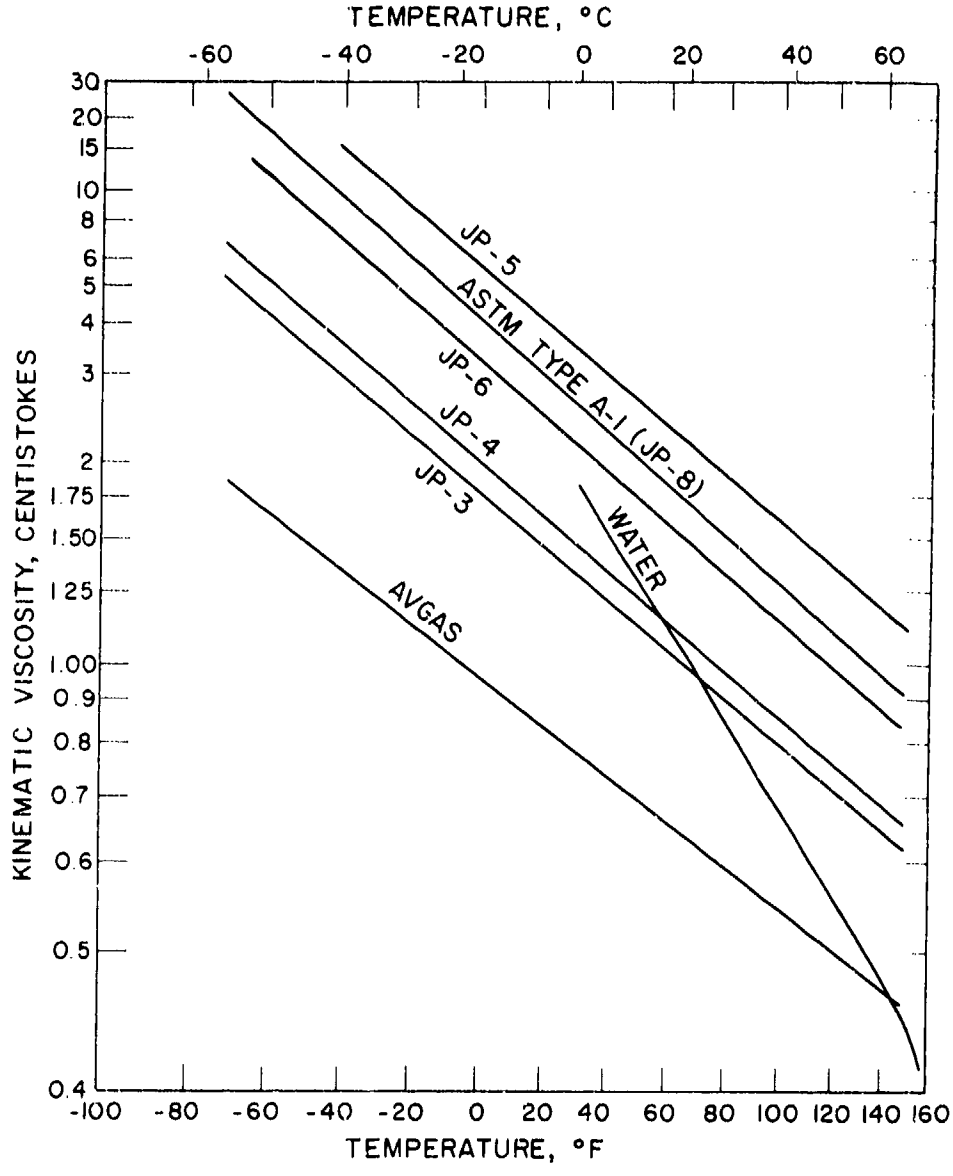

Figure 2. Kinematic Viscosity ($\nu = \eta / \rho$) Versus Temperature.

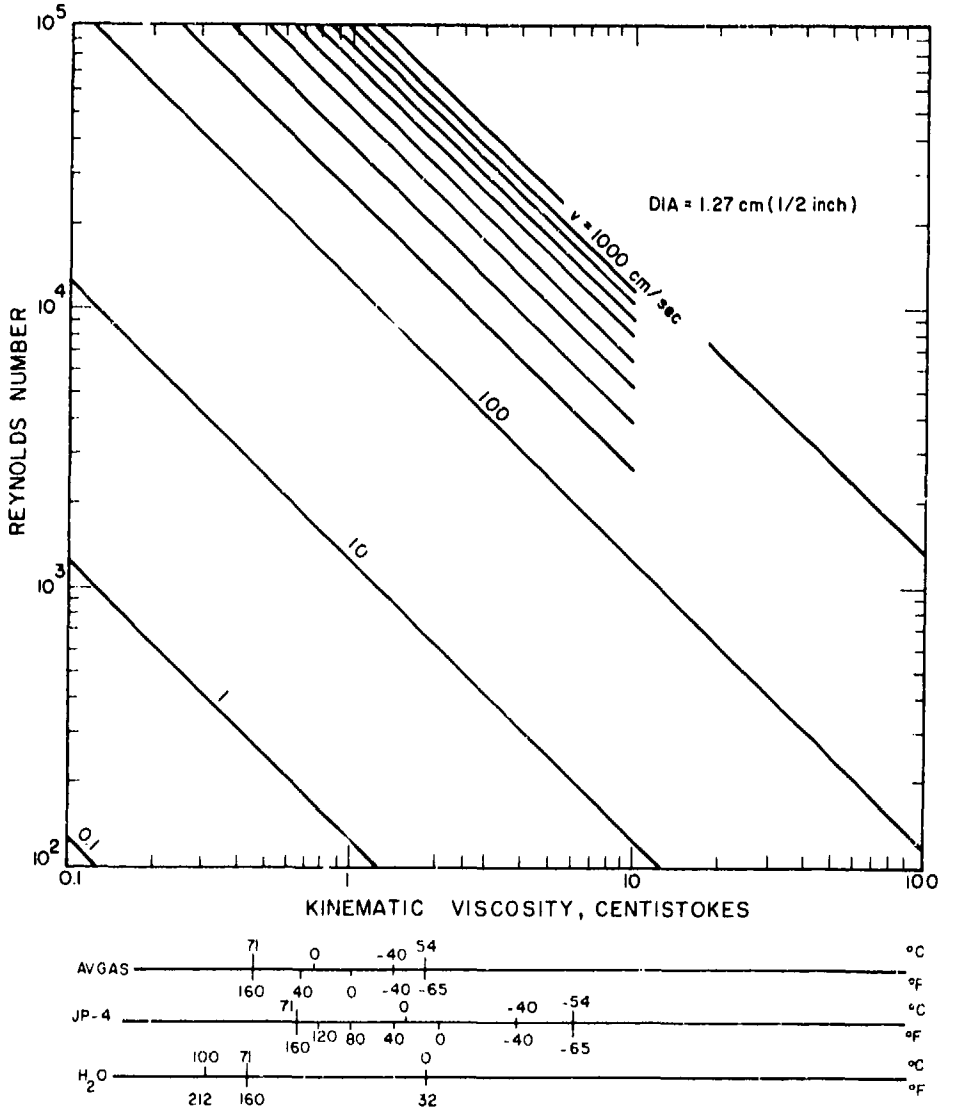

Figure 3. Reynolds Number Nomogram.

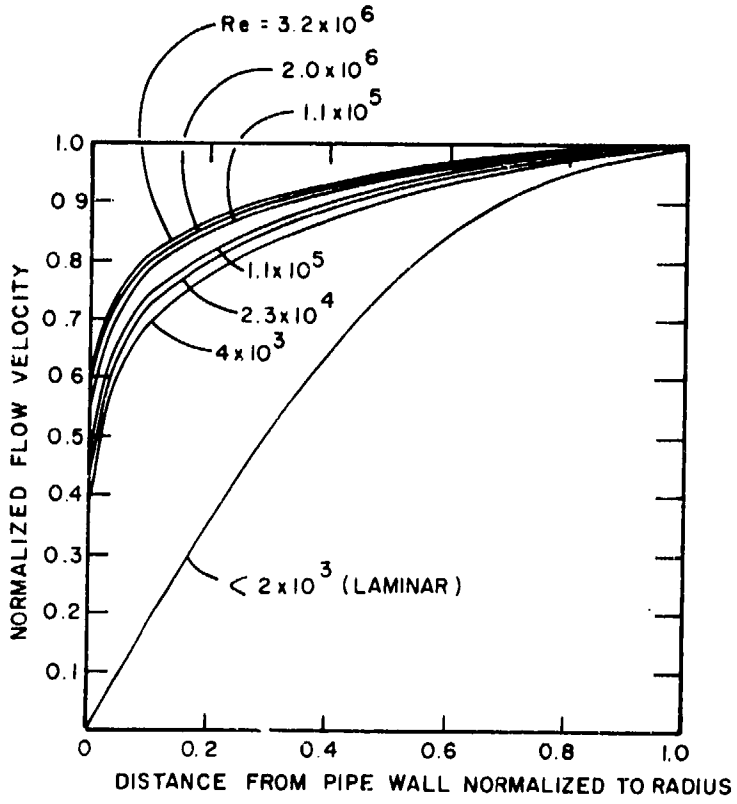

Figure 4. Flow Velocity Distribution in a Pipe.

For n = 6, $v_a/v(0) = 0.791$. For n = 7, $v_a/v(0) = 0.817$. For laminar flow, the profile is parabolic:

$$v(r)/v(0) = 1 - (y/R - 1)^2 = 1 - (r/R)^2 \tag{3}$$

and $v_a/v(0) = 0.5$.

If one interrogates the fluid with a wave that effectively samples the diameter, but not the whole area, one measures $v_d = v_a/K$, where K is less than unity and depends on Re, as mentioned before. In terms of the pipe friction coefficient Λ, $K = 1/(1 + 0.44194\sqrt{\Lambda})$. For Λ between 0.01 and 0.06, K ranges between 0.9023 and 0.9577. Various oblique paths that measure v_d are shown in Figure 5, and their projections are shown in Figures 6 and 7. Relative to a clamp-on flowmeter, Figure 7d shows a v_d measurement.

The profile correction factor $K = v_a/v_d$ may be expressed in terms of the velocity distribution $v(r)$:

$$K = \frac{v_a}{v_d} = \frac{\frac{1}{\pi R^2}\int_0^R 2\pi r v(r)\,dr}{\frac{1}{R}\int_0^R v(r)\,dr} = \frac{2}{R}\,\frac{\int_0^R r v(r)\,dr}{\int_0^R v(r)\,dr} \tag{4}$$

For parabolic flow, this becomes

$$K = \frac{2}{R}\,\frac{\int_0^R r\left[1 - (r/R^2\right]\,dr}{\int_0^R \left[1 - (r/R)^2\right]\,dr} = 3/4 = 0.750 \tag{5}$$

while for turbulent flow, K is typically about 0.90 to 0.96.

Graphically, deviations due to the dependence of K on Re have been drawn by Kritz in his nomogram.[8] Kritz's nomogram is derived from Prandtl's velocity-distribution equation

$$v(r) = v(0) + 2.5v^* \ln\frac{R - r}{R} \tag{6}$$

where v^* = friction velocity. From this,

$$v_d = v_a\,(1 + 0.19\,Re^{-0.1}) \tag{7}$$

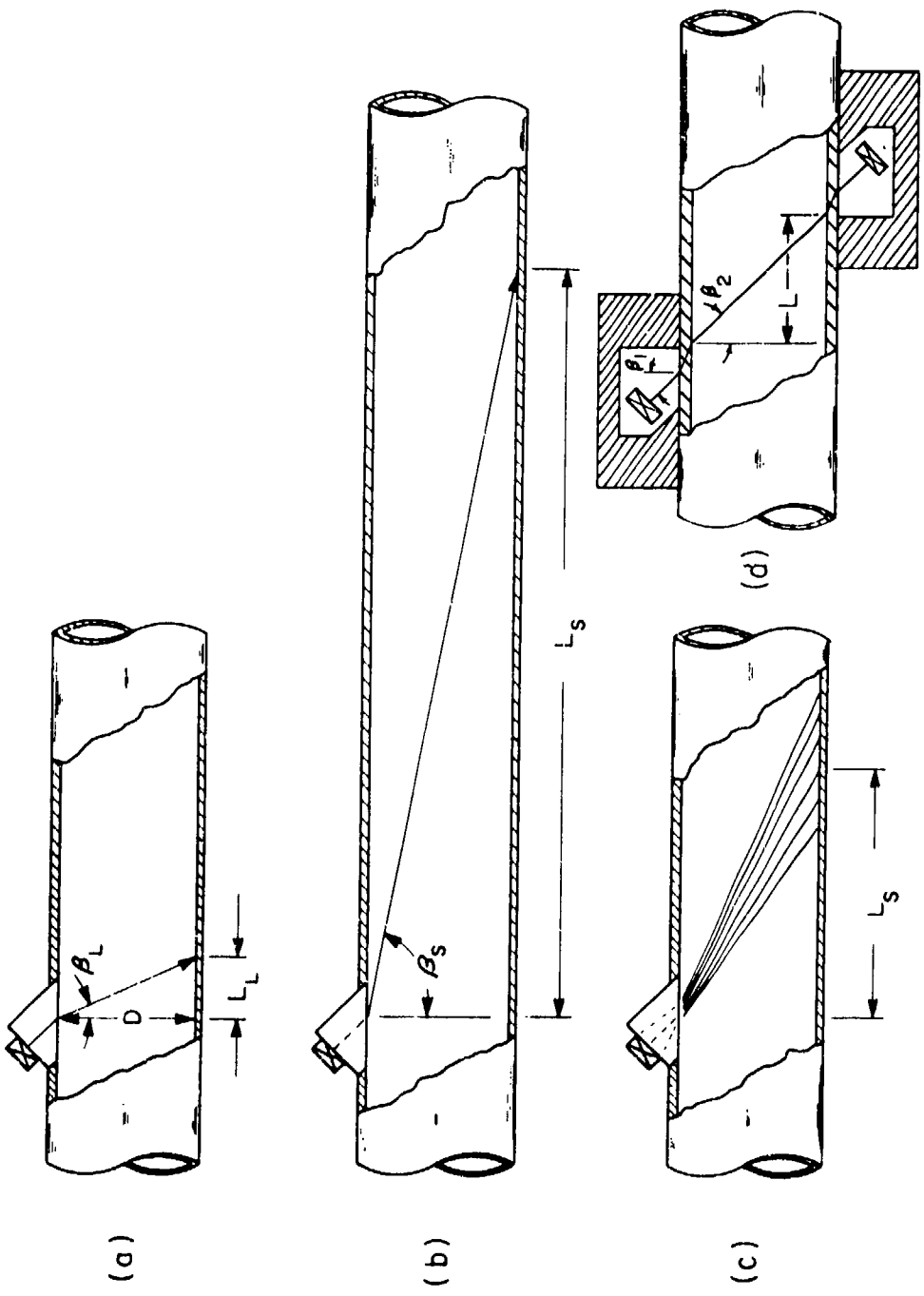

Figure 5. Comparison of Obliquely Incident (45^{o}) Longitudinal and Shear Waves.

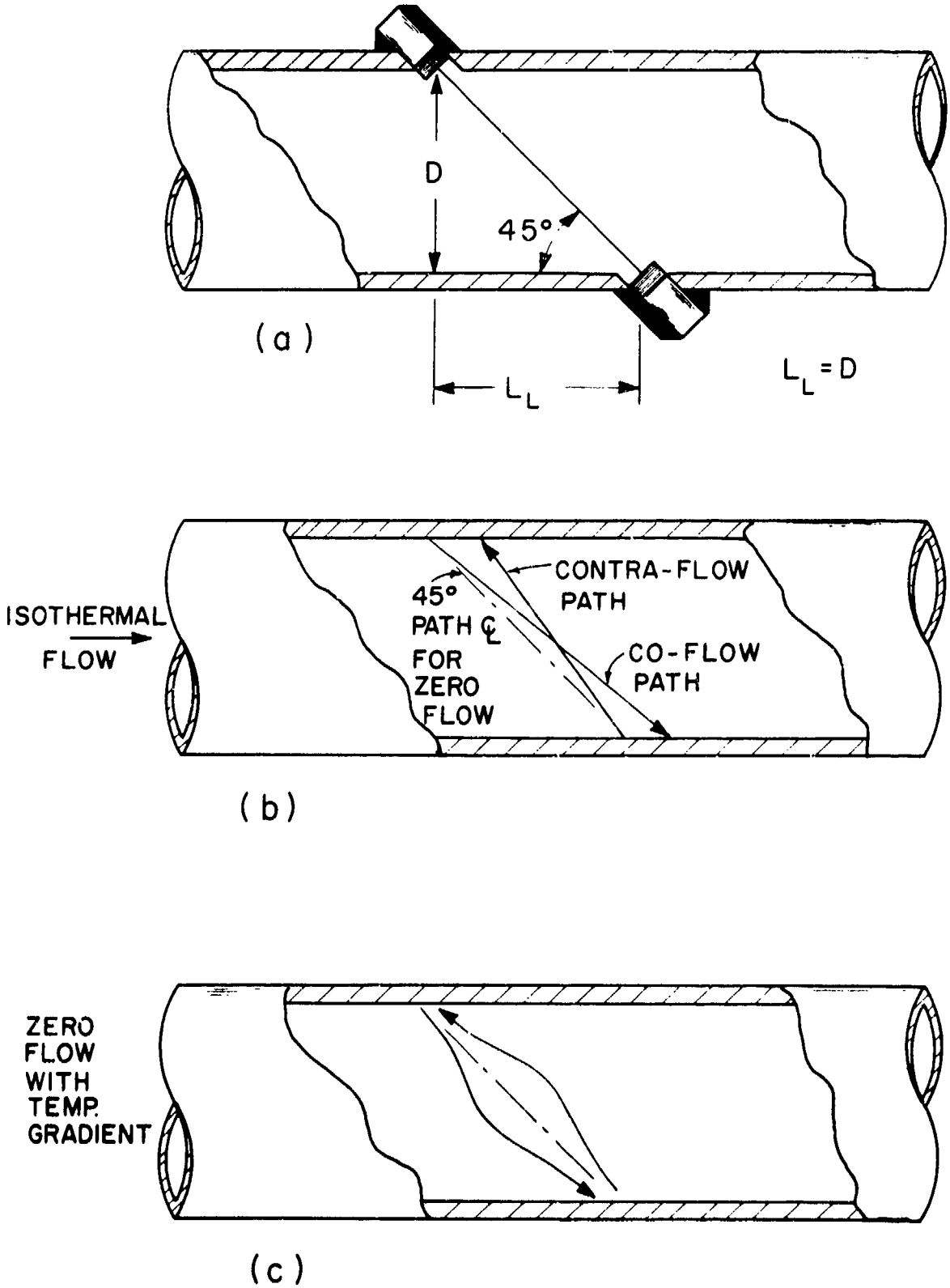

Figure 6. Ray Path Projections for Oblique Propagation.

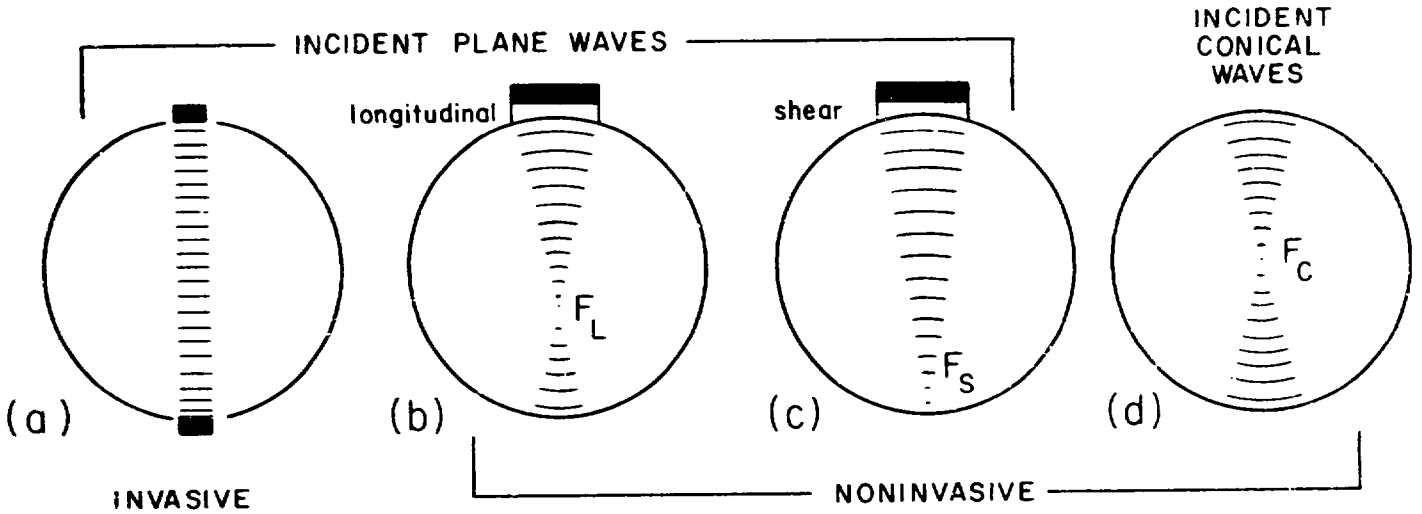

Figure 7. Comparison of Wave Patterns, Looking Axially.

which we may easily relate to our $K = v_a/v_d$ if we write $K_{Kritz} = 1/(1 + 0.19\ Re^{-0.1})$.

Typical errors, according to Kritz, are listed in Table IV, together with errors we calculated for laminar flow. The discrepancies for laminar flow may be explained as follows. Prandtl's equation is for turbulent flow, with its underlying assumptions most valid for large Re.[7] Kritz erroneously used this equation for $Re < 2000$, for which the deviation is in fact not 9.5% but 25%, as we have shown, and not a function of Re, for $Re < 2000$ (i.e., laminar flow). Kritz's nomogram is questionable for transitional flow too ($2000 < Re < 40,000$), although here the errors would not be as serious. It appears valid above 40,000, except, as he points out, his calculations neglect the disturbance to the effective profile due to transducer cavities of the nonflush type (Figure 5a). A plot of the error versus Re, for $Re > 5000$, has been presented recently by McShane,[9] based on an empirical equation of the form

$$v_d = v_a\ (1.119 - 0.011 \log Re). \qquad (8)$$

Table IV shows that errors computed from (8) or (7) agree within 0.5% for $10^4 < Re < 10^5$.

TABLE IV. CALCULATED ERRORS DUE TO NONUNIFORM FLOW PROFILE

Reynolds Number	Calculated Error, v_d-v_a (%)		
	Kritz[8]	McShane[9]	Present Work
1,000	9.5	-	25
2,000	8.9	-	25
10,000	7.6	7.5	-
50,000	6.5	6.7	-
70,000	6.2	6.6	-
100,000	6.0	6.5	-

In many industrial situations, where flow is turbulent, temperature and composition of the process fluid are sufficiently constant so that Reynolds number can be estimated from v_a. Since K is relatively insensitive to Re, the estimated Re is sufficient to determine K to a small fraction of 1%, which means v_a can be determined to that accuracy too.

In our case, however, at a given flow velocity v, kinematic viscosity ν and hence Re can change by an order to magnitude for JP-4 over the full

temperature range (Figures 1 and 2). Therefore, our Re compensator, if used, could not be based only on an iteration using the flow velocity v(r) at a point, or v_d averaged across a diameter, if errors are to be kept below 1%. To calculate how accurately Re must be determined to keep errors in K less than a prescribed amount, say, 0.1%, we may differentiate the error term $(1 - v_d/v_a)$ with respect to Re. This leads to the result that, for relatively small changes in Re, the percentage change in K is approximately half of the fractional change in Re. For example, if $\Delta Re/Re = 0.2$, K changes by about 0.1%. (For an order of magnitude change in Re, K changes by ~1%.) While these results are limited to turbulent flow, they suggest that determination of Re to $\pm$ 20% could permit one to convert to v_a rather accurately, an ultrasonic measurement of v_d.

Let us examine the expression $Re = \rho v D/\eta$. Under turbulent flow, v(0) is equal to ~1.16 $v_d \pm 3\%$. Assuming ρ and D are known to better than 1%, the principal uncertainty in Re is due to η. One approach to obtaining η is indicated by the graph in Figure 8. This graph is constructed using the data in Figures 1 and 2, and shows that viscosity may be computed from measurements of density and temperature, provided the fuel behaves as part of a homologous series.[10]

Another approach to overcoming the uncertainty in Re is to mix the profile to achieve, ideally, K = 1. Assuming one uses a Kenics mixer, as described in the next section, one can calculate the distance that the mixed or flat, uniform profile is maintained. For low flow this distance is about (.03) (Re) (diameter), while for high flow this distance increases to ~50 to 100 diameters.

The above profile considerations may be summarized as follows:

1. Transducers should not be allowed to increase the uncertainty in flow profile in the region of interaction between sound wave and flow.

2. For the range of conditions expected in this contract, flow profile could require compensation (K) factors from 0.75 to 0.94.

3. For laminar flow or for fully developed turbulent flow, but not necessarily for transitional flow, the correct K factor could be applied to the extent that Re were known and to the extent that the profile had traveled down a sufficient length of smooth pipe to become established. (As a test, flow could be measured, in principle, at two distances down the pipe.)

4. If the fuel were perfectly mixed, the profile would be uniform, and K would equal unity. This condition may be nearly achieved close to the exit of a Kenics static mixer at high flow, and to a lesser extent, at low flow.

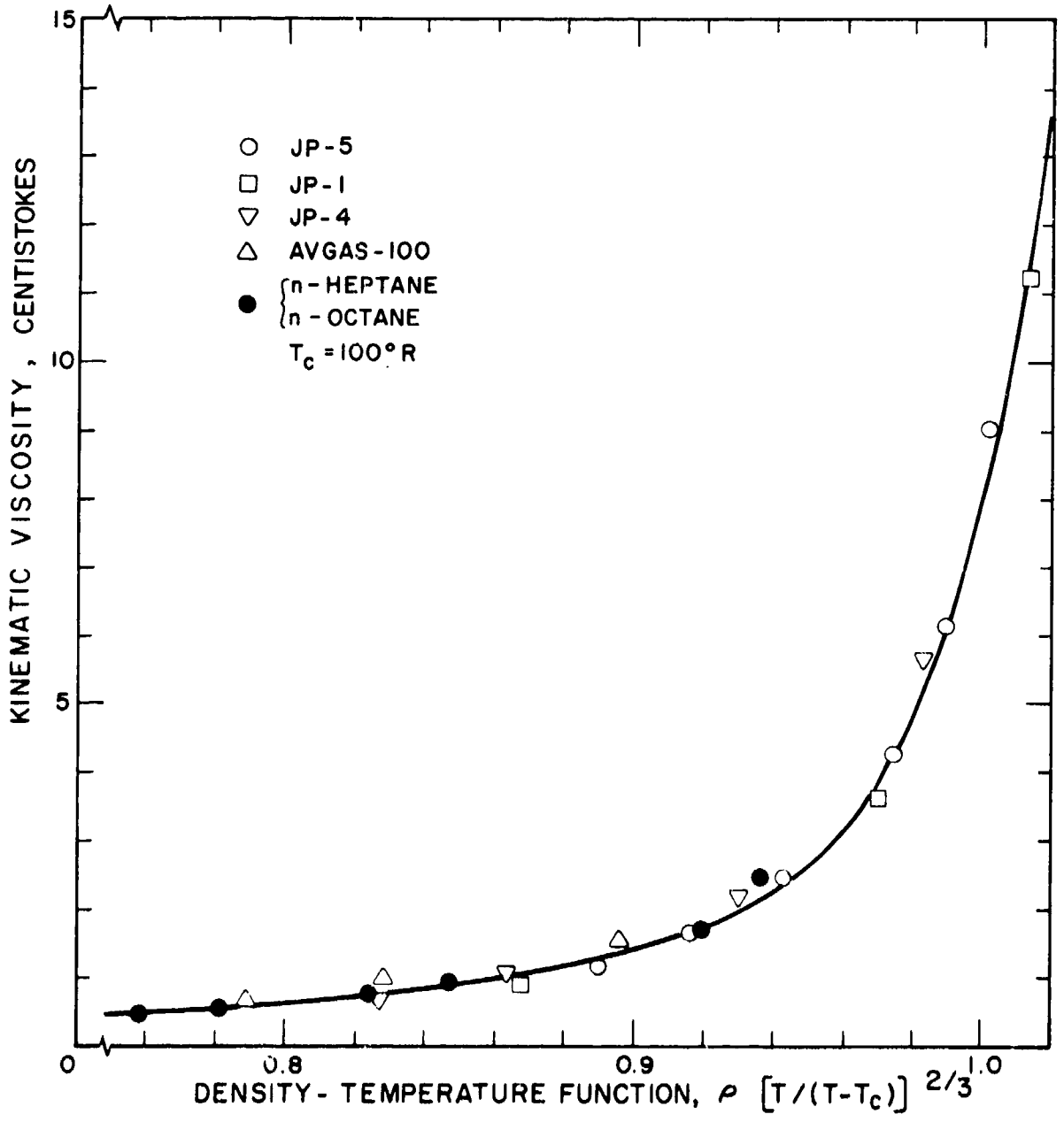

Figure 8. Kinematic Viscosity Versus Density-Temperature Function, for Six Fuels.

5. To the extent that scatterers are uniformly distributed, and uniformly insonified, the average Doppler shift can be processed to yield average flow velocity, independent of the flow profile.

6. To the extent that a plane wave can interrogate the entire cross section of flowing fluid without becoming curved, its transit time can be processed to yield average flow velocity, independent of the flow profile. This new result is of major significance.

SCATTERING

The Doppler scattering method automatically weights the flow profile correctly, provided insonification is uniform and provided scatterers are uniformly distributed. To distribute scatterers as uniformly as possible, and, incidentally, to flatten the profile, we used a Kenics static mixer. This mixer is a helical flow divider with a 180° twist per section. It is virtually clog-free. When $\dot{M}$ = 2000 lb/hr, seven sections typically introduce a pressure drop of about 6 psi in a 1/2-inch-diameter pipe, and about 2 psi in a 3/4-inch-diameter pipe.

To optimally locate the interrogation zone, one needs to know how far the flat profile is maintained after exiting from the mixer. This distance depends on Reynolds number, which in this work ranges from about 100 to about 70,000.

For high Reynolds numbers (>50,000), the initially flat profile transforms to its final shape after ~50 to 100 diameters. Therefore, measurements close enough to the mixer to avoid the transformation, i.e., within 5 to 10 diameters after the mixer, will see the flat profile. This location contributes to highest accuracy at the highest flow rate.

For low Reynolds numbers ($\lesssim$ 1000), the initially flat profile will transform (relaminarize) to parabolic in a distance of ~(0.03) (Re) (diameter), or 3 diameters at Re = 100.[7] This means that, as before, to avoid the transformed profile, one should interrogate as close as possible to the mixer. But even within ~1 or 2 diameters, since the profile is already curved at minimum flow rate, small errors accrue to the extent that illumination is nonuniform. Note that the scatterers should still be uniformly distributed, even though flow profile is parabolic. Therefore, uniform illumination could avoid the profile-dependent errors.

A diagram of a dual-frequency Doppler flow velocimeter is shown in Figure 9. Since the basic Doppler shift is proportional to v/c, an input in terms of fuel type and temperature, or c (where c depends[8] on fuel type and temperature, as in Figure 10) is required if v is one of the desired outputs. Figure 11 indicates the theoretical improvement which

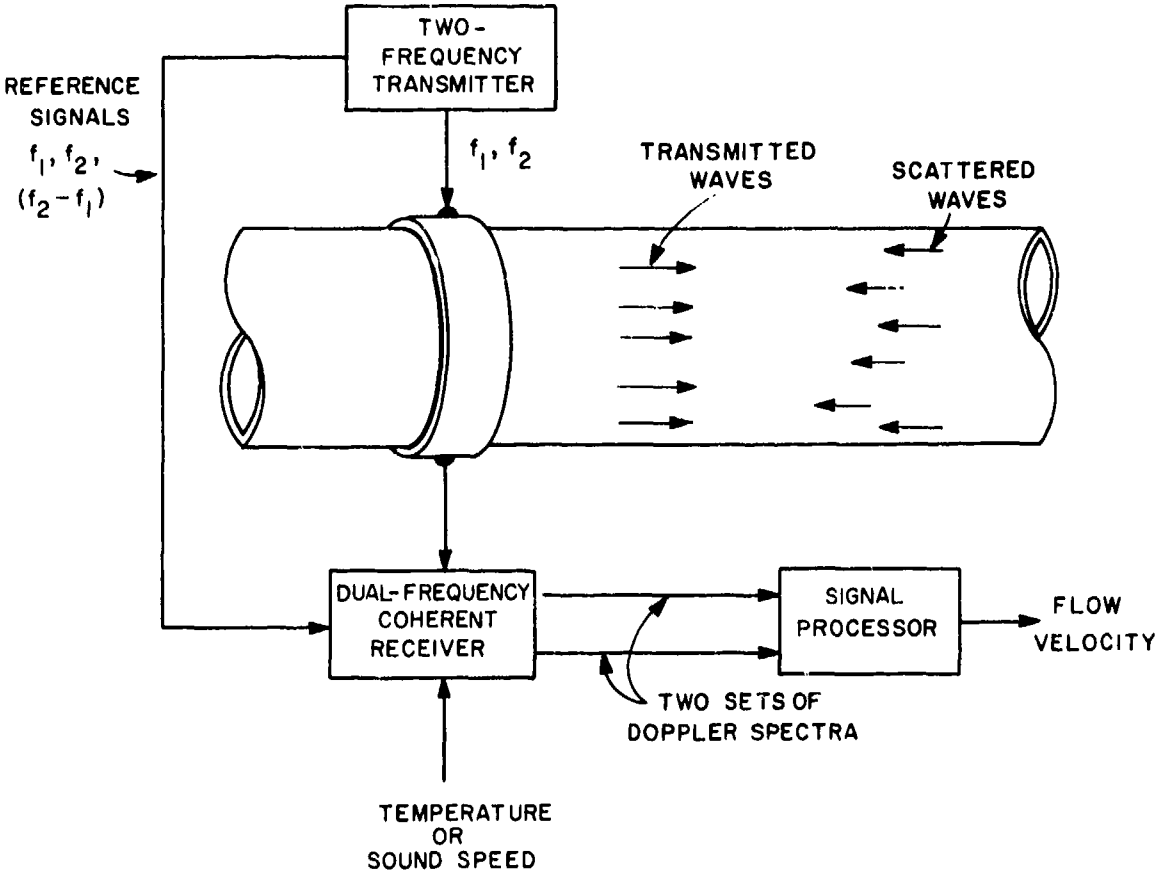

Figure 9. Doppler Flow Velocimeter Using Two Transmitted Frequencies.

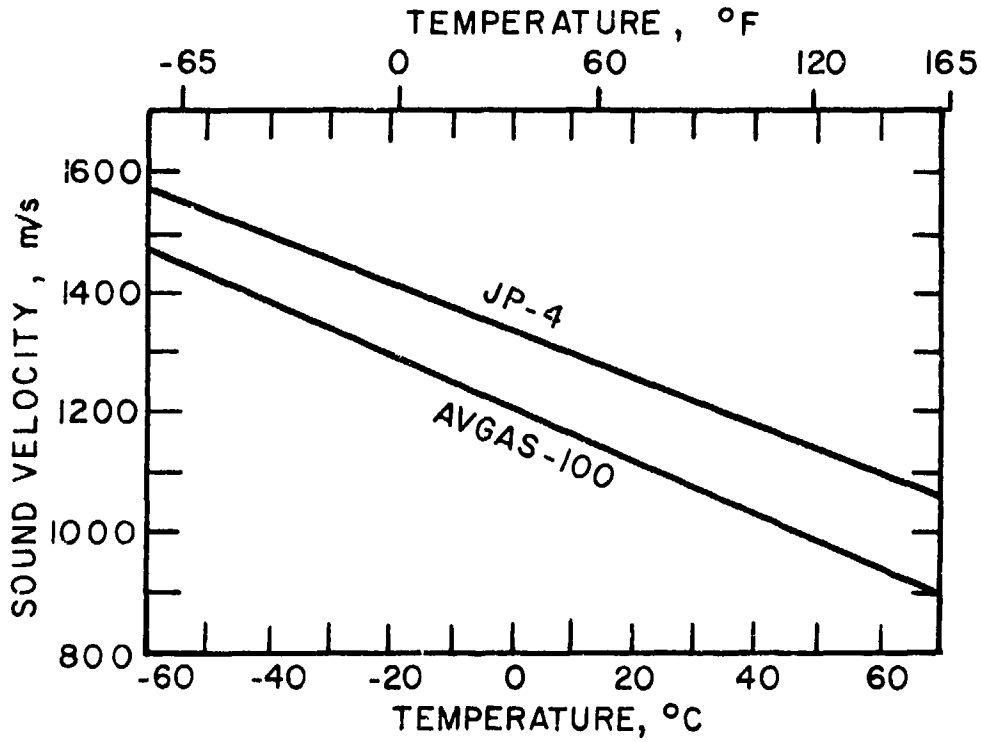

Figure 10. Sound Velocity Versus Temperature for JP-4 and Avgas-100.[8]

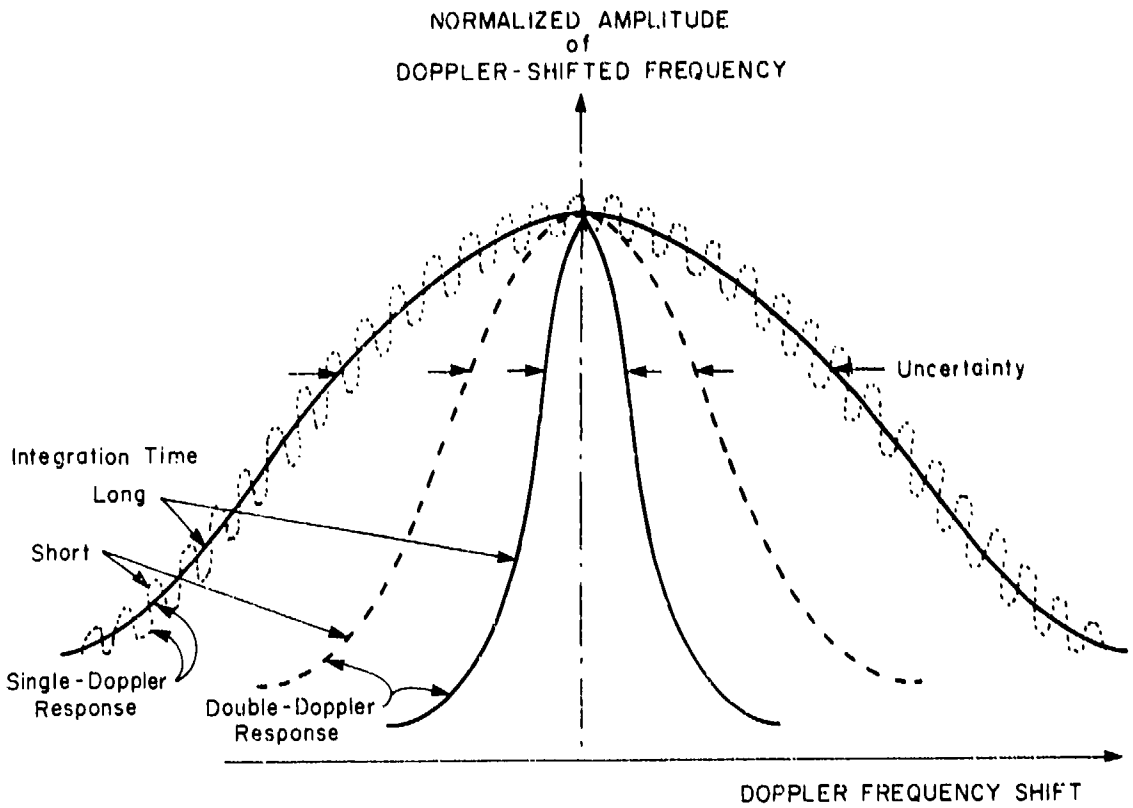

Figure 11. Comparison of Uncertainties Obtained With Single- and Double-Frequency Doppler Flow Velocity Meters.

may be obtained by processing Dopplers from two different transmitted frequencies f_1 and f_2.

Scattering and Frequency Selection

Several design calculations were done in order to more precisely determine the operating parameters of the dual frequency flow velocity measuring system. First, on the basis of the contaminants specified in MIL-E-5007C, the scattering levels per unit volume of fuel due to each of the various contaminant categories were determined. Second, the overall scattering cross section per unit volume of fuel at 20 MHz was computed and found to be $\sim 0.3 \times 10^{-3}$ cm^2/cc. Assuming a pipe diameter of 1/2 in. and an interrogation length of 1/2 in., the volume of fuel from which scattering is being measured is about 3 cm^3. This will, therefore, provide an overall backscatter cross section of about 10^{-3} cm^2 Third, the received power due to this bulk scattering cross section was computed, and, assuming a delivered power to the transducer of one watt per channel, a signal-to-noise ratio of 40 dB was determined. See Appendix I.

A number of trade-offs exist in the selection of operating frequency. These are summarized below.

The frequency f of the wave to be scattered should be high enough to avoid most engine noise and to avoid reverberation in the pipe wall and fluid. Yet it should not be so high that attenuation is excessive. Extensive data[11] is available on α in liquids similar to aviation fuels. For our temperature range the measured $10^{17}\,\alpha/f^2$ is less than 100. This means at f = 10 MHz, $\alpha_{max} < (10^{-17})\,(10^7)^2\,(100) = 0.1$ Np/cm $\approx$ 1 dB/cm. At 20 MHz, $\alpha_{max} \approx 4$ dB/cm. Since the total path is expected to be $\sim$5 to 10 cm, the maximum usable frequency should be selected in the above range, namely, 10 to 20 MHz. (α is denoted the attenuation coefficient.)

Again, the acoustic attenuation coefficient in the medium is roughly proportional to f^2. Therefore, subject to geometrical constraints, too high an operating frequency range will give rise to a prohibitively low signal-to-noise ratio. On the other hand, the overall scattering cross section of the medium increases with frequency, and the statistics of the measurement improve with increasing frequency. Consideration of these factors leads to the choice of operating frequencies at approximately 20 MHz.

Response Time

For performance diagnostics in this contract, response time of 0.5 sec is desired. For control, <30 ms is the objective.

These values were interpreted as the time it takes the output signal to reach 1/e of its final value, in response to a step change in mass flow rate $\dot{M}$. It appears that only the flow velocity (v) part of the system need be this fast, as it seems unlikely that fuel temperature (density, viscosity) could change so quickly. That is, temperature functions (density, viscosity) can be monitored with longer integration times, with smoothed outputs always available for multiplication with v, to yield $\dot{M}$. This simplifies the determination of $\dot{M}$ without sacrificing the essential fast response to sudden changes in flow velocity.

The minimum response time is limited in one respect by the number of scatterers interrogated in the integration period. This depends in part on the gate width, which may be ~20 to 30μ s wide. For colinear transducers, if the gate is too wide, the profile may be smeared towards the transducer end of the gate, which smears the Doppler returns. If the gate is too narrow, longer integration times are required, to sample statistically, enough scatterers. A gate width corresponding to flow along an axial path equal to one diameter, for 1/2-in.-diameter pipe, would be about 25μ s. For transducers oriented at a right angle to one another, the intersection of the two beam patterns defines the measuring zone, even for a wide gate. This permits the use of continuous waves, without gating.

Transducers

The simplest piezoelectric transducers are the plane wave types. We also considered annular types such as the phased array and the related diffraction grating. Annular types could be either phased array or obliquely incident shear. However, it turned out that the simplest plane wave offered two important features. First, it permitted the use of continuous waves. Second, by locating one of the transducers in Figure 12 or 13 adjacent to the interaction (scattering) zone, the total path x is nearly halved. This means attenuation may be reduced by a factor of nearly e^2 or 7.3. Conversely, for a given allowable total attenuation $e^{\alpha x}$, frequency f can be increased by $e \doteq 2.7$, since α is proportional to f^2. Again, higher frequency leads to scattering contributions by smaller particles, and provides better statistical averaging over more particles.

One potential drawback of the right angle transducer configuration is due to the changing profile between the wall and the measuring zone. Therefore we analyzed, for transient conditions, the effect of different average flow velocities along different paths between interaction zone and receiver transducer. It turns out that such effects are negligibly small. This results from the dual-frequency Doppler output being of the form

$$I = \int_0^{\bar{T}} (S_1 \dot{S}_2 - S_2 \dot{S}_1)\, dt \qquad (9)$$

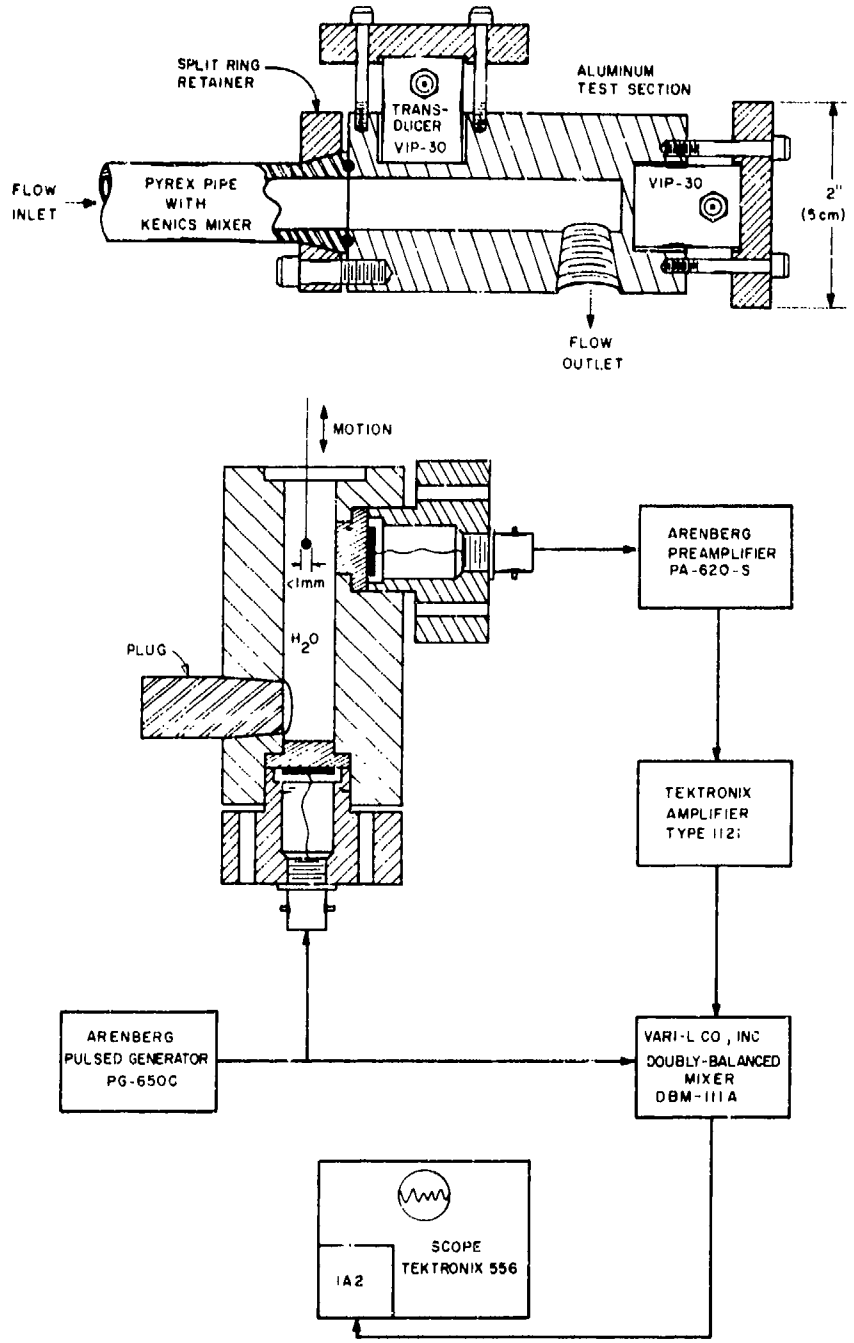

Figure 12. Cross Section Assembly View of Laboratory Test Fixture (Top) for Doppler Flow Velocimeter Using Flowing Liquids, and also (Bottom) Verification of Doppler Effect on a Single Scatterer in Water Under No-Flow Conditions.

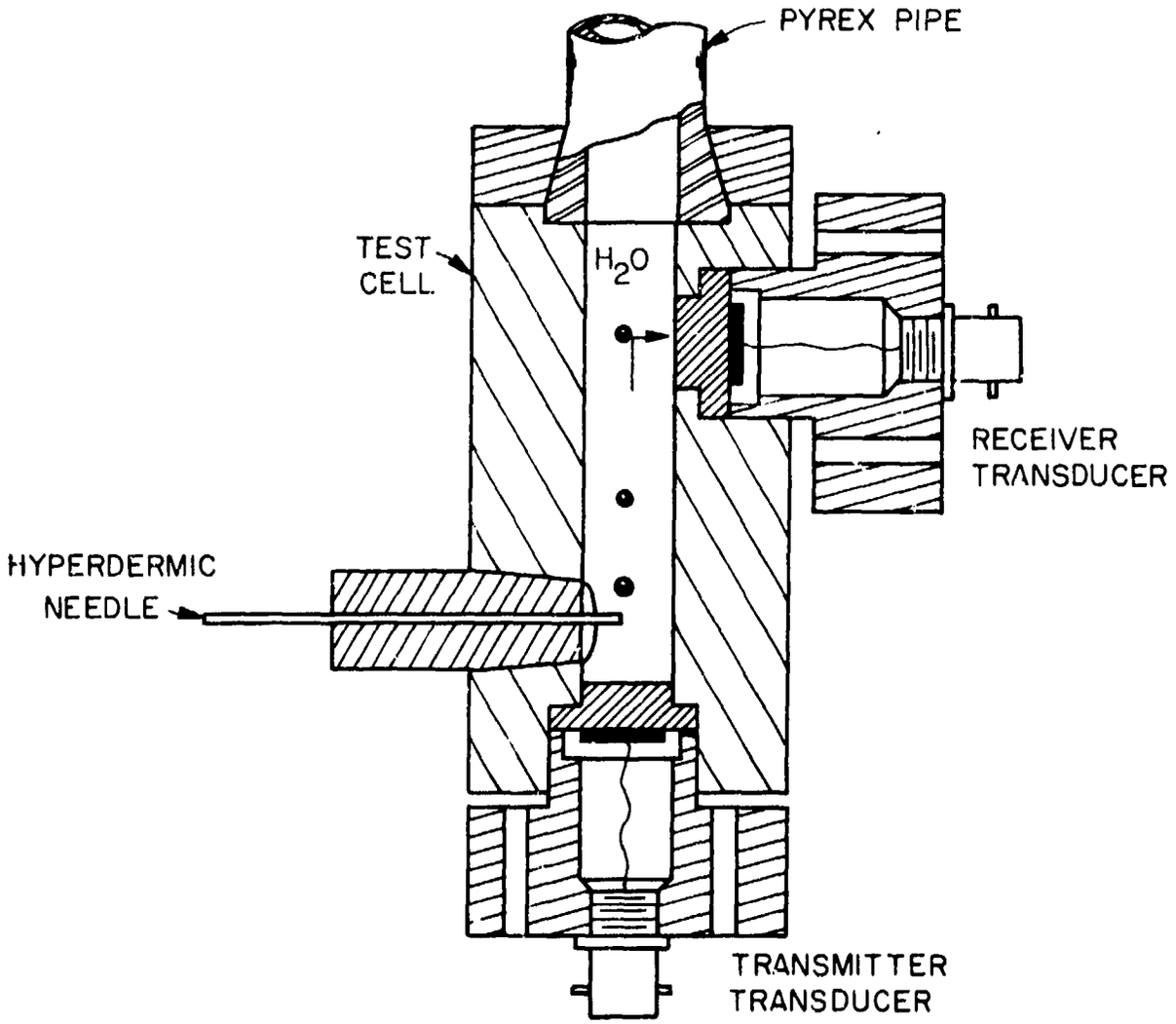

Figure 13. Demonstration of Doppler Effect Under No-Flow Conditions, Using Gas Bubbles as Moving Scatterer.

where the signals S are of the form

$$S_1 = \sin [\, \omega_1 t + \omega_1 \hat{R}/(v + c)] \tag{10}$$

$$\dot{S}_1 = \frac{\partial S_1}{\partial (v + c)} \cdot \frac{d (v + c)}{dt} = \frac{-\omega_1 \hat{R}}{(v + c)^2} \frac{d (v + c)}{dt} \cos [\, \Delta] \tag{11}$$

and S_2 and $\dot{S}_2$ are similar, with subscript 2 instead of 1. ($\hat{R}$ is the range.) For transients shorter than the system response time,

$$I = \int_{(v+c)_0}^{(v+c)_{\bar{T}}} \frac{\Delta \omega \hat{R}}{(v + c)} \sin \left[\Delta \omega + \frac{\Delta \omega \hat{R}}{(v + c)} \right] \frac{d (v + c)}{(v + c)} \tag{12}$$

which is negligibly small, since the flow velocity $v << c$, the sound speed.

In the case of the desired signals, however, we have integrals of the form

$$I = \int_{\hat{R}(0)}^{\hat{R}(\bar{T})} \frac{\Delta \omega}{(v + c)} \sin \left[\Delta \omega t + \frac{\Delta \omega \hat{R}}{(v + c)} \right] d\hat{R} \tag{13}$$

which are relatively large since $\hat{R}(\bar{T})-\hat{R}(0)$ is substantial. The system output would thus depend mainly on flow in the selected scattering zone, and not on flow velocity fluctuations outside this zone.

Scattering Observations

The method and equipment used to observe scattering from moving particles are shown in Figures 12 and 13. The oscillator provides a stable source of continuous waves essentially independent of transducer temperature. Laboratory tests were conducted on moving scatterers in a stationary liquid, and also on scatterers carried at the moving liquid' s flow velocity. These tests used uncontaminated Avgas-100 and also water as the fluid media. In these tests, using 20 MHz continuous waves, scattered waves were not detected except when one or more bubbles were present naturally or present by controlled introduction. Calculations predicted that fuel contaminated above 1% of the maximum levels specified in MIL-E-5007C, paragraph 3.4.1.3, Table 1, would yield detectable scatter. However, the need for high accuracy and, ultimately, fast response, means that scatter must be not merely detectable, but ample. Instead of pursuing methods of increasing the scatter, or increasing sensitivity to scatter, we reexamined alternative transmission approaches.

TRANSMISSION METHODS

Various ultrasonic transmission methods were analyzed for measuring v and c. In many cases one would prefer to either eliminate the need for a c measurement, or choose a method that yields both v and c. In this program, however, our approach required both variables to be determined independently.

Flow Velocimeter

Translation of the 40:1 $\dot{M}$ range of 50 to 2000 lb/hr, for fuels having densities ranging from about 0.65 to nearly 0.90 g/cm^3, leads to the requirement to measure flow velocity over a ~60:1 range, from ~0.05 to ~3 m/s (~2 to ~120 in./s) in a 1.27-cm (1/2-inch) diameter pipe. A nomogram relating $\dot{M}$, v, ρ, pipe diameter, and volumetric flow rate at 2000 lb/hr is shown as Figure 14.

Pulse Time of Flight

Let us first estimate the axial path length L required to meet accuracy requirements of 5% at minimum flow and 0.5% at maximum flow. The upstream and downstream travel times are $L/(c + v)$ and $L/(c - v)$. Their difference is $\Delta t \approx 2Lv/c^2$, from which $L = c^2 \Delta t/2v$. Assuming a time interval resolution of $\pm$ 1 ns, and c = 1500 m/s, we compute L = 45 cm (~18 in.) when v = .05 m/s, and L = 7.5 cm (~3 in.) when v = 3 m/s. These L's are minima, since they cause us to use up our entire $\dot{M}$ error allotment in determining v, without allowing any margins of error in ρ or c.

If we allocate half our $\dot{M}$ error to v, then we must double L to 90 cm (~36 in.) to meet the accuracy requirement at minimum flow. If the unwieldy values of L between 45 and 90 cm are not yet sufficient reason to force abandoning this method, two further considerations certainly clinch this decision. First, to achieve $\pm$ 1 ns resolution, the pulse width should be 100 ns or shorter, corresponding to a frequency of ~10 MHz. Attenuation of 10 MHz pulses is estimated to be ~1 dB/cm, which value leads to signal loss of 45 to 90 dB in the fuel.

Second, in propagating over such long paths, well into the far field (Fraunhoffer zone) the initially plane wavefront will be increasingly distorted at increasing velocities of laminar flow (Re $\rightarrow$ 2000) and somewhat distorted even in the flatter profile associated with turbulent flow (Re $\rightarrow$ 70,000). These considerations show that while one might achieve acceptable accuracy over the upper half of the flow range using an $L \lesssim 20$ cm (~8 in.), the pulse time of flight method is unsuitable for the lower flow velocities. Appendix II supports this

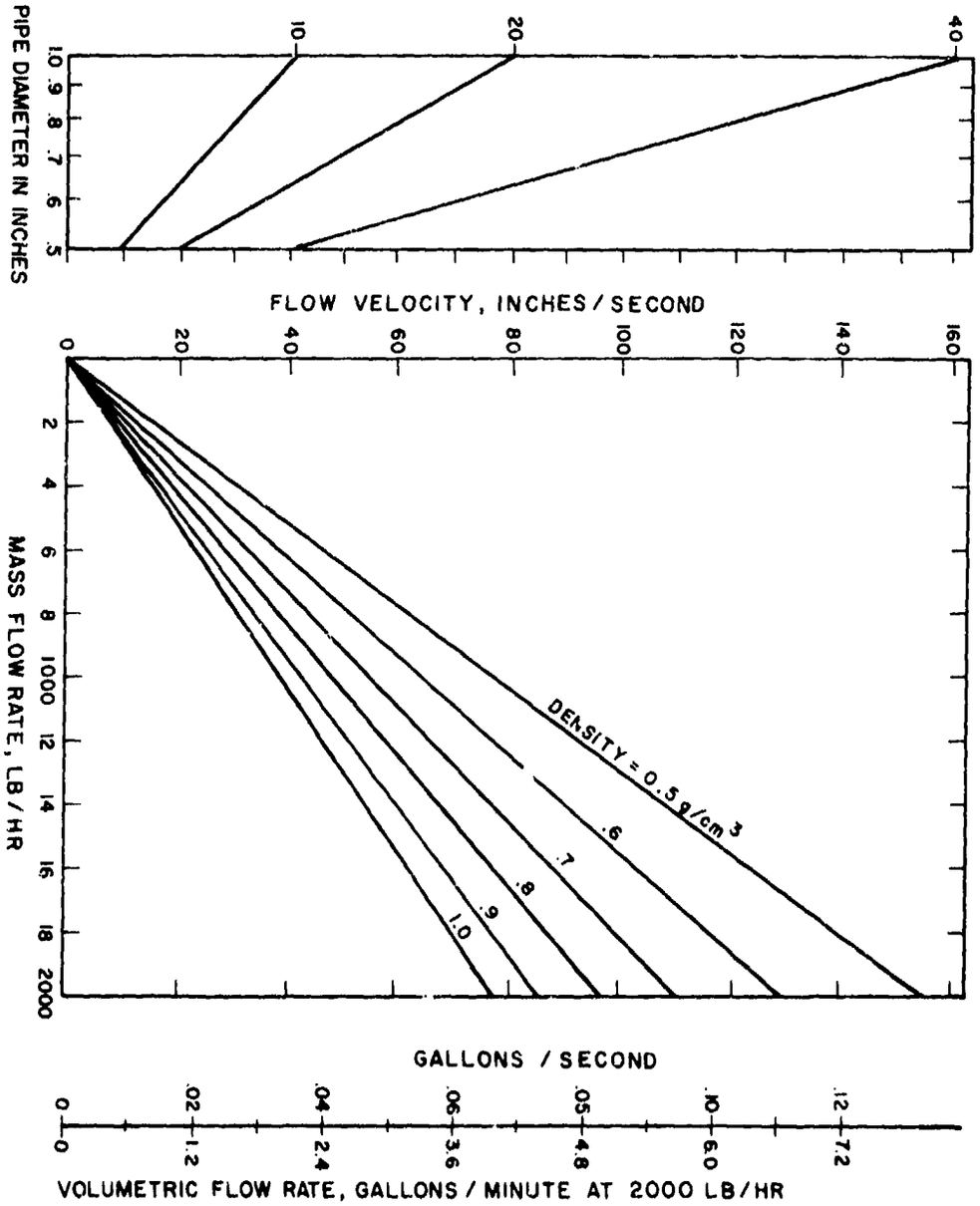

Figure 14. Flow Velocity Nomogram

conclusion with an analysis of far field errors under laminar flow conditions.

Since wavefront curvature under laminar flow forces us to abandon long paths, and the accuracy requirement at low flow forces us to abandon the pulse time of flight method for short paths, we are apparently left with only two alternative short path ultrasonic transmission methods: phase measurement at fixed frequency, or frequency measurement at fixed phase. In the present program, we investigated the former alternative.

Continuous Wave Phase Measurement

Based on the values of v, c, α, taking 10 cm (~4 in.) as the maximum cell dimension, and setting the maximum phase shift difference equal to 180°, we selected 5 MHz as the operating frequency. Measurement of this phase difference to $\pm 0.3^{\circ}$ corresponds to an error in v_{max}/c^2 of about $\pm 0.2\%$. At the low flow limit, $\pm 0.3^{\circ}$ corresponds to an error of about $\pm 10\%$. Phase meters are now available with digital and analog phase accuracy of $\pm 0.3^{\circ}$ at 0.01 to 3V single frequencies up to 11 MHz (e.g., Dranetz Engineering Laboratories' model 305C phase meter with 305-PA-3005 plug-in). It therefore appears that errors in flow velocity of 0.5% or less at v_{max}, and 10% at v_{min}, are to be associated with presently available electronic instruments that measure phase shift. By doubling the operating frequency to 10 MHz, to provide 360° phase difference at v_{max} and 6° at v_{min}, it appears that these percentage errors could be halved, to 0.25% and 5%, respectively.

The measurement to be described next involves the processing of essentially plane 5 MHz continuous waves (cw) propagated in the transducer's near field through 100% of the flow cross section. Flow is measured in a square channel, with a rectangularly-collimated beam inclined at 45° to the flow. This approach, while it may still need some refinement relative to inlet geometry and channel interruptions, provides a new instrumentation method for responding essentially linearly and accurately to flow velocity in transmission measurements over laminar, transitional and turbulent flow conditions, without requiring knowledge of or compensation for the Reynolds number or flow profile.

Similar to previous ultrasonic transmission flowmeters, the system to be described now measures the phase difference between waves transmitted upstream and downstream. The two cw waves traverse virtually the same path at virtually the same time. The two waves have the same carrier frequency, yet can be separated, or identified, by the manner in which they are each modulated and then demodulated.

This advanced flow velocimeter is shown in Figure 15. In this system, a 5 MHz crystal controlled oscillator signal is divided into two isolated channels. The waves in the upper and lower channels are phase coded by means of a dual coherent pseudo-random-noise code generator, producing a sequence of 1's and 0's such that the resulting code displays all the characteristics of perfect randomness. The length of the code, as well as the clock rate (which is derived by dividing down from a 6.2 MHz carrier) are arbitrarily variable. Each "1" produces a $+90^{\circ}$ phase shift of the carrier, while each "0" produces a -90° phase shift. The resulting spectrum strongly resembles a gaussian noise spectrum centered at the carrier frequency and has a half width equal to the reciprocal of the clock rate. The codes in the upper and lower channels are different codes. These pseudo-random sequences have the property of being orthogonal, which means that a signal coded with code C_1 but detected with a code C_2 will be rejected by a factor 1/N in voltage (where N = number of bits in the code) as compared with a signal coded with C_1 and detected by C_1. Thus, a code having 10^2 bits will have a correlation function of 40 dB; while 10^4 bits will provide a correlation function of 80 dB!* Another property of these (shift register) codes is that a code which is shifted by one or more bits is orthogonal to the unshifted code. Thus, it is possible to provide range gating of a high order of isolation, as well as the isolation of two separately coded signals. The use of phase coding permits simultaneous and continuous operation of one or more systems operating on exactly the same basic carrier.

Going back to Figure 15, we see that the two 5 MHz waves are independently phase code modulated (C_1 and C_2) by the double balanced mixers (DBM's) at the left. These are then fed, via circulators (which are actually hybrid power dividers) to the two transducers. The received waves, which of course resemble wide band noise, are fed (via the circulators) to the top and bottom double balanced mixers on the right. The demodulating codes, C_{2d} and C_{1d}, which are delayed just the proper amount, are also fed to these DBM's. The outputs of the DBM's are two cw signals, as well as wide band noise. The "noise" results from noncorrelation of unwanted signals from either the wrong channel or from stray reflections and reverberations within the pipe. Only that wave which is due to a reverberation-free straight-through-transmission results in a cw wave at the demodulator DBM's. We next go through a pair of tuned 5 MHz amplifiers which strip off most of the uncorrelated information, and finally feed into a pair of phase-locked loops. These devices are essentially self-tracking filters and employ a voltage controlled oscillator (VCO) and a phase detector in a feedback configuration such that the VCO is forced to track the cw input signal. The bandwidth

*An electromagnetic system recently completed, using coding techniques identical to this, exhibits 80 dB correlation/decorrelation ratio.

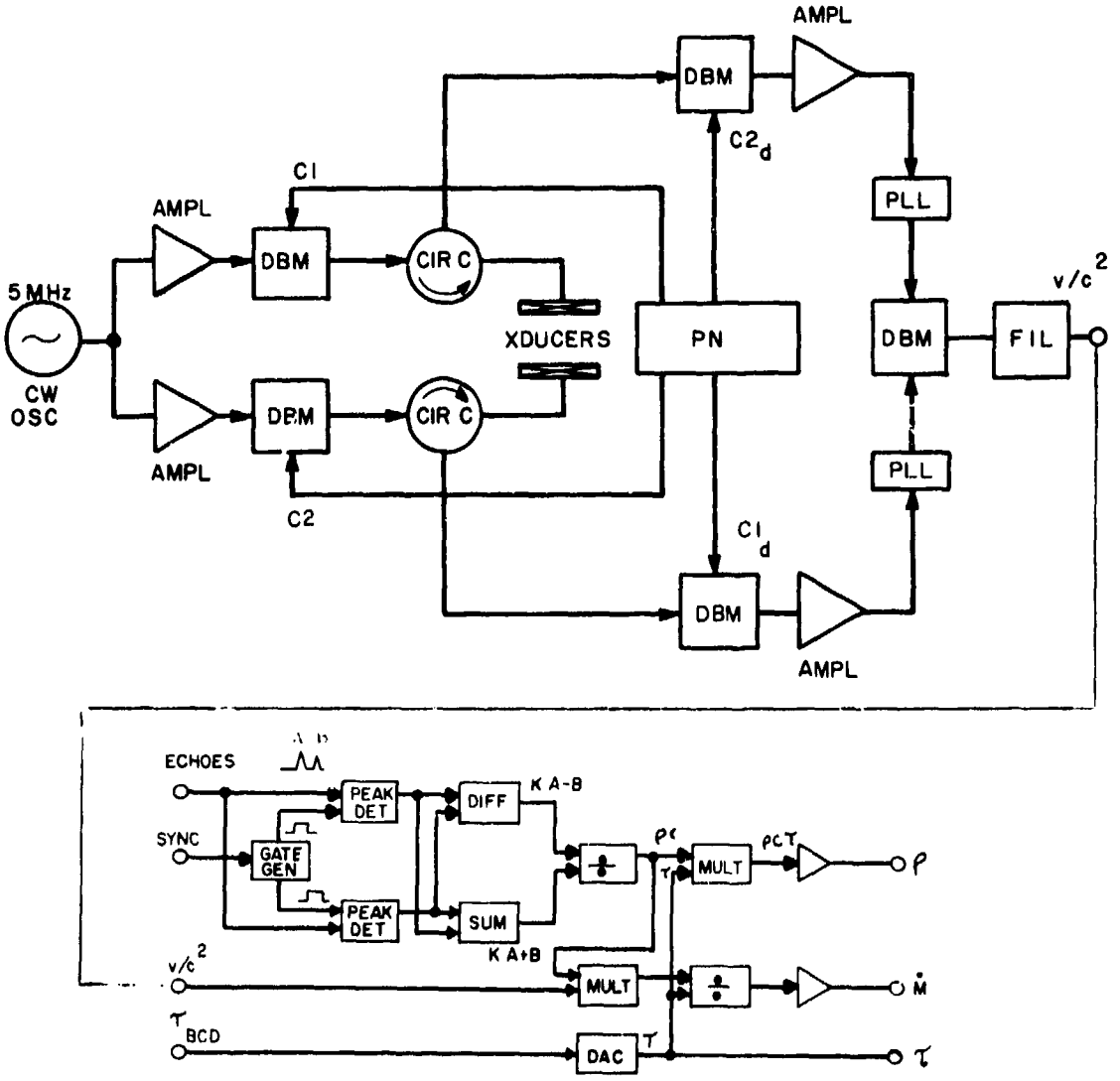

ABBREVIATION

CW OSC	Continuous wave oscillator
AMPL	Amplifier
DBM	Double balanced mixer
CIRC	Circulator (power divider)
XDUCERS	Transducers
PN	Dual coherent pseudo-random-noise code generator
PLL	Phase Locked Loop
C1	Code 1 (pseudo-random-code)
C2	Code 2 (pseudo-random-code)
$C1_d$	Code 1, delayed
$C2_d$	Code 2, delayed

Figure 15. Block Diagram of Ultrasonic Mass Flowmeter.

of the feedback loop is adjustable to be arbitrarily narrow, e.g., 100 Hz. The outputs of the phase-locked loops are square waves whose phases are equal to the phases of the cw $\pm$ up to 100 Hz components of the input signals, and whose amplitudes are independent of the input amplitudes. These square waves are next multiplied in the right-hand DBM to produce a voltage which is precisely proportional to the phase difference. Instead of phase-locked loops, one may use a standard phase meter. Another simplification involves using just one code for both directions.

One might ask about the residual uncorrelated signal within the 100 Hz bandwidth of the phase-locked loops. The answer is that there isn't any! The reason is that the overall time duration of the sequence is made to be short enough so that the frequency components associated with uncorrelated signals fall well outside the bandpass of the feedback loop in the phase-locked loops.

To obtain $\dot{M}$, the v/c^2 output of the flow velocimeter is combined with τ and ρc as shown in the lower portion of Figure 15. Details on the τ and ρc measurements are given below.

Time Intervalometer

Measurement of the time interval τ across a fixed or known path in a direction orthogonal to the flow is required in order to obtain $\dot{M}$ from measurements of v/c^2 and ρc. That is, $\dot{M}$ is proportional to $(1/\tau)$ (v/c^2) (ρc), or $\dot{M} = k' v \rho / c \tau$ where k' depends on the pipe area and units of measure.

The method used to measure τ is illustrated in Figure 16. It utilizes a damped 5 MHz transducer mounted outside the flow channel. The transducer is energized, and selected echoes of like polarity are measured, with a modified Panametrics 5220 gage operated as a time intervalometer. This gage automatically averages the transit time between ten pairs of selected echoes. The reason the echoes need to be selected, is that following the initial energizing pulse, the wall supports many reverberations of the pulse. The frequency is chosen high enough so these are substantially attenuated by the time echoes arrive from the far wall of the channel. Since the 5220 is designed to read between echoes of only positive polarity, the measurement is made between two successive reverberations in the fluid, rather than between the first pair of wall/fuel, fuel/wall echoes. If the transducer were in direct contact with the fuel, τ could be measured from the initial pulse to the first echo from the fuel/wall interface.

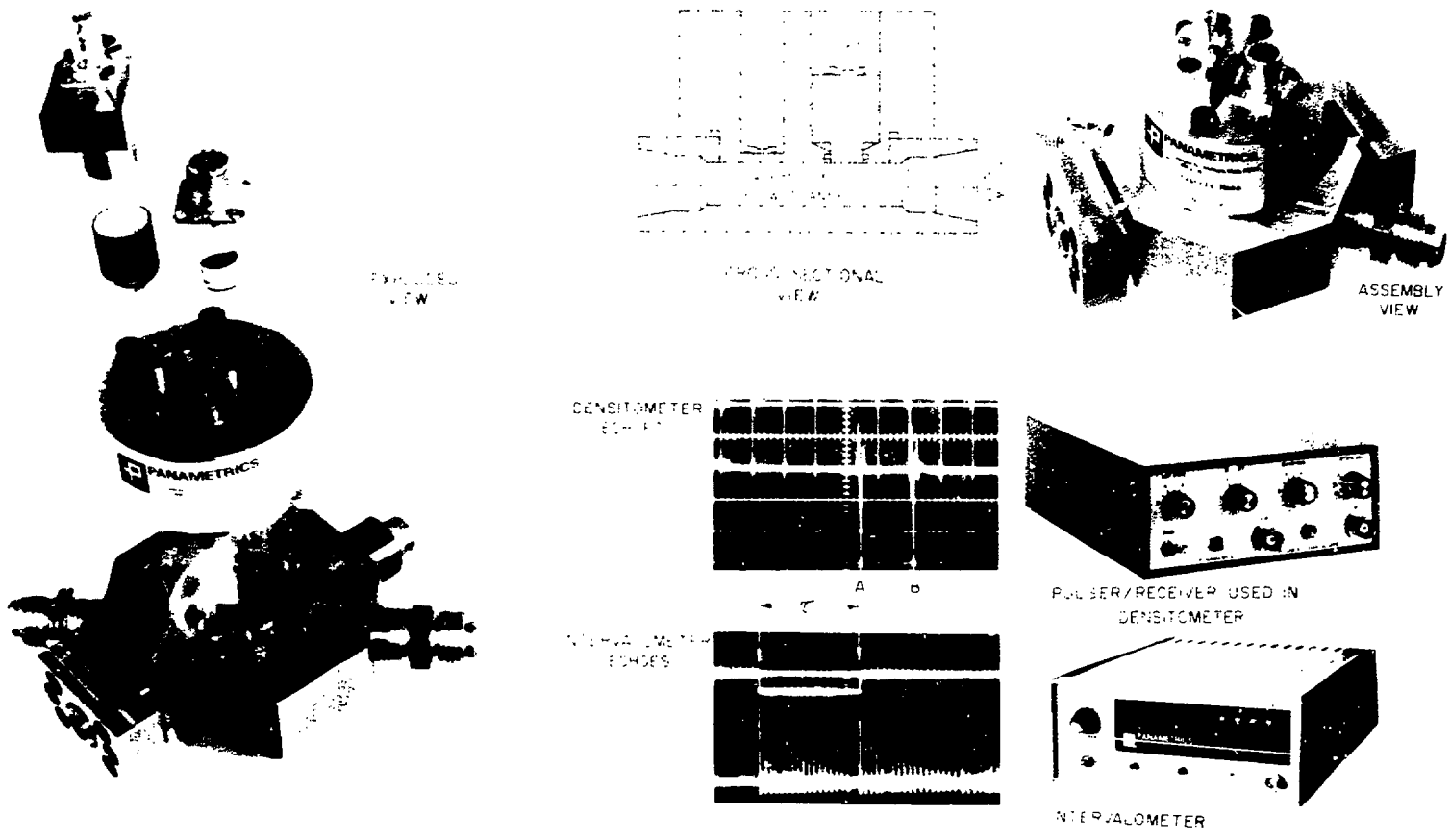

Figure 16. Ultrasonic Mass Flowmeter Measuring Cell.

REFLECTION METHODS

The present ultrasonic reflection coefficient densitometer, where $R = (\rho_2 c_2 - Z_1)/(\rho_2 c_2 + Z_1)$, may be compared with two other types of ultrasonic densitometers. In one type, first investigated in connection with mass flowmeters by Kritz[8] and later by Dalke and Welkowitz,[12] the output voltage in a resonant circuit is a measure of the liquid's characteristic impedance $\rho_2 c_2$. This $\rho_2 c_2$ is coupled into the resonant circuit by its loading effect on a piezoelectric crystal which radiates into the liquid. For operation at high pressure, a half-wave protection plate separates the crystal from the liquid.

In a second type, the distributed-spring-mass vibration densitometer, now commercially available from ITT-Barton (Series 650), the resonant frequency of a metal tube is measured, the square of this frequency being inversely proportional to the fluid density ρ_2. As presently constructed, this tube of monel and 316 SS is normally centered within a pipe tee section of 3.8 cm (1.5 in.) diameter. Since the tube materials have moduli of elasticity which are temperature-dependent (readout could vary up to $\pm$ 1% over range -65°to+160°F), some correction is required for operation over the full temperature range. (One approach to minimizing the temperature dependence of a resonating probe is to build the probe's resonant shell out of a quartz crystal whose longitudinal axis is inclined at about 5° to the Z-axis, or optical axis, of the crystal.[13]) Provided the ITT densitometer's size, intrusiveness and temperature-dependence are allowable, however, its precision of $\pm$ 0.001 specific gravity units for liquids is attractive. Effects of vibration and contaminants should be negligible.

In contrast to these two types, the reflection coefficient densitometer probe can respond to a very small volume of liquid (e.g., using focussed waves, it could theoretically measure a droplet); it can operate over wide pressure ranges without compensation, and when the probe is fabricated of certain materials such as AT quartz, it can operate over wide temperature ranges without compensation. It can be recessed or flush-mounted. Sensitivity is limited by echo amplitude resolution; using 5 MHz video pulses, density should be resolvable to about 0.2%.

Referring to Figure 17, we show the reflection coefficient densitometer schematically in two configurations. (Figure 16 shows the actual cross section as used in the mass flowmeter.) The stepped-diameter probe yields echoes A and B which ring for one or more cycles, depending on acoustical and electrical terminations. A Panametrics pulser/receiver, model 5050 PR, was used to obtain these echoes. In Figure 16 the time interval across the liquid is measured separately. This is accomplished by

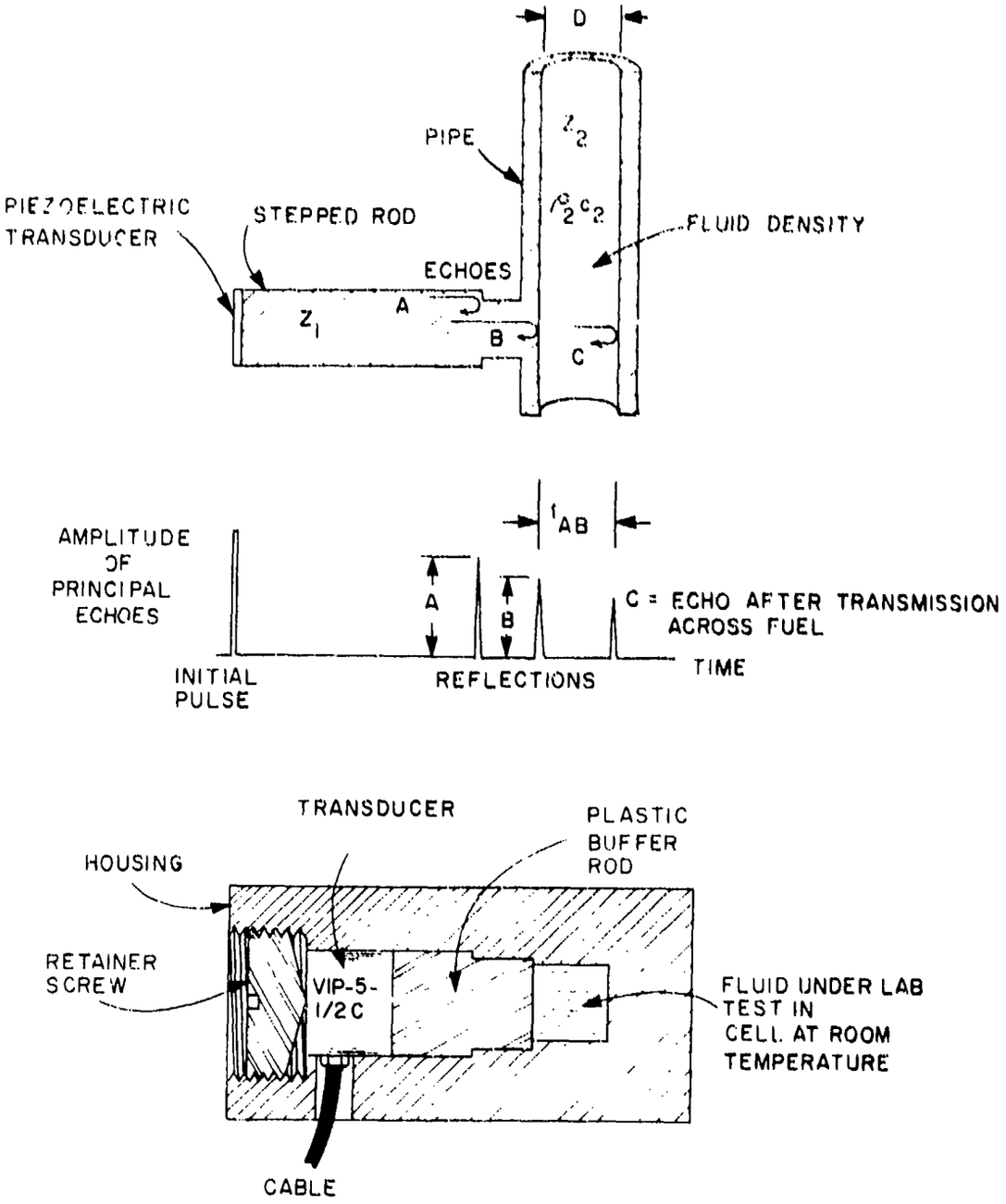

Figure 17. Schematic of Ultrasonic Densitometer and Sound Velocimeter Measuring Cells.

using the lower transducer and a modified Panametrics thickness gage, model 5220, to measure between two selected echoes of like polarity, to ± 10 ns.[14]

The reflection part of the density measurement responds to $\rho_2 c_2 / Z_1$. This $\rho_2 c_2$ product is called the characteristic impedance of the (fuel) medium. By measuring the amplitude of the wave reflected at the pipe/fuel interface, $\rho_2 c_2$ is determined in terms of Z_1. To the extent that Z_2 sensed near the pipe wall is representative of the average Z_2 in the fluid, the method should provide a valid measure of fuel density (Figures 16, 17).

The transmission part of the density measurement responds to c_2 alone, by arranging to measure the time T it takes for a sound pulse to traverse the test cell. For a measurement across the inside diameter D, the sound speed is $c = 2D/T$. For simplicity, let us assume A ≅ B when $\rho = 0$.

To compute fuel density we simply take the ratio

$$\rho_2 = (Z_1/c_2)(1 + R)/(1 - R) \quad (Z_1/c_2)[(A - B)/(A + B)] \qquad (14)$$

where R is the sound pressure reflection coefficient at the probe/fuel interface. Calculations show that, for interface reflections of about 1V, A and B echo amplitude measurements accurate to 0.1 mV will determine the reflection coefficient R to 0.1%, and $\rho_2 c_2$ to 0.5%. These calculations assume an all-stainless-steel pipe or test cell and plane waves. One can improve on the $\rho_2 c_2$ determination by using a probe of characteristic impedance closer to that of the fuel. For example, using a fused silica, AT quartz or T-40 glass probe, $\rho_2 c_2$ and hence ρ improves to ≈0.3%. For a plastic probe one could resolve ρ_2 to 0.1%, theoretically, using this reflectometer method.

A more detailed analysis of this method is given below.

Ultrasonic Densitometer Sensitivity

The sound pressure reflection coefficient R at the buffer/fuel interface is R = (r-1)/(r+1) where r = impedance ratio Z_2/Z_1. Z_2 is the fuel characteristic impedance $\rho_2 c_2$, and Z_1 is the buffer characteristic impedance $\rho_1 c_1$. What value of Z_1 maximizes the sensitivity of this measurement to fuel density? That is, what value of Z_1 maximizes sensitivity with respect to Z_2 or r?

Since we propose to measure R, one may first suppose that maximum sensitivity occurs when dR/dr is maximum (see Figure 18). This maximum

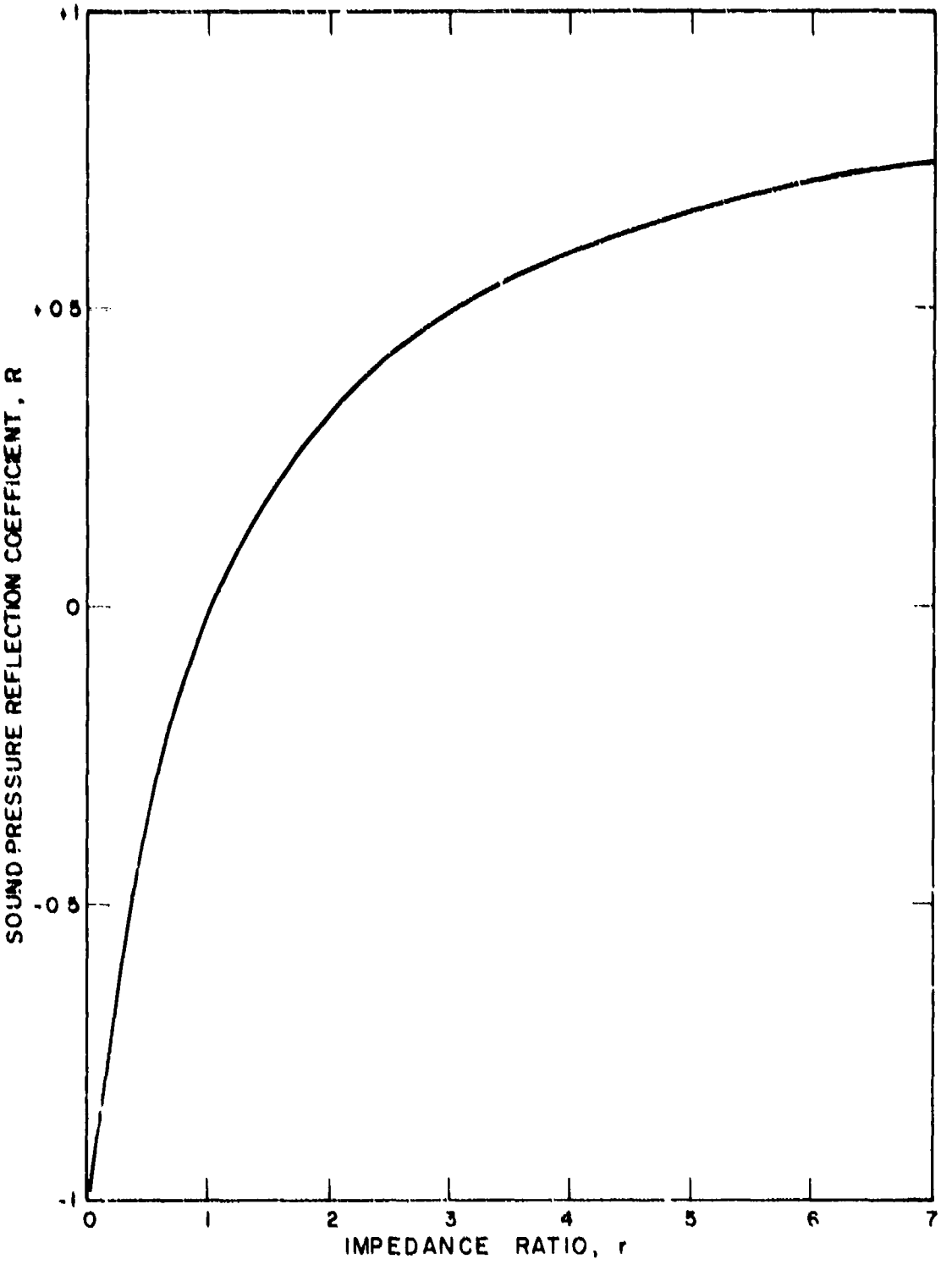

Figure 18. Reflection Coefficient Functions.

is readily found to occur at $r = 0$, for which the slope of R versus r is $dR/dr = 2/(r+1)^2 = 2$. However, near $r = 0$, $R \approx -1$ While ΔR is indeed largest here, for a given Δr, we would be sensing a relatively small change ΔR in a large number R.

Thus we are led to consider $(1/R)(dR/dr)$ as the densitometer sensitivity function to be maximized with respect to r. This has maxima when $r = 1$, that is, when $Z_1 \equiv Z_2$. This function has positive and negative branches, as is readily seen by evaluating $(1/R)(dR/dr) = 2/(r^2 - 1)$ for r over a range straddling $r = 1$ (see Figure 19). In this work we are concerned with the negative branch, since fuel impedances Z_2 are less than solid buffer impedances Z_1; i.e., $r = Z_2/Z_1 < 1$.

The above analysis leads us to conclude that as far as ultrasonic reflection coefficient measurements of fuel density are concerned, the buffer rod should preferably be chosen to have an impedance Z_1 as close as practical to the fuel Z_2.

In any given installation, other requirements may dictate how close the design can approach this "acoustic" objective.

For comparison purposes, we list the characteristic impedances of Avgas-100, JP-4, water and several solids, at room temperature, in Table V.

TABLE V. CHARACTERISTIC IMPEDANCES

Medium	Characteristic Impedance, g/cm^2-μ s
Avgas-100	0.087
JP-4	0.095
Water	0.150
Polystyrene	0.25
Acrylic (Lucite, Plexiglas)	0.32
Teflon	0.59
Magnesium	1.01
Pyrex	1.24
Fused Silica	1.30
Aluminum	1.75
Titanium	2.77
Stainless Steel 302	4.55
Tungsten	9.98

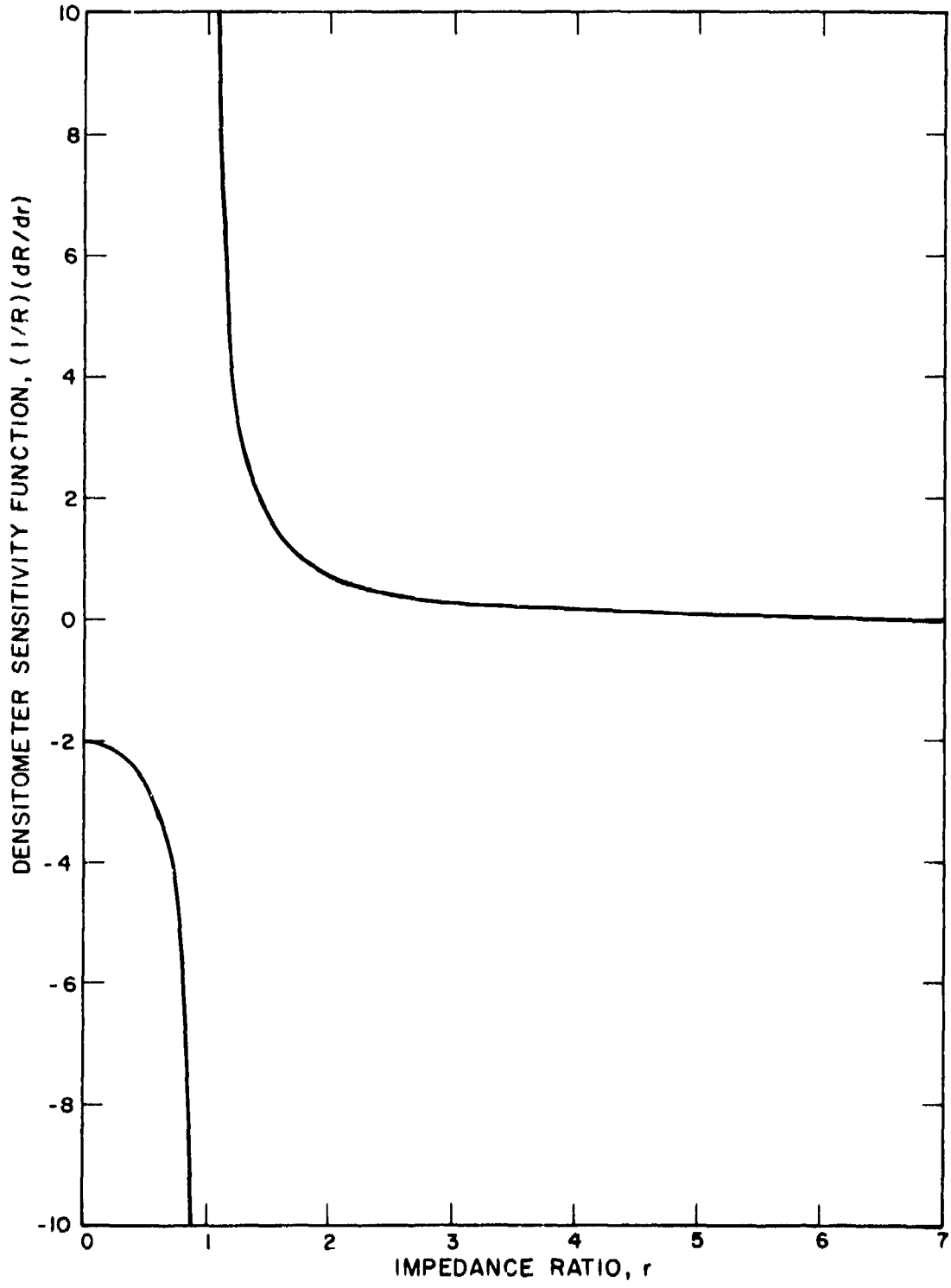

Figure 19. Densitometer Sensitivity Function.

We describe next the main considerations underlying the optimization of the reflection method.

To select the proper material for the probe, consider the following: A plastic buffer ($Z_1 \approx 0.3$ g/cm^2-μs) provides relatively good sensitivity, but unfortunately plastics are too temperature-sensitive. To temperature-compensate Z_1 to $\pm$ 0.1% for a plastic such as delrin, one would need to monitor the probe temperature to about 1°F.

A better approach is to use a more brittle material such as glassy carbon ($Z_1 = 0.7$) or fused silica ($Z_1 = 1.3$) whose Z_1's change very little from -65° to +160°F. Z_1 in these buffer materials is 1 to 2 orders of magnitude less sensitive to temperature. The trade-off is a factor of 2 or 4 less R sensitivity to Z_2. Fused silica is known to exhibit a small but ultimately undesirable temperature-dependence, since its sound velocity V_L increases with temperature at the rate of ~81 ppm per $^{\circ}$C. Over a temperature range of ~120°C (-65° to +160°F), this leads to $\Delta V_L / V_L \approx 1\%$. To avoid the need for electronic temperature compensation, we fabricated identically-shaped probes of AT quartz and T-40 glass. A comparison of these materials is given in Table VI.

The AT quartz has the lowest $\Delta V_L / \Delta T$, but must be carefully oriented. Therefore the T-40 glass, which is isotropic, may provide, ultimately, a more practical, and certainly lower cost, solution.

Z_1 and c_2 can be measured with errors in the range of 0.1 to 0.01%. Therefore the practical limit in this method is imposed by one's ability to peak-detect and measure A and B, or their ratio, A/B. If A and B are video (nonoscillatory) shaped, peak detector accuracy of better than 0.5% is achievable at present only if A and B are at least 1 μs wide. Such wide pulses can be generated, but they do not propagate as plane waves, and therefore may complicate the probe design. However, if A and B pulse shapes remain constant, a circuit that measures a fixed proportion of the peaks will be adequate (Figure 20). Also, if A and B were rf bursts, say, 10 cycles of a 10 MHz carrier, the detected 1 μs envelopes can be measured by 1 MHz peak detectors, or by a standard instrument such as a Matec 2470 Attenuation Comparator, which resolves 0.01 dB with a 2.5s response time.

The circuit of Figure 20 operates as follows. On receipt of a plus or minus trigger, a bipolar switch-selectable comparator starts a timing sequence. This sequence is adjusted so that two 2 μs gates straddle the A and B echoes from the densitometer probe. The peak detectors, built using Fairchild's μA710 and Dynamic Measurement's FST-160B generate dc voltages proportional to A and B peak magnitudes.

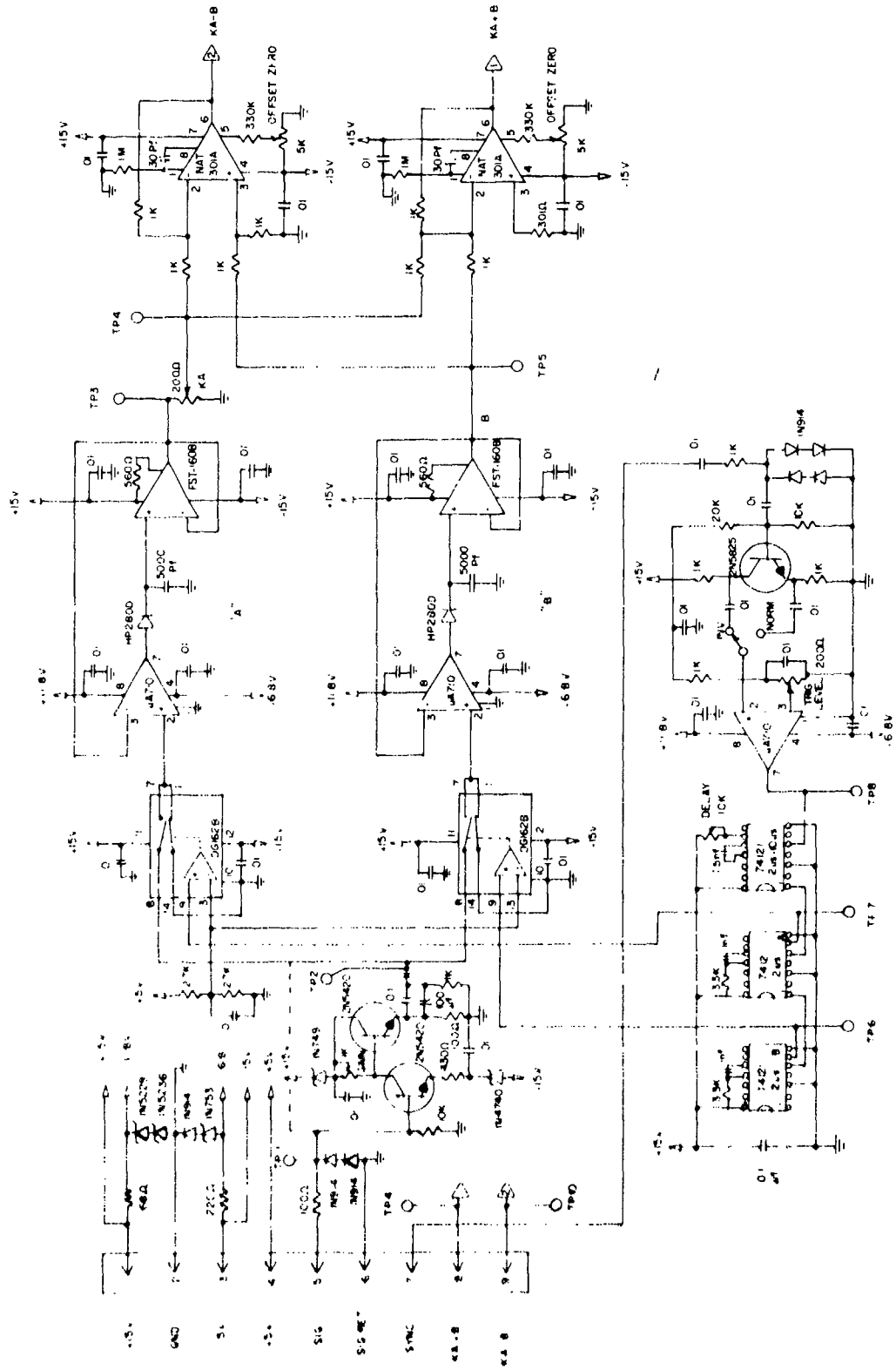

Figure 20. Circuitry for Densitometer Including Two Channel Peak Detector and Sum and Difference Amplifiers.

TABLE VI. COMPARISON OF DENSITOMETER PROBE MATERIALS: FUSED QUARTZ, AT QUARTZ, T-40 GLASS

Material	Velocity Temp. Coef. (ppm/°C)	Expansion Coefficient (ppm/°C)	Density (g/cm^3)	Longitudinal Velocity (cm/μs)	Char. Acoust. Impedance (g/cm^2-μs)
Fused Quartz*	81.4	0.55	2.20	0.590	1.30
AT Quartz**	-2.0	$\alpha_3 = 7.8$ $\alpha_1 = \alpha_2 = 14.3$	2.65	0.688	1.85
T-40 Glass***	-2.8	~8	3.39	0.435	1.47

*Data from Amersil, Inc., 685 Ramsey Avenue, Hillside, N. J.

**Data from W. P. Mason, Piezoelectric Crystals and Their Application to Ultrasonics, 102-105, Van Nostrand (1950), longitudinal mode.

***Data from Bausch & Lomb, Inc., Special Products Division, 635 St. Paul Street, Rochester, N. Y. 14602; private communications, Dr. Hensler. Average temperature coefficient of -2.8 ppm/°C is over the range -20° to +37°C, with zero point of 37°C. Zero point temperatures vary from -10°C to 70°C. See also: J. T. Krause, IEEE Trans. Sonics and Ultrasonics SU-19 (1), 34-40 (Jan. 1972); J. T. Krause, private communication.

The sum and difference amplifiers, National 301 A's, together with a "k" potentiometer, yield the terms $kA \pm B$. The quotient of these terms, when multiplied by the time intervalometer output T, yields a result proportional to density ρ_2. An operational amplifier scales this result, to end up with the final output value for ρ_2.

The circuit is aligned using the following laboratory procedure.

1) Select proper sync polarity with switch located at back of board.

2) Set Trigger Level potentiometer to reject any noise in sync signal if noise is present.

3) Set Delay potentiometer so that gate pulses at TP6 and TP7 overlap display of desired portions of waveform.

4) Turn off source.

5) Set kA to 0 (full ccw).

6) Set kA + B offset potentiometer for 0 mV at TP9 (Pin 8).

7) Set kA - B offset potentiometer for 0 mV at TP10 (Pin 9).

8) Turn source on and adjust kA potentiometer for null at TP10.

Densitometer Noise Analysis

If noise were absent, the density would be determined as

$$\rho_2 = \frac{Z_1}{c_2} \frac{A - B}{A + B} \tag{15}$$

But suppose noise of magnitude ϵ is added to A and subtracted from B. Then

$$\rho_2(\epsilon) = \frac{Z_1}{c_2} \frac{(A + \epsilon) - (B - \epsilon)}{(A + \epsilon) + (B - \epsilon)} \tag{16}$$

$$= \frac{Z_1}{c_2} \frac{A - B - 2\epsilon}{A + B} \tag{17}$$

Let $$\frac{\Delta\rho_2}{\rho_2} \equiv \frac{\rho_2(\epsilon) - \rho_2}{\rho_2} = \frac{-2\epsilon}{A - B} \tag{18}$$

Now if $\Delta\rho_2/\rho_2 \leq 0.2\%$, and if A = 1V, B ≈ 0.9V, we require that

$$\epsilon \leq 100\ \mu V. \tag{19}$$

This analysis shows that error voltages up to 0.1% of (A-B) are tolerable.

OTHER ULTRASONIC METHODS

The foregoing discussion has covered those scattering, transmission and reflection methods which comprised the major effort in this program. It is to be understood, however, that several variations may be of interest in the future, depending on changes in technical requirements regarding the types of fuels, flow range, temperature range, accuracy, response time, geometry, etc. Such changes might occur, for example, as a result of emphasizing equipment simplicity rather than emphasizing versatility.

To illustrate the nature of these variations, we briefly indicate several other ultrasonic methods of measuring v or v/c^2, and ρ.

Determination of Flow Velocity v

A direct determination of v, without requiring a c measurement, may be achieved by controlling two variable frequencies f_1, f_2 such that the number of wavelengths in the upstream and downstream directions are each maintained constant. The f_1 loop for such a system is shown in Figure 21. The f_2 loop would be similar, and the readout could be the frequency difference $\Delta f = f_2 - f_1$, which would be proportional to v. This method may be considered as the cw analog of certain ultrasonic pulse "singaround" flowmeters presently available as commercial instruments.[15]

Determination of v/c^2

There are a variety of other methods of generating a phase shift proportional to v/c^2. For example, if one assumes that a pair of opposed transducers could be made identical, and that a pair of identical circulators could be perfectly terminated, then uncoded upstream and downstream cw signals could be fed to a differential amplifier whose output would be, ideally, proportional to the sine of the phase angle between the two waves. Offsetting the apparent electronic simplicity of this method, however, is the flow range limit imposed by the lack of sensitivity of the sine function for arguments near 90°, as well as the systematic errors and noise due to departures from the above assumptions on transducers and circulators. Still other methods of separating upstream from downstream waves over a common path include rf bursts of fixed or variable frequency, two continuous waves of fixed but different frequencies,[3] and cw alternately switched upstream and downstream.

Some earlier investigators used symmetrical dual path arrangements which employed a single fixed frequency to drive the transducer(s) radiating both upstream and downstream, and a phase meter to sense the phase difference between upstream and downstream receiving transducers.[16] This simple method cannot provide adequate absolute accuracy, because of minor path differences, but perhaps could be calibrated over a sufficient range of fuel combinations and flow conditions to be useful in some instances.

Continuous Wave Reflection Densitometer Method

Consider a main section of buffer rod of impedance Z_0, with an end plate of impedance Z_1 coupled to the fuel of impedance Z_2. The specific acoustic input impedance at the 01 interface is[17]

$$Z_{IN} = Z_1 \left[\frac{Z_2 \cos k''d + j Z_1 \sin k''d}{Z_1 \cos k''d + j Z_2 \sin k''d} \right] \qquad (20)$$

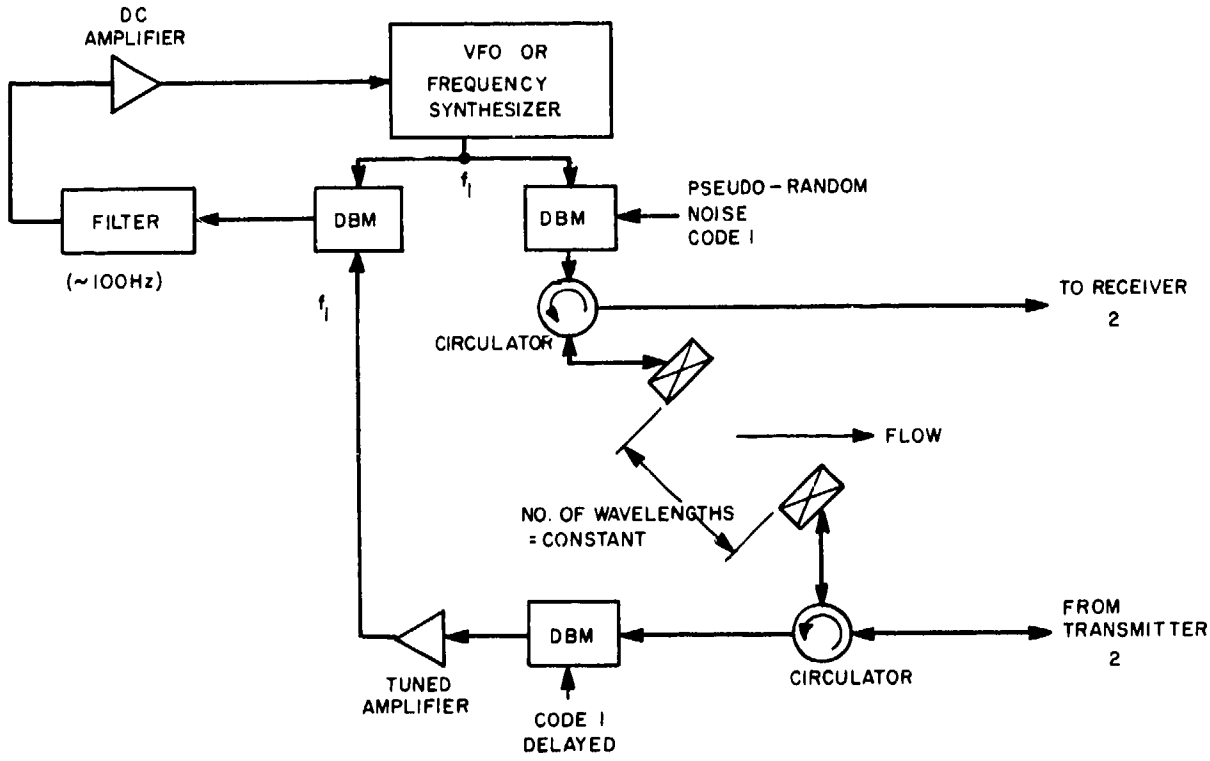

Figure 21. Flow Velocimeter Schematic Showing One of Two Loops for Maintaining a Fixed Number of Wavelengths by Varying the Frequency.

where the wave number for the incident cw wave is $k'' = 2\pi/\lambda$ and d = thickness of the end plate member. When the plate is a quarter-wave thick, $k''d = \pi/2$ and Z_{IN} simplifies to Z_1^2/Z_2.

This permits one to "transform" the relatively low fluid impedance Z_2 up to a value increased by the factor Z_1^2/Z_2. Theory shows that this can substantially increase the sensitivity of the reflection coefficient R_{01} to changes in Z_2:

$$R_{01} = \frac{Z_{IN} - Z_0}{Z_{IN} + Z_0} = \frac{(Z_1^2/Z_2) - Z_0}{(Z_1^2/Z_2) + Z_0} \tag{21}$$

Table VII shows how R_{01} depends on Z_2, the fluid impedance, for different combinations of buffer impedances Z_0 and Z_1. Theoretically, this approach could achieve a density accuracy of 0.3% despite an error in R_{01} of 2 to 3%.

For the present application, however, we rejected this method because of complications to be expected in a cw or long rf burst approach.

TABLE VII. CW REFLECTION COEFFICIENT R_{01} VERSUS FUEL IMPEDANCE Z_2, FOR DIFFERENT COMBINATIONS OF BUFFER IMPEDANCES Z_0 AND Z_1

Z_2	$Z_0 = 10$ $Z_1 = 1.0$	$Z_0 = 10$ $Z_1 = 1.23$	$Z_0 = 10$ $Z_1 = 0.707$	$Z_0 = 1.0$ $Z_1 = 0.316$	$Z_0 = 6.67$ $Z_1 = 1.0$
0.05	.333	.500	0	.333	.500
.06	.250	.430	-.091	.250	.430
.07	.177	.363	-.166	.177	.363
.08	.111	.306	-.230	.111	.306
.09	.052	.248	-.288	.052	.248
.10	0	.200	-.333	0	.200
.11	-.047	.156	-.375	-.047	.156
.12	-.091	.111	-.412	-.091	.111
.13	-.130	.074	-.444	-.130	.074
.14	-.167	.034	-.473	-.167	.034
.15	-.200	0	-.500	-.200	0

Indirect Determination of Density

Since ρ and c are both linear functions of fuel temperature, it may be possible to determine ρ indirectly by measuring c and/or temperature. Figure 22 shows that for fuel compositions near JP-4 this method does not appear sensitive to ρ. For compositions near JP-1, however, sensitivity might be adequate. As a corollary, if the density of virtually any unknown aviation fuel or fuel mixture could be independently measured, such as with a hydrometer, at one or two known temperatures, the density's subsequent variation could be determined by measuring the fuel temperature. This method, while undesirable for control purposes, may be appropriate for some diagnostic studies.

In passing, we may note that some present fuel control systems require that the fuel be known, such that one of five fuel types can be selected manually on a dial control. For such systems, where fuel type is known, a simple temperature measurement would provide the data for determining density to 1% or better. For this special case, an ultrasonic flow velocimeter of the type developed in this program could provide an output which, combined with fuel type and temperature data, would measure $\dot{M}$.

To summarize, and to place the principal foregoing methods in perspective, we present Table VIII. For example, Table VIII shows that if one measures flow velocity by a Doppler or phase method, then theoretically the better choice for the densitometer is the reflection coefficient type, since the outputs will be immune to, or less sensitive to, errors in c. Fundamentally, however, the best of all these combinations appears to be the last. Here, both the flow velocity and density measurements are each independent of c, and naturally, so is their product, $\dot{M}$.

TABLE VIII. COMPARISON OF OUTPUT PRODUCTS OF SIX COMBINATIONS OF CONTINUOUS WAVE FLOW VELOCIMETERS AND ULTRASONIC DENSITOMETERS

Flow Velocimeter \ Densitometer	Reflection Coefficient (ρ c)	Resonant Frequency (ρ)
Doppler (v/c)	$\dot{M}$	$\dot{M}/c$
Phase Difference (v/c^2)	$\dot{M}/c$	$\dot{M}/c^2$
Frequency Difference (v)	$\dot{M}c$	$\dot{M}$

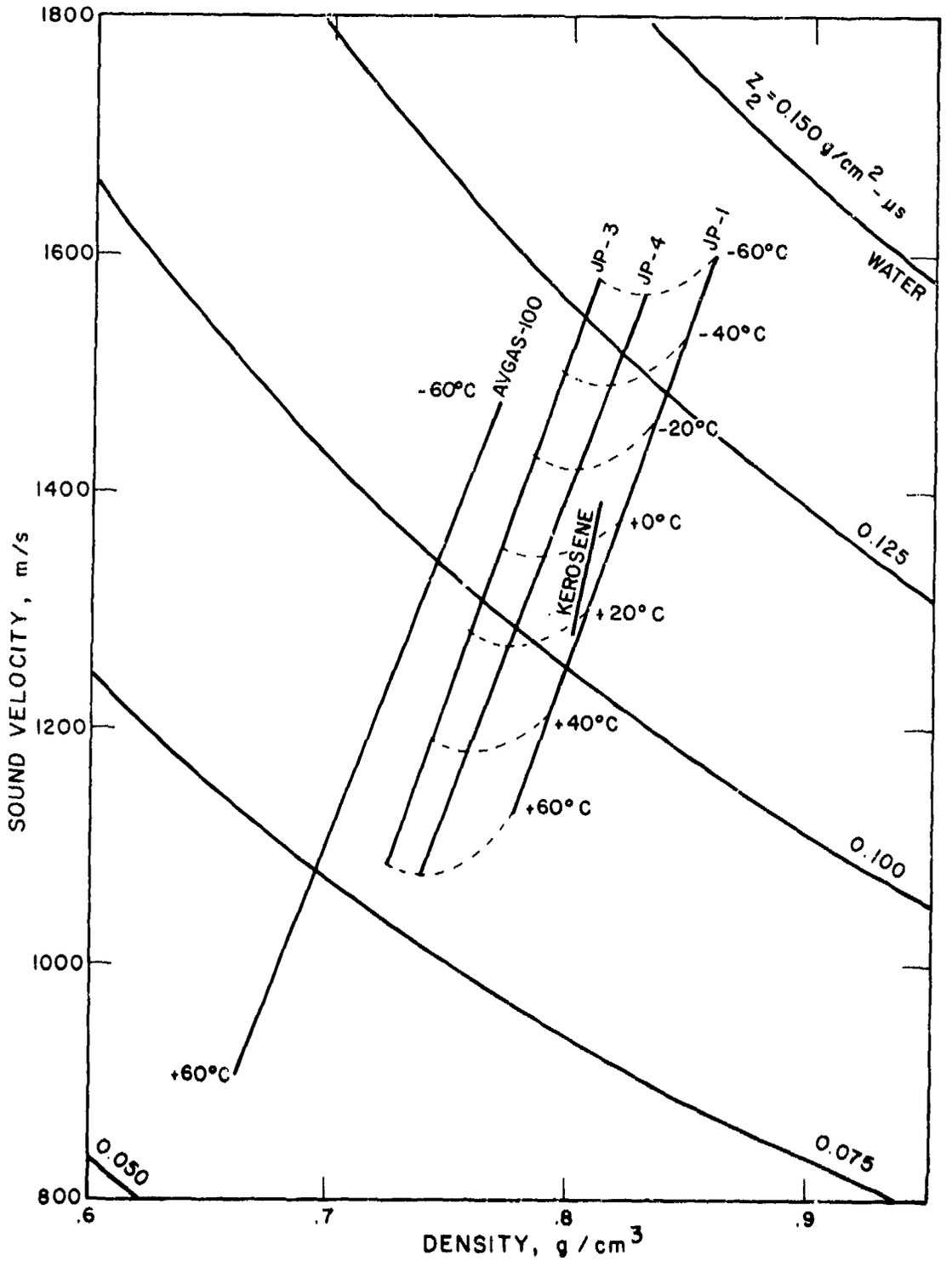

Figure 22. Graph for Estimating Sensitivity of Indirect Density Determination Based on Sound Speed and Temperature Data.

TEST AND RESULTS

DOPPLER FLOW VELOCIMETER TESTS AT PANAMETRICS

The Doppler effect was demonstrated in the test cell shown in Figures 12 and 13. Scattering of the 20 MHz transmitted beam was observed by introducing one or more small (diameter < 1 mm) gas bubbles into the water-filled test cell. As the bubbles rose, they scattered the incident beam at 90° to the receiver transducer.

The Doppler shifts were roughly estimated at 2 kHz from observations on a time-domain oscilloscope. This agreed with the bubble velocity through water. Since gas bubbles of $\approx 5\ \mu m$ diameter have been reportedly detected by ultrasonic waves even at frequencies below 20 MHz, it was not surprising to see large scattered returns.(18)

To permit a more quantitative comparison between theory and experiment, a spherical glass reflector of ≈ 0.1 mm diameter was melted onto the end of a glass thread. When this single reflector was moved, the corresponding Doppler amplitude was measured. Then the scattered power was calculated. As a result of these calculations, it was concluded that contaminant levels of ~1% of those specified in MIL-E-5007, paragraph 3.4.1.3, would be sufficient to yield detectable scattered returns. It was also recognized that scattering off vortices in the fluid could turn out to provide even more scattered power, and might also permit use of frequencies below 20 MHz. The transmission approach to be described ultimately used continuous waves, whereas most previous transmission approaches used pulses. In our tests we used both pulse and continuous wave techniques.

Tests on flowing tap water, however, showed that this fluid did not provide detectable scattering, using the lead metaniobate transducers available. Therefore we decided to build two improved transducers, matched, cut, ground and lapped to 21 MHz, 1/2 inch diameter, of lithium iodate. Even with these improved transducers, however, tests on flowing water and flowing Avgas-100 did not yield a sufficiently high level of scattered power to assure meeting the accuracy goal. At this point, we abandoned the scattering approach in favor of a transmission approach.

TRANSMISSION FLOW VELOCIMETER TESTS AT PANAMETRICS

The oscillograms in Figures 23 and 24 show that in pulse transmission tests at Panametrics on water and Avgas-100, good signal-to-noise was

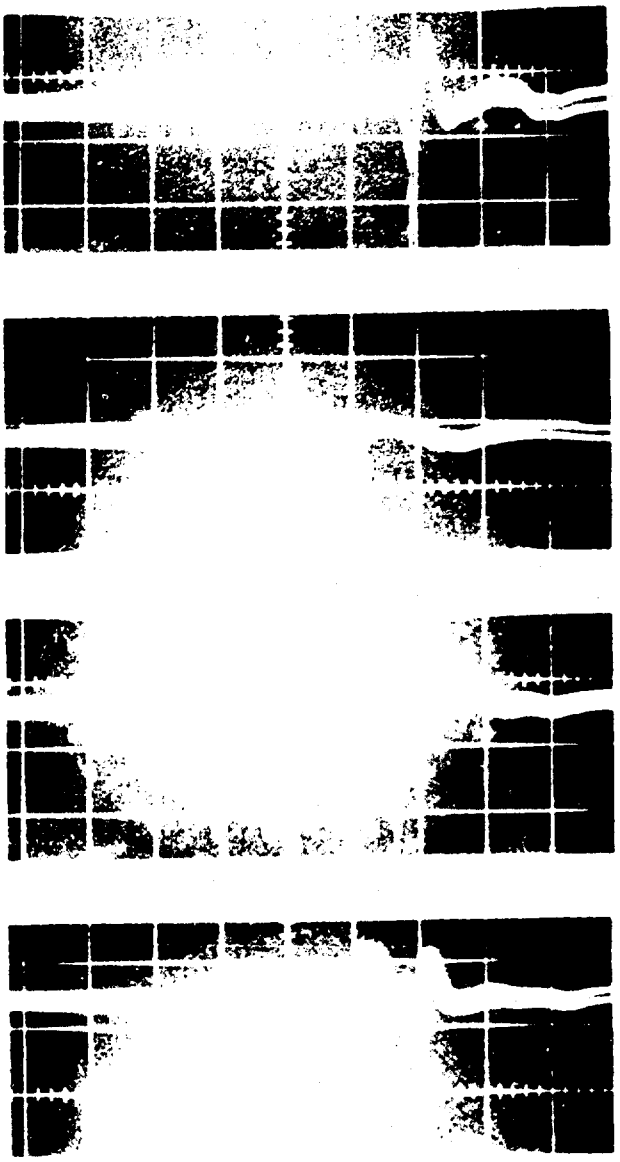

Figure 23. Simultaneous Upstream and Downstream Pulse Transmission Measurements in Flowing Avgas-100.

Reproduced from best available copy.

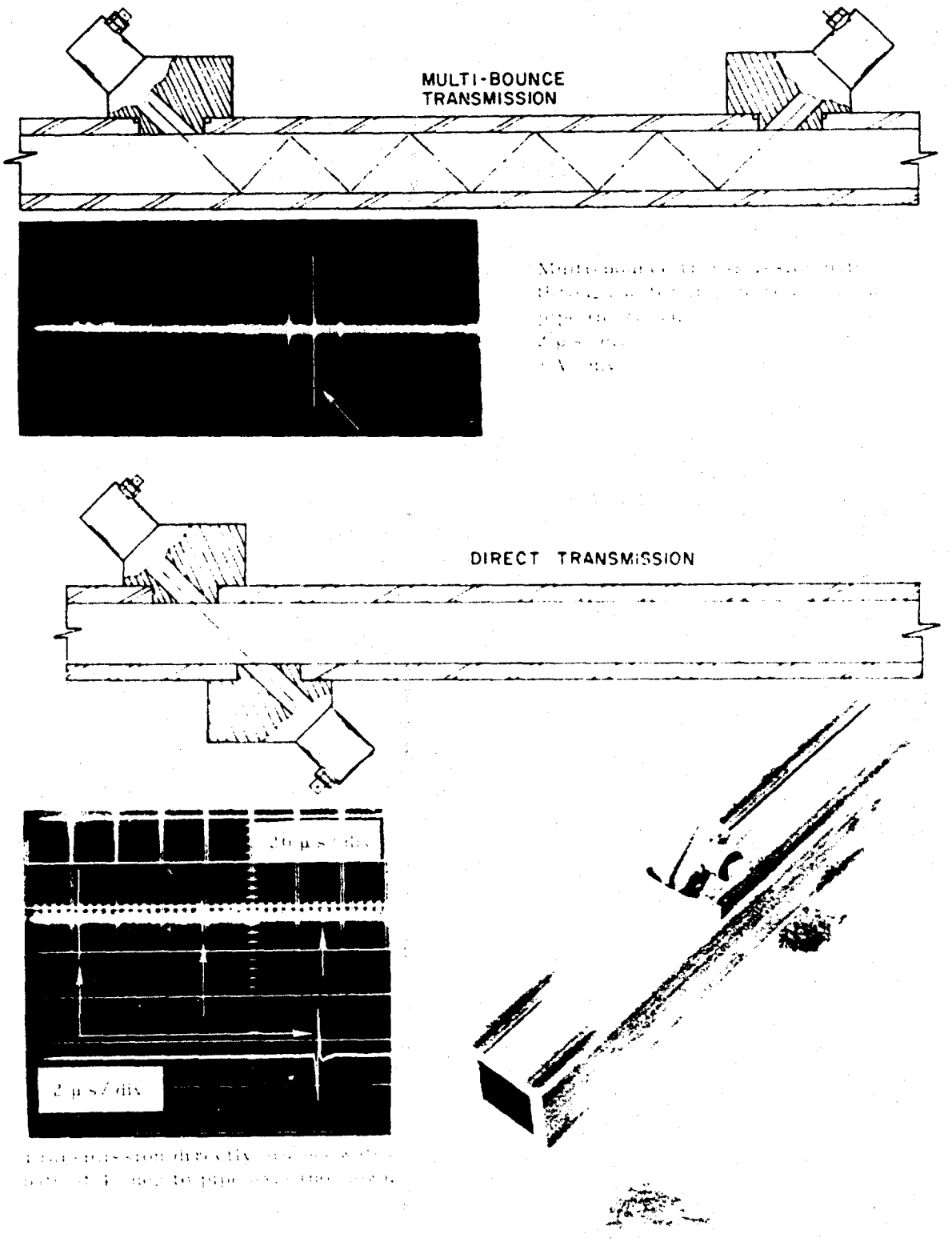

Figure 24. Multi-Bounce and Direct Transmission of 10 MHz Pulses Through Stationary Water in Square Aluminum Pipe.

obtained. Figure 25 illustrates an earlier ultrasonic magnetostrictive wire experiment which simulated the separation of video pulses due to flow. Subsequently, the design using rectangular channels, and the coded upstream-downstream interrogation method, was tested on flowing water. The measuring cell was fabricated of 2024 aluminum. Actual cross-sectional dimensions of the flow channel were 0.502 in. wide x 0.503 in. deep. Cross-sectional dimensions of the sound beam channel were 0.251 in. wide x 0.503 in. deep. In these tests an Ad-Yu phase meter, model 422A, sensed the phase angle, which was proportional to v/c^2. The phase meter was calibrated using a maximum water flow rate of ~3.5 gpm, or ~1750 lb/hr.

Figure 26 shows that the measured increase in phase angle is approximately in direct proportion to the volumetric flow rate of the water. To the extent that the temperature was constant, this graph shows that the phase shift is approximately proportional to $\dot{M}$.

These tests also showed that electrical matching of the transducer impedances at the circulators (Figure 15) was critical, and depended on the transducer temperature and on the acoustic impedance of the transducer backing and that of the liquid. This problem was partly overcome by adjusting the matching network not at zero flow, but at low flow.

These tests further showed that new transducers, replacing the pair which had been originally electroded in a rectangular pattern to match the interrogation slot, could operate despite being circularly electroded. Thus, this design simplification appears satisfactory.

When flow was stopped, the phase angle did not return immediately to its "zero" value. The delay appears to be due to curl or eddies, in the vicinity of the rectangular slot. It is expected that these can be eliminated by flow guides or acoustic windows analogous to the method of Figure 6d.

Following these tests, which had been conducted at pressures below 100 psig, the test cell, including transducers, was cyclically subjected to internal hydraulic pressure up to 1500 psig. No leaks were observed. At high pressure, minor fluctuations in transmission were observed but were not considered to be significant.

DENSITOMETER TESTS AT PANAMETRICS

Tests were made on various reflectometer-type probe materials (polystyrene, glassy carbon, fused silica, T-40 glass, AT quartz and titanium), on transducers (both backed and unbacked), and on two electronic approaches

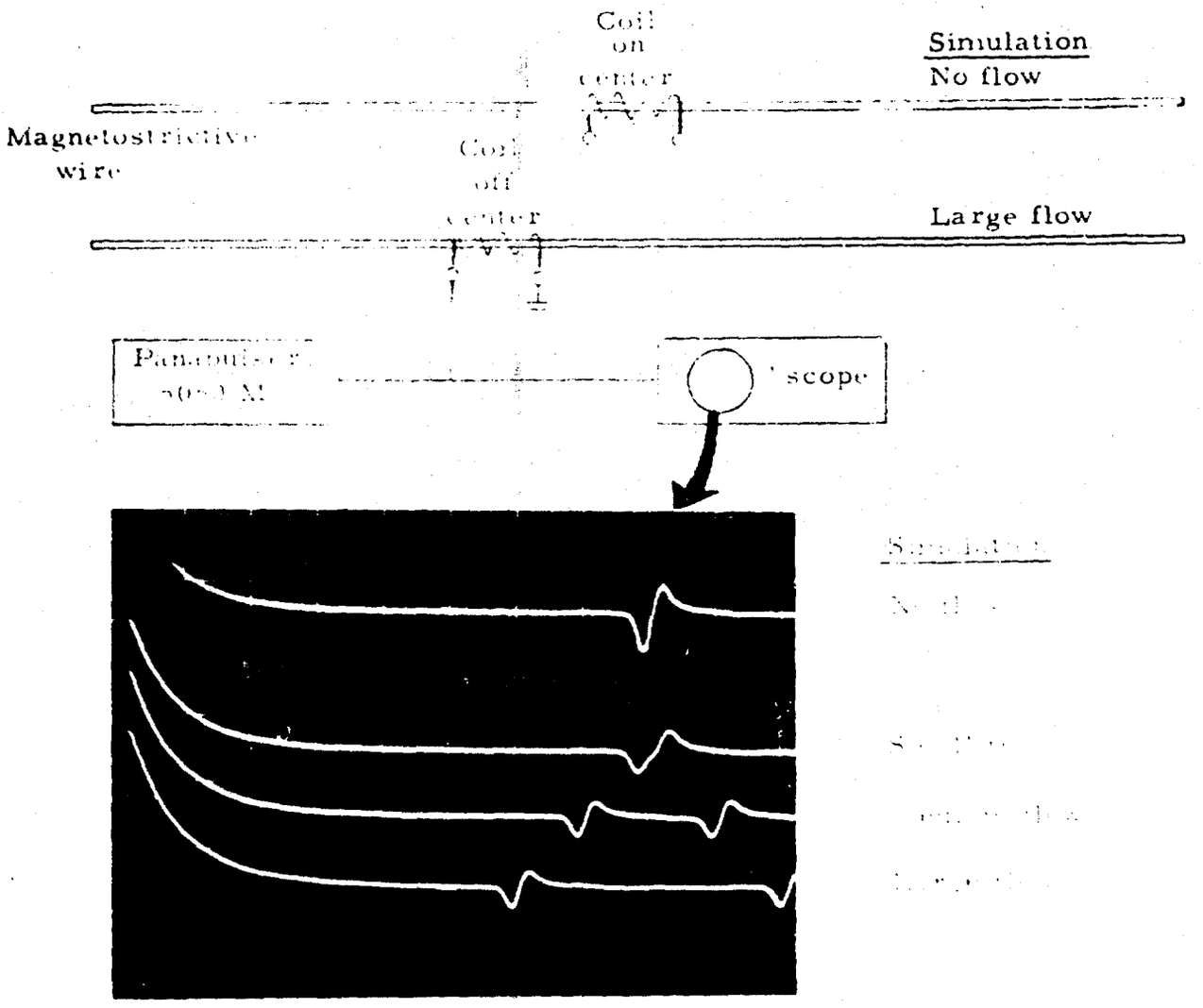

Figure 25. Signals Obtained in Laboratory-Simulated Flow, Where Time Interval Between Pulse Pair is Proportional to Distance That Coil is Away From Center of Magnetostrictive Wire.

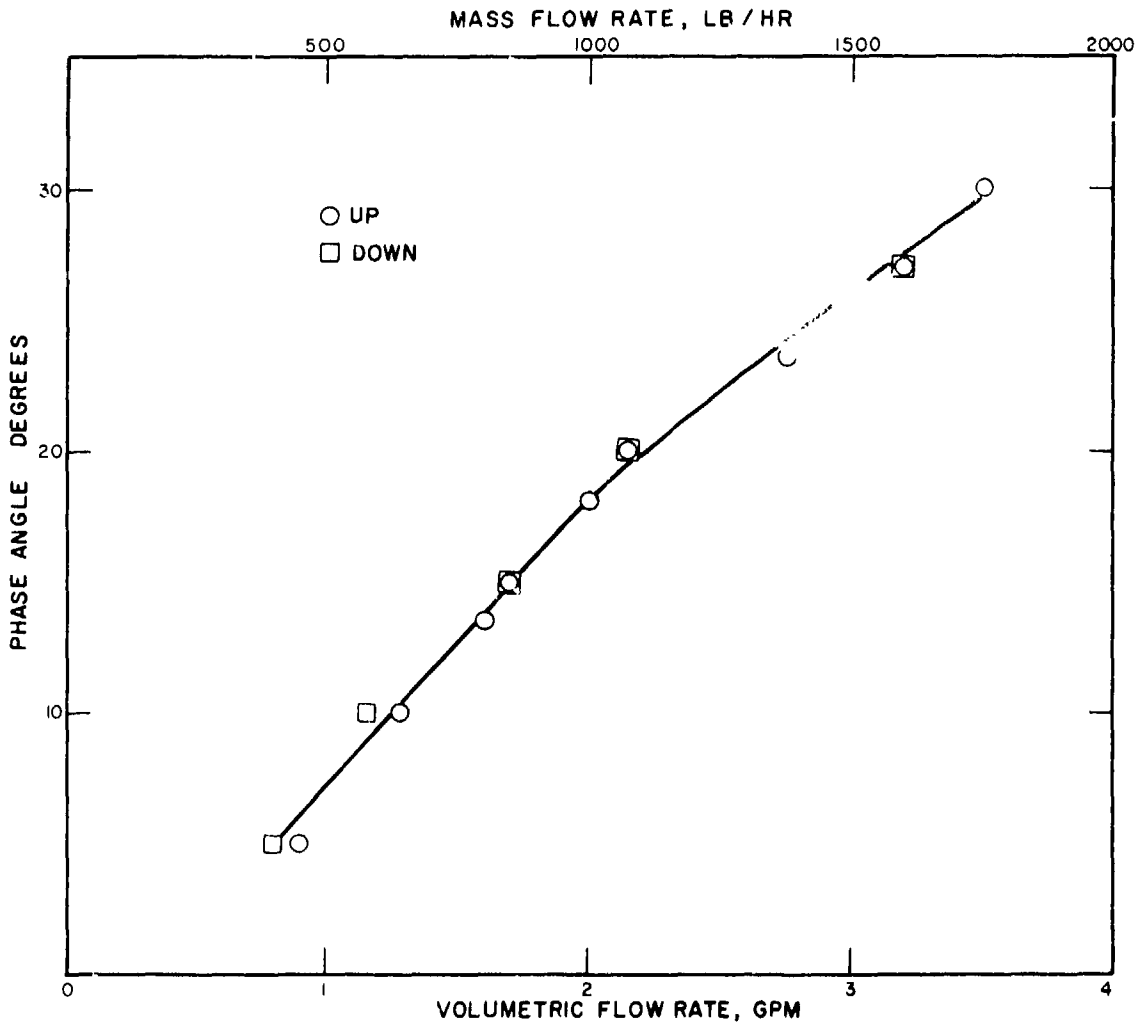

Figure 26. Phase Shift Versus Volumetric Flow Rate for Water.

(logarithmic comparison of rf bursts and linear comparison of the peaks of spike-excited pulses). Densitometer calibration tests used water, Avgas-100, acetone, CS_2 and CCl_4.

Probe Materials. Based on the data in Table VI, it appears that AT quartz exhibits the best acoustic properties among available ceramic materials, for the probe. This material was used in the Avco-Lycoming tests.

While the AT quartz densitometer probe was tested only near room temperature, we calculated the change in probe impedance Z_1 due to changes in density and longitudinal mode sound velocity over the range -65° to $+160^{\circ}F$ (-54° to $+71^{\circ}C$).

At room temperature, $\rho_1 = 2.65\ g/cm^3$. The temperature coefficient of density $= -36.4 \times 10^{-6}$ per $^{\circ}C$. Therefore over the full temperature range, ρ_1 changes by $(71 + 54)(36.4 \times 10^{-6}) = 0.00455\ g/cm^3$, or 0.172%.

The temperature coefficient of velocity T_v in a quartz crystal is given by Mason[19] in terms of various elastic constants and the crystal orientation by the following equation:

$$T_v = 3.9 + 6.5 \sin^2\theta \cos^2\psi$$

$$- \frac{1}{2} \left[\begin{array}{l} s_{11}^E Ts_{11}^E (\cos^2\theta \cos^2\psi + \sin^2\psi)^2 \\ + (2s_{13} Ts_{13} + s_{44}^E Ts_{44}^E) \sin^2\theta \cos^2\psi (\cos^2\theta \cos^2\psi + \sin^2\psi) \\ + s_{33} Ts_{33} \sin^4\theta \cos^4\psi - 2s_{14}^E Ts_{14}^E \sin\theta \\ \times \sin\psi \cos\psi [3 (\cos\theta \cos\phi \cos\psi - \sin\phi \sin\psi)^2 \\ - (\sin\phi \cos\theta \cos\psi + \cos\phi \sin\psi)^2] \end{array} \right] \quad (22)$$

$$\frac{}{s_{11}^E (\cos^2\theta \cos^2\psi + \sin^2\psi)^2 + (2s_{13} + s_{44}^E) \sin^2\theta \cos^2\psi}$$

$$\times (\cos^2\theta \cos^2\psi + \sin^2\psi) + s_{33} \sin^4\theta \cos^4\psi$$

$$- 2s_{14}^E \sin\theta \sin\psi \cos\psi [3 (\cos\phi \cos\theta \cos\psi - \sin\phi \sin\psi)^2$$

$$- (\sin\phi \cos\theta \cos\psi + \cos\phi \sin\psi)^2]$$

Retaining Mason's notation, we observe that for an AT cut of quartz, $\phi = 90^{\circ}$, $\psi = 90^{\circ}$, and $\theta = 35^{\circ}\,17'$. Therefore most of the terms in Eq. (22) drop out and we find $T_v = -2 \times 10^{-6}$ per $^{\circ}C$. The total change in velocity is $125 \times 2 \times 10^{-6}$, or 0.025%. As both density and velocity coefficients are negative, the percentage impedance change is their sum: $\Delta Z_1 / Z_1 = -0.197\%$, or approximately $\pm$ 0.1% for $\mp$ 112°F excursions from a mean temperature of 48°F.

We measured the longitudinal velocity in AT quartz as 0.697 cm/μs. (This may be compared with the AT mode velocity of 0.336 cm/μs corresponding to the AT frequency-thickness constant of 1.68 MHz-mm.) The longitudinal wave impedance $Z_1 = 2.65 \times 0.697 = 1.85$ g/cm^2-μs for AT quartz. These values appear in Table VI.

Transducer Backing. Backings were found unnecessary, provided the acoustic impedances of the probe and transducer were comparable, and provided the bond between them was sufficiently thin and complete.

Logarithmic Comparison of Echoes

Theoretically, the apparent attenuation (α L) increases as density increases, where $\alpha L \equiv \ln(A/B)$, with A and B defined in Figure 17. Tests were run with a commercial instrument which measures $\ln(A/B)$, the Matec model 2470. These tests verified that the model 2470 could measure the ratio of A to B to $\pm$ 0.01 dB, corresponding to B measurement accuracy of $\pm$ 0.1%. For a buffer rod having $Z_1 \leq 2$ g/cm^2-μs, this would give density resolution of better than $\pm$ 0.3%. That is, aluminum, quartz, fused silica or glassy carbon exhibit suitable impedances.

Model 2470 stability tests showed drift and jitter $\approx$ 0.01 dB over 110 minutes. But some drift, ~0.06 dB, occurred at the beginning and end of the run. This drift probably could be identified as to source, and then reduced to an acceptable level. However, this problem, plus consideration of the cost and size of the complete consoles required to operate the 2470, including conversion of readout to density, led us to concentrate on the alternative linear comparison of echoes approach, discussed next.

Densitometer Calibration Tests in Various Liquids

The object of this test was to check our calculations of the sensitivity of reflection coefficient measurements to density. (The possibility of increasing this sensitivity by measuring reflection amplitudes after n reverberations was also explored.) This test was conducted using several liquids of appropriate density and sound velocity, to simulate part of the ranges experienced by Avgas-100 and JP-4, as listed in Table IX.

TABLE IX. DENSITY, SOUND VELOCITY AND ACOUSTIC IMPEDANCE OF AVGAS-100 AND JP-4

Property	Avgas-100		JP-4	
	T = -60°C	T = +70°C	T = -60°C	T = +70°C
Density (g/cm^3)	0.77	0.45	0.83	0.62
Sound Velocity[8] (m/s)	1470	900	1570	1070
Acoustic Impedance (g/cm^2-μs)	0.113	0.0405	0.130	0.0664
$m = d\rho / dT$ (g/cm^3-°C	0.00246		0.00162	

Liquids considered for simulating these ranges in room temperature tests (~25°C) are listed in Table X.

TABLE X. PROPERTIES OF LIQUIDS FOR DENSITOMETER CALIBRATION

Liquid	Density (g/cm^3)	Sound Velocity (m/s)	Acoustic Impedance (g/cm^2-μs)
Acetone	0.79	1174	.0930
Carbon tetrachloride	1.595	926	.148
Kerosene	.81	1324	.107
Water, distilled	.998	1498	.150
Carbon Disulfide (25°C)	1.26	1149	.145
Iso-octane (25°C)	.687	-	-

Using the circuit of Figure 20, and a fused silica probe, $kA \pm B$ was measured, and density was then calculated by the formula $\rho_2 = (Z_1/c_2)(kA-B)/(kA+B)$ where $Z_1 = 1.30$ g/cm^2-μs. Results for acetone, water, CS_2 and CCl_4 are plotted in Figure 27, covering densities from ~0.8 to 1.6 g/cm^3. It is seen that the data generally parallel the theoretical line, but errors

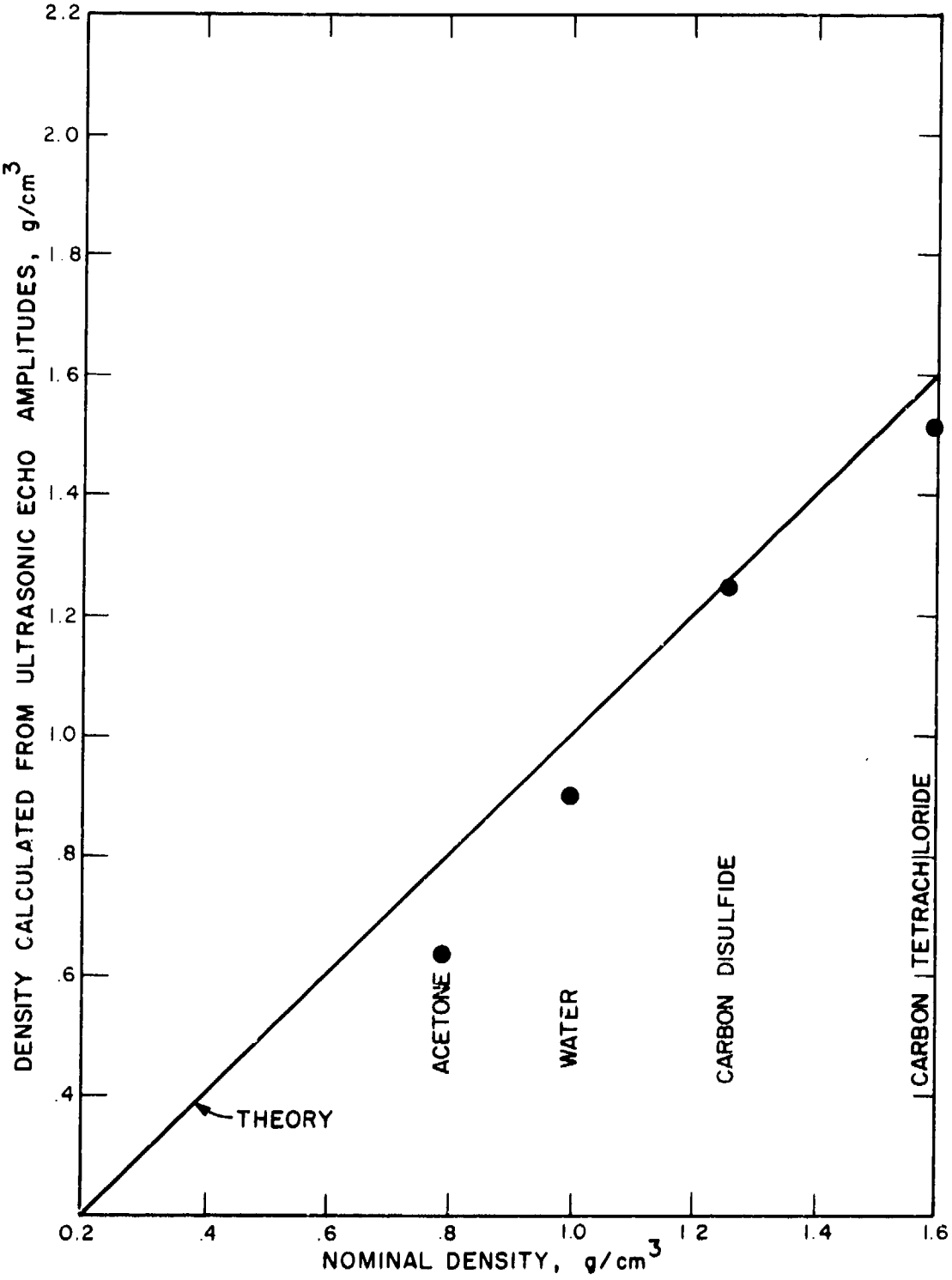

Figure 27. Calibration Test on Ultrasonic Reflection Coefficient Densitometer.

are unacceptably large. The errors appear largely due to drift and noise. For example, typical data for acetone were as follows: kA - B = 47 mV, and kA + B = 607 mV. That is, kA = 327 mV and B = 280 mV. In taking the difference of these two large numbers, 1 mV of noise produces a 2% error in ρ_2. Since the rms noise level for some present broadband receivers is ~40 μV referred to in the input, it was expected that a circuit such as Figure 20 would not have been subject to noise as large as 1 mV. Initial attempts at shielding and filtering were not sufficient. More work would be required to reduce the drift and noise to ~40 μV, so terms like kA - B will be repeatable to ~0.1%, leading to errors in ρ_2 of ~0.3%.

PRELIMINARY TESTS AT AVCO-LYCOMING

Preliminary transmission tests using video pulses were conducted at Avco-Lycoming on February 22, 1972. The fluid was Stoddard solvent, MIL-F7024A, Type 2. Mass flow rate was varied from zero up to 2800 lb/hr at 35 psig. The ultrasonic test cell is shown in Figure 28 (except for Aeroquip pipe/AN adapters, 2021-8-18). Because of the long ultrasonic transmission path, 12 in., signal identification was poor at low flow. But at turbulent high flow, pulse separation was clearer. Pulse separations were similar to those of Figure 23. Results appeared to be similar to those obtained earlier at Panametrics using Avgas-100 (Figure 29), circulated in a closed loop (Figure 30).

To determine the effect of engine noise on the ultrasonic transmission measurement, the ultrasonic unit, still filled with the calibrating fluid, was strapped with wire to a T43 L13 full engine. The unit was located next to an accelerometer, directly over the fuel control part of the engine, to subject it to realistic vibration levels. The engine was then run for about 5 minutes at speeds up to 97%. Rig vibration was measured as 0.001 in. (double amplitude, filtered below 600 Hz). Using a 6 MHz portable oscilloscope, the noise was observed to be < 50 mV peak-peak, at ~100 kHz. The no-flow 10 MHz signal was 200 mV peak-peak, for a pulse-echo total path of 24 in.

TESTS ON JP-4, JP-5 AND A CONTAMINATED FLUID

The main purpose of these tests, conducted at Avco-Lycoming between June and August 1972, was to determine the accuracy, reproducibility and linearity of the ultrasonic mass flowmeter system, and to demonstrate operation on uncontaminated fuel as well as on fuel contaminated in accordance with MIL-E-5007C, paragraph 3.4.1.3. The response time was not determined in these tests, but was calculated from the system bandwidth to be 20 ms.

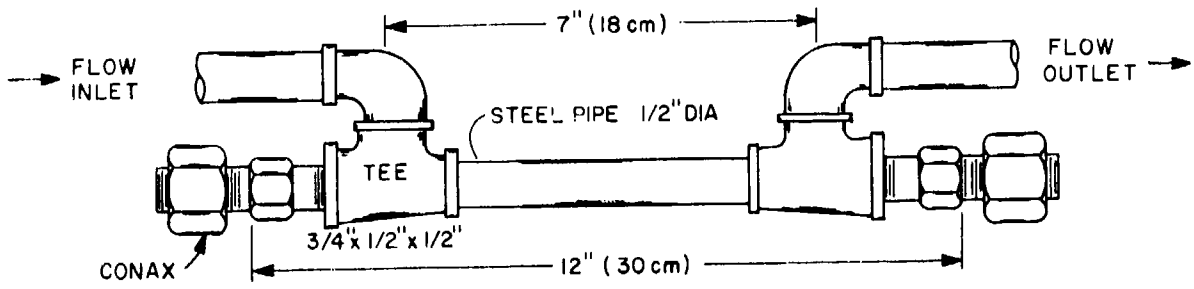

Figure 28. Transmission Test Cell Utilizing Standard Fittings in Which Transducers are Mounted.

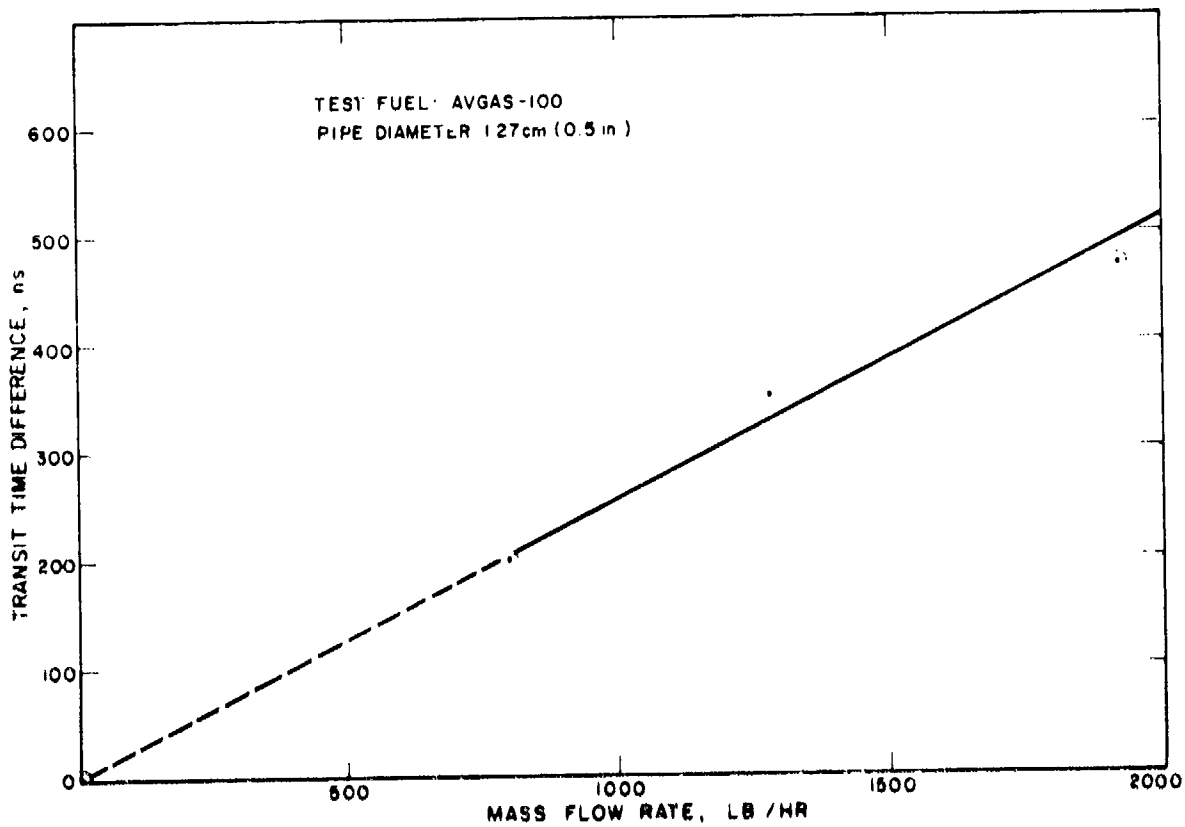

Figure 29. Pulse Transmission Measurement for Turbulent Flow of Avgas-100.

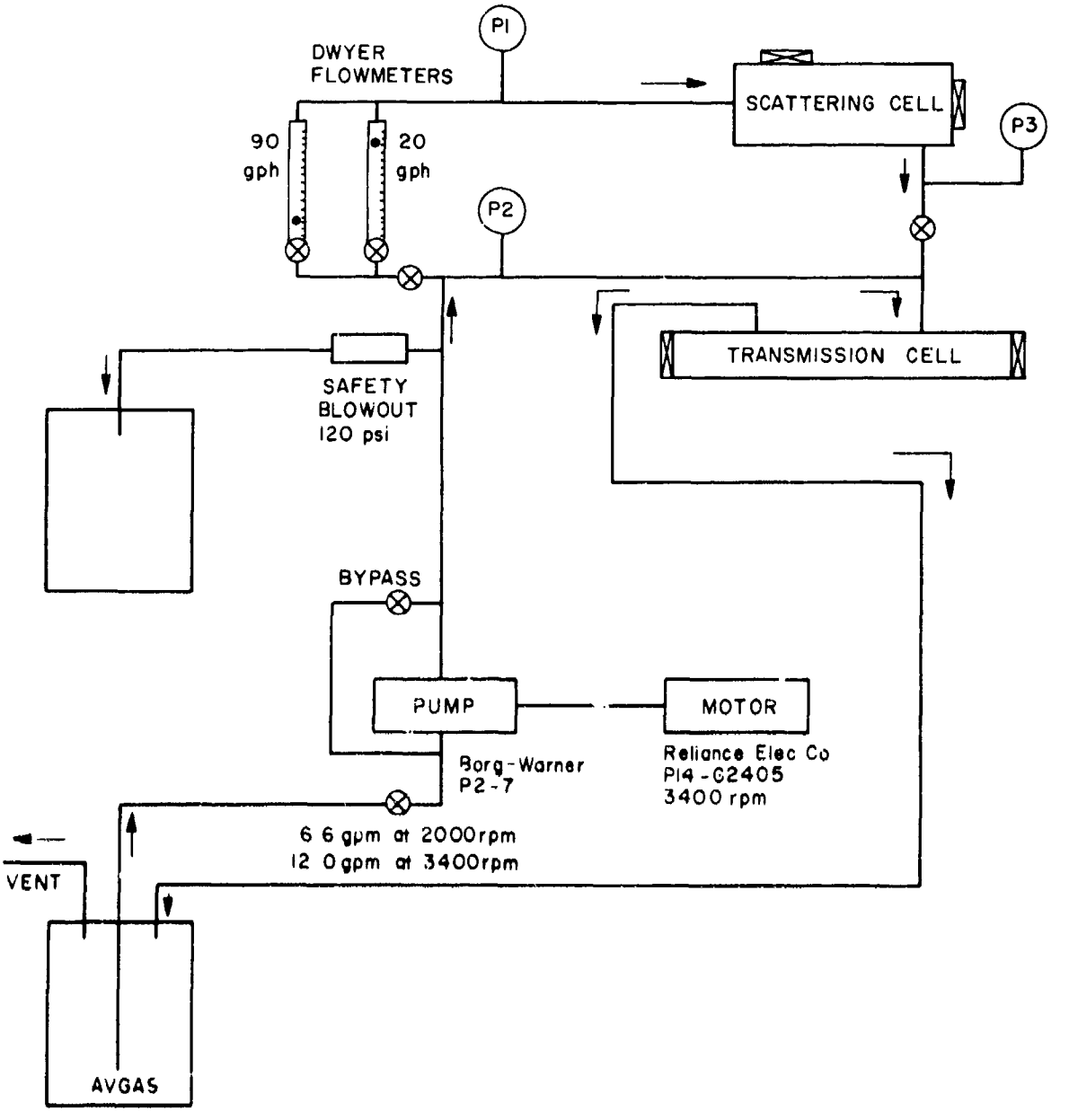

Figure 30. Flow Loop for Testing Scattering and Transmission Methods of Measuring Flow Velocity.

Description of Test Stand. The flowmeter calibrating stand was manufactured by Cox's Commercial Research Division, the George L. Nankervis Company, Detroit. It is denoted Part No. T-303T, Serial No. 6602-A, and includes readouts such as a timer, weigh switch, hydrometer, viscometer, fuel temperature, fuel pressure, and was used with two turbine-type flow sensors to cover the flow ranges of interest. Figures 31 and 32 illustrate the calibration test arrangement.

The following results were obtained in JP-4 and JP-5 prior to contaminant-testing of the ultrasonic measuring cell.

Calibration Results on JP-4. Calibration data for JP-4 is given in Table XI for the following conditions: Date: June 12, 1972. Cox turbine flowmeter Serial No. 8463, size AN8-6, range 188.4 to 2062.8 lb/hr. Temperature: 76°F. Fuel specific gravity: 0.760. Kinematic viscosity: 1.04 centistokes. The ultrasonic transit time across a 1-in. path perpendicular to the flow was 20.85 μs, measured with the 5220 gage. Thus the sound speed was 0.480 in./μs or 1220 m/s, and the fuel's characteristic acoustic impedance was Z_2 = 0.0926 g/cm^2-μs, or about 62% of that of water at the same temperature.

TABLE XI. FLOWMETER CALIBRATION TEST DATA FOR JP-4

Cox Cal. Pts. (Hz)	Cal. Wt. (lb)	Avg. Flow Time (s)	Computed Mass Flow Rate (lb/hr)	Ultrasonic Readings of Phase Angle (Deg)	Density (Relative Units on DVM)		M
1320	11	19.197	2062.8	25	862	2409	3000
1200	10	19.193	1876.7	24	817	2411	2800
1080	9	19.213	1686.4	22	750	2415	2550
900	7.5	19.197	1406.5	15.5	510	2400	1670
720	6	19.147	1128.1	13	430	2400	1200
600	5	19.120	941.4	7	250	2407	499
480	4	-	-	-	-	-	-
360	3	19.027	567.6	2.5	100	2409	181
300	2.5	-	-	-	-	-	-
180	1.5	19.133	282.2	-	-	-	-
120	1	19.110	188.4	-	-	-	-

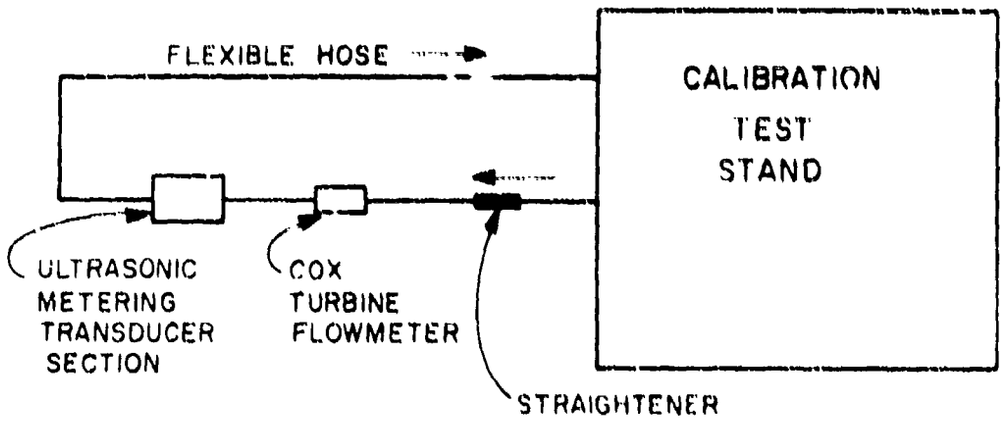

Figure 31. Block Diagram of Calibration Test Arrangement.

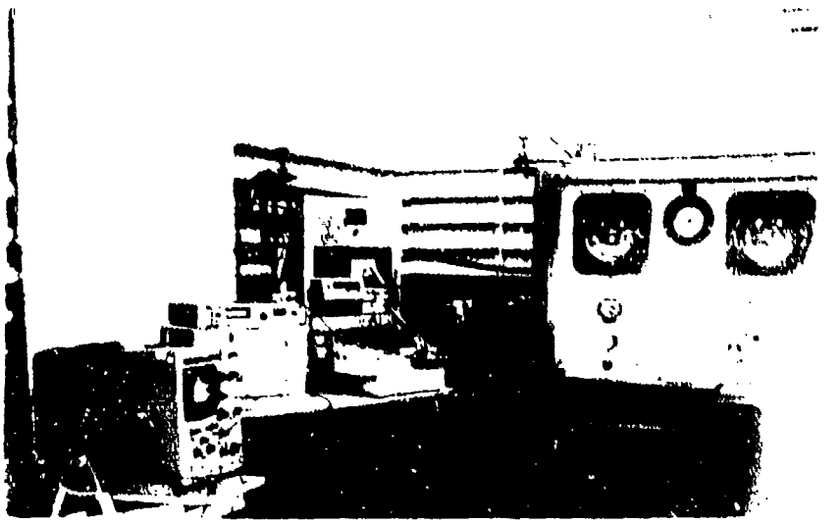

Figure 32. View of Ultrasonic Equipment and Calibration Test Stand.

The ultrasonically-determined $\dot{M}$ is plotted against the standard computed mass flow rate in Figure 33. It is seen that the results appear to be nearly linear, with deviations from a straight line fit of about $\pm$ 100 lb/hr, or $\pm$ 5% of range. More data are needed, however, for better curve definition.

Besides the JP-4 data tabulated above, additional measurements were obtained of phase angle versus Cox $\dot{M}$ calibration points. These data are plotted in Figure 34.

Results are similar, but not identical. Drift or scatter may be mainly accounted for by the phase meter. In future tests, phase accuracy of 0.3^{o} would eliminate this possible source of error.

Calibration Results on JP-5. Calibration data for JP-5 is given in Table XII for the following conditions: Date: June 13, 1972. Cox turbine flowmeters, Serial Nos. 8463 (as before) and 5903, size AN10, range 817.1 to 4957.9 lb/hr. Temperature: 74^{o}F. Pressure: 22 psig. Fuel specific gravity: 0.820. Kinematic viscosity: 2 centistokes. The ultrasonic transit time across a 1-in. path perpendicular to the flow was 19.24 μs, measured with the 5220 gage. Thus the sound speed was 0.052 in./μs or 1320 m/s, and the fuel's acoustic impedance was $Z_2 = 0.108$ g/cm^2-μs, or about 72% of that of water at the same temperature.

The ultrasonically-determined $\dot{M}$ is plotted against the standard computed mass flow rate in Figure 35. Significantly, for 3 of 4 runs in Figure 35, the data are within $\pm$ 4% of one straight line. Disregarding the anomalous fourth run, these data are quite encouraging, in that they demonstrate the basic linearity and reproducibility of the $\dot{M}$ system. In Figure 36, where $\dot{M}$ ranged to 5000 lb/hr, beyond the range of our multiplier, we show that the measured phase angle may be approximated as a piecewise linear function. Departures from linearity are apparently due to eddies.

Contamination Tests. The stand used in these tests was manufactured by Engineered Devices of Agawam, Massachusetts. Tests were run at ~1900 lb/hr, as measured by the Cox Series 12 rig rotameter. The fluid, contaminated essentially in conformance with MIL-E-5007C, paragraph 3.4.1.3, was introduced without filtering at ~35 psig and ~75^{o}F, with at least one brief temperature rise of ~105^{o}F. Tests began on June 14 and ended on August 24, 1972.

The MIL-E-5007C types and distributions of contaminants are given in Table XIII. (Instrumentation specification MIL-F-8615B is the same except

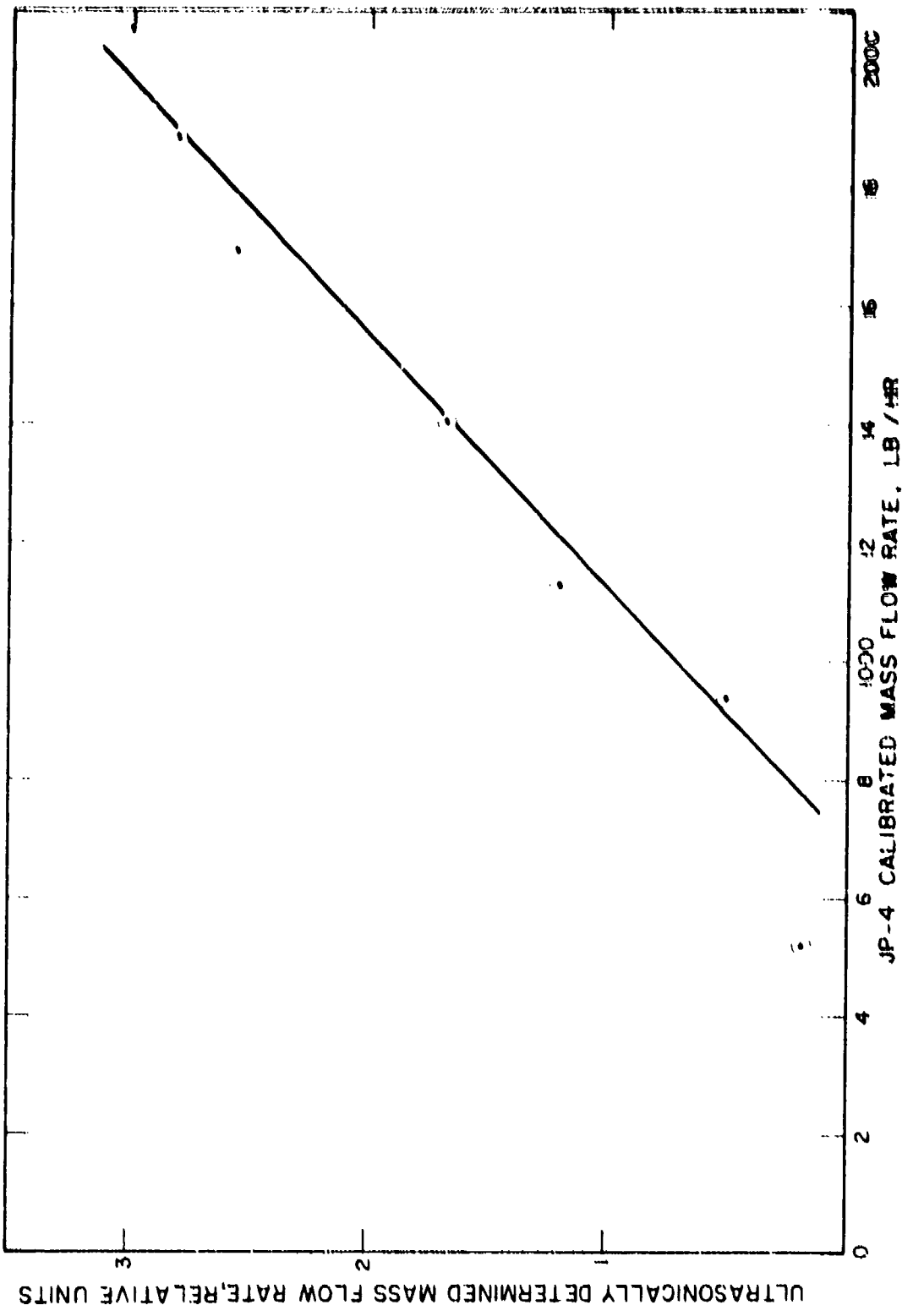

Figure 33. Ultrasonically Determined M for JP-4.

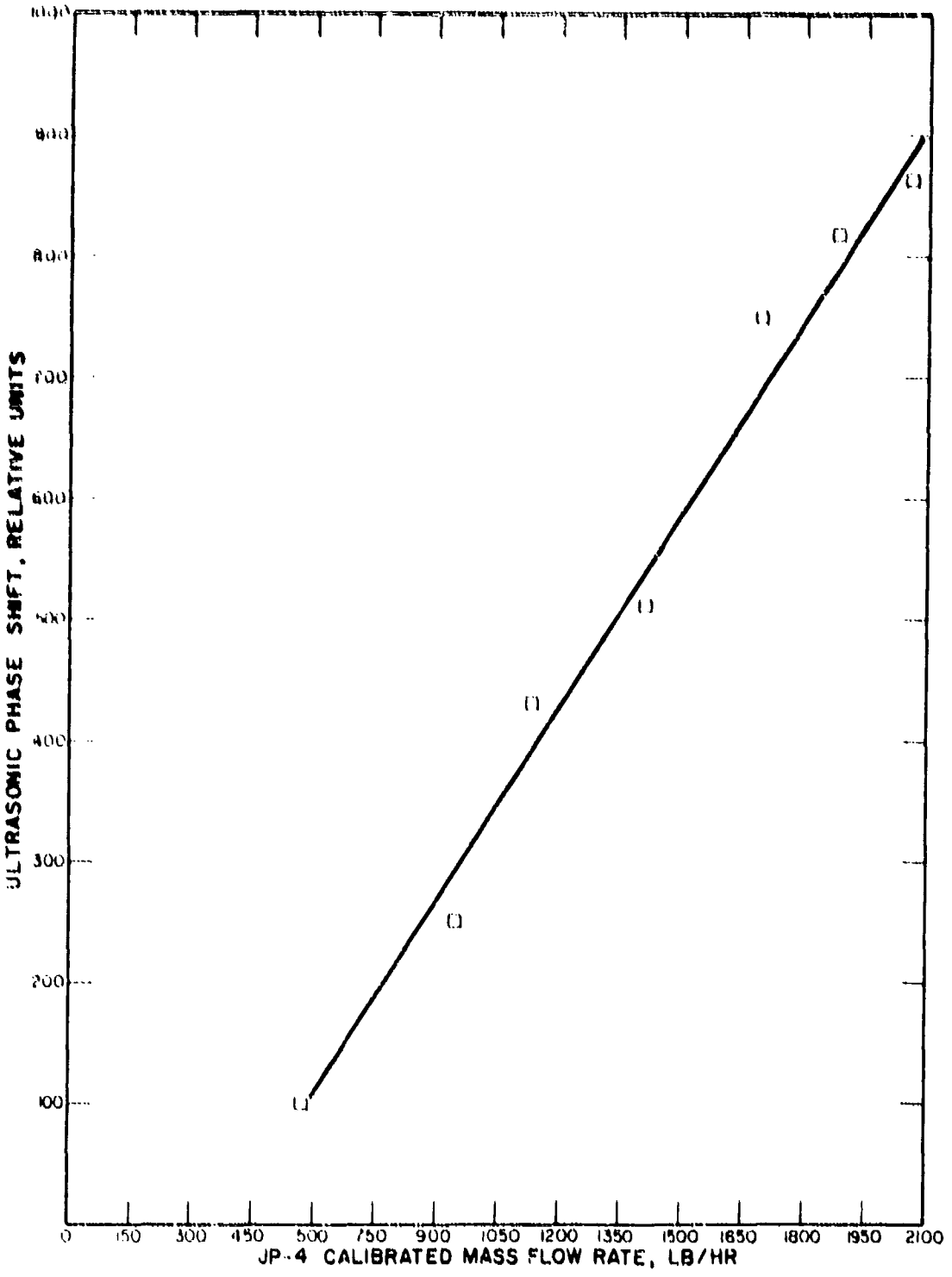

Figure 34. Ultrasonically Determined Phase Angle Versus M for JP-4.

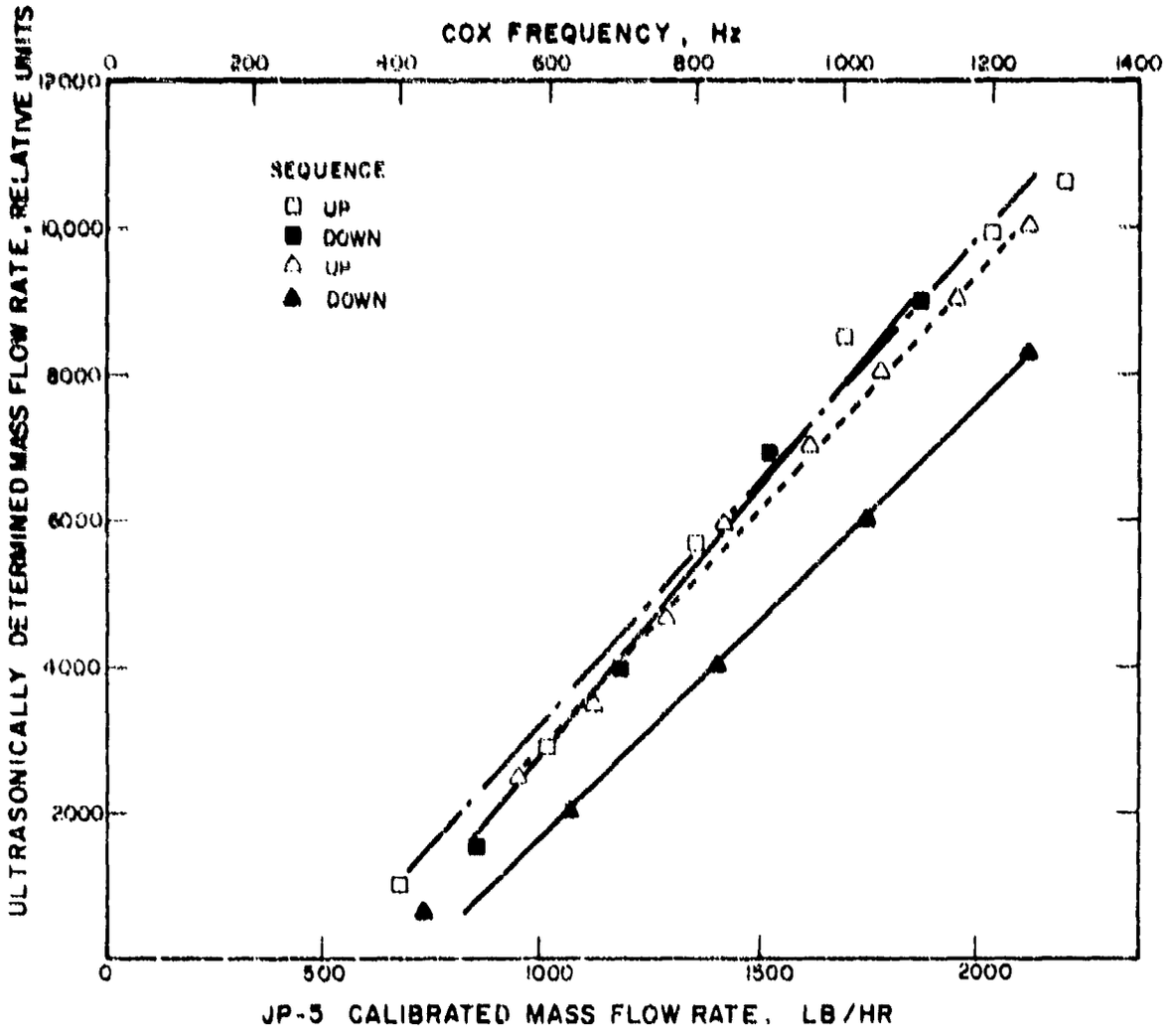

Figure 35. Ultrasonically Determined $\dot{M}$ for JP-5.

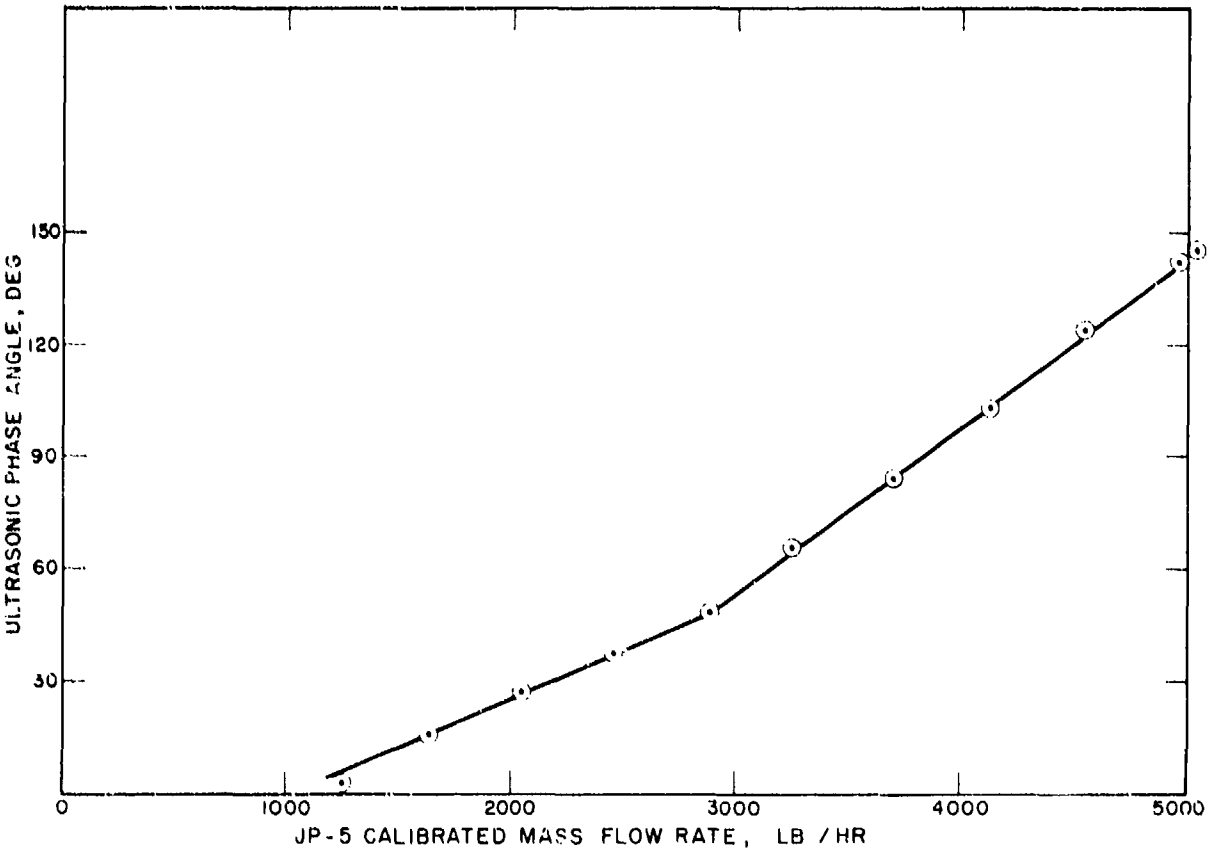

Figure 36. Ultrasonically Determined Phase Angle Versus $\dot{M}$ for JP-5.

TABLE XII. FLOWMETER CALIBRATION TEST DATA FOR JP-5

Cox Cal. Pts. (Hz)	Cal. Wt. (lb)	Avg. Flow Time (s)	Computed Mass Flow Rate (lb/hr)	Ultrasonic Readings of Phase Angle (Deg)	Density (Relative Units on DVM)		M
1320	11	17.710	2236	84	2700	2175	12000
1200	10	17.690	2035	66.5	2152	2134	7650
1080	9	17.680	1833	56	1830	2131	8350
900	7.5	17.680	1527	41	1233	2133	5400
720	6	17.687	1221	28	925	2139	4150
600	5	17.700	1017	19.5	650	2127	2850
480	4	17.693	814	11	388	2141	1630
360	3	17.740	609	4	180	2150	750
300	2.5	17.713	508	3	214	2148	548
180	1.5	17.800	303	-	-	-	-
120	1	17.710	203	-	-	-	-
		(Above: Cox S/N 8463) (Below: Cox S/N 5903)					
1220	25	17.853	5041	145	4580	2172	13061
1200	25	18.153	4958	142	4510	2174	13061
1100	25	19.827	4539	124	3961	2179	13062
1000	25	21.817	4125	103	3251	2180	13061
900	25	24.270	3708	84	2660	2177	11400
800	25	27.307	3296	66	2127	2198	8893
700	25	31.250	2880	49	1566	2198	6200
600	25	36.490	2466	38	1198	2183	4387
500	10	17.550	2051	27	851	2190	2882
400	10	21.983	1638	16	499	2181	1109
300	10	29.330	1227	2.5	85	2189	395
200	10	44.060	817	-	-	-	-

the concentrations of the first four types are increased by 2.5 by requiring the same quantities per 400 gallons instead of per 1000 gallons.)

TABLE XIII. FUEL ENDURANCE TEST CONTAMINANT

Contaminant	Particle Size	Quantity
Iron oxide	0-5 microns	28.5 gm/1000 gallons
	5-10 microns	1.5 gm/1000 gallons
Sharp silica sand	150-300 microns	1.0 gm/1000 gallons
	300-420 microns	1.0 gm/1000 gallons
Prepared dirt conforming to AC Spark Plug Co. Part No. 1543637 (coarse Arizona road dust)	Mixture as follows: 0-5 microns (12%) 5-10 microns (12%) 10-20 microns (14%) 20-40 microns (23%) 40-80 microns (30%) 80-200 microns (9%)	8.0 gm/1000 gallons
Cotton linters	Grade 6, staple below 7, second cut linters (U. S. Department of Agriculture Grading Standards).	0.1 gm/1000 gallons
Crude naphthenic acid		0.03% by volume
Salt water solution shall contain 4 parts NaCl to 96 parts H_2O by wt.		0.01% entrained

The tests were originally scheduled to continue on a one-shift basis for 100 hours. However, loss of signal at 25 hours caused an interruption. Examination of the test cell and transducers at Avco-Lycoming (Figures 37, 38) showed some discoloration and corrosion, and some minor slurry accumulation, but not enough to account for loss of signal. The complete system was returned to Panametrics, where it was found that the 5 MHz frequency had drifted outside the narrow range of the receiver circuitry. Retuning, and readjustment of the code delay, restored the signals.

Prior to returning the system to Avco-Lycoming, it was endurance-tested for 100 hours on unfiltered tap water at ~800 lb/hr, plus overnight and

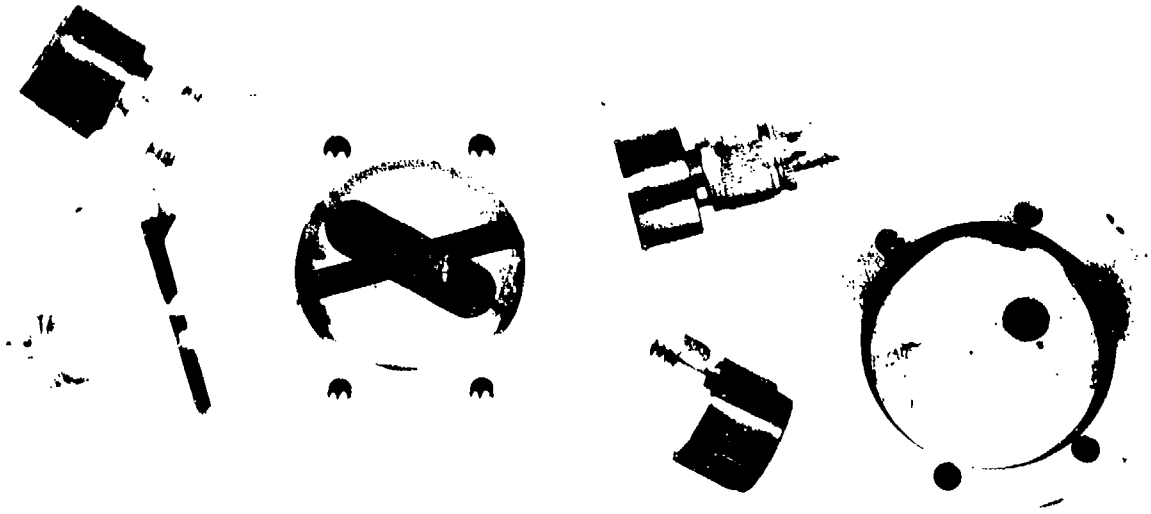

Figure 37. View of Cell After 25-Hour Exposure to Flowing Contaminant.

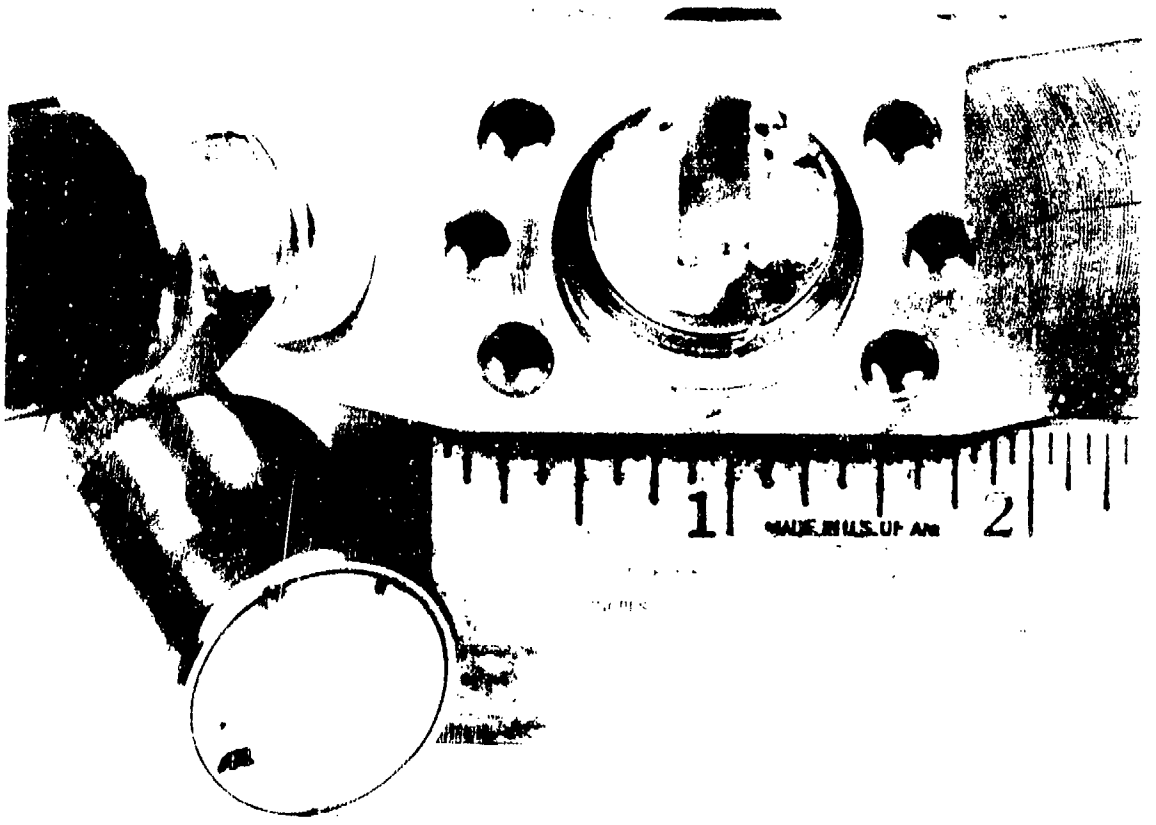

Figure 38. Close-Up of Cell and Transducer.

Reproduced from best available copy.

weekend soaks at no-flow, with periodic calibration checks against an accumulated volume of water. The flow velocimeter appeared quite reproducible.

The system was returned to Avco-Lycoming and contamination testing was resumed on August 10, continuing until August 24, 1972. At this termination, exposure totaled 104 hours at 1840 to 1940 lb/hr, plus 16 hours of filtered contaminant at ~1900 lb/hr, plus second- and third-shift and weekend soaks at no-flow totaling 428 hours. Signal levels decreased in these tests from a maximum of 2V to a minimum of 0.06V. This decrease however appears to be mainly a result of amplifier malfunction, not transducer degrading. Since phase meters are now available which maintain their accuracy for signals above 0.01V, this decrease of signal amplitude is not considered significant.

The ultrasonic measuring cell was opened for inspection prior to recalibration. It was observed that: the transducer vertical faces were partly covered with a dark red residue; the densitometer probe's horizontal face showed one red speck; some dark red slurry had accumulated at the bottom of the transducer cavities; and some corrosion and deposits were evident at mating surfaces. The mating surfaces were wiped clean to ease reassembly, and then the cell was tapped together again. No residue was removed from the flow channel nor from the ultrasonic measuring channel.

Next, the system was transferred back to the Cox calibration test stand (Figures 31, 32) and then recalibrated on JP-4 at 77.5°F and at 92°F. Figure 39 shows the measured phase difference versus M, obtained using the flow velocimeter portion of Figure 15. At 77.5°F we also measured the phase difference versus M by manually switching the uncoded 5 MHz wave alternately upstream and downstream. This method is valid to the extent that the average c remains constant for both directions. Note that the use of coded waves continuously transmitted both ways avoids this limitation, and is obviously to be preferred.

Recalibration Results on JP-4. Recalibration data for JP-4 is given in Table XIV for the following conditions: Test Date: August 24, 1972. Cox turbine flowmeter Serial No. 8932, size AN8, range 214 to 3561 lb/hr, calibrated March 20, 1972. Test temperature: 77.5°F. Fuel specific gravity: 0.751.

The essential corresponding data for JP-4 at 92°F is given in Table XV. Fuel specific gravity was 0.746. Coded 5 MHz waves were continuously transmitted both ways.

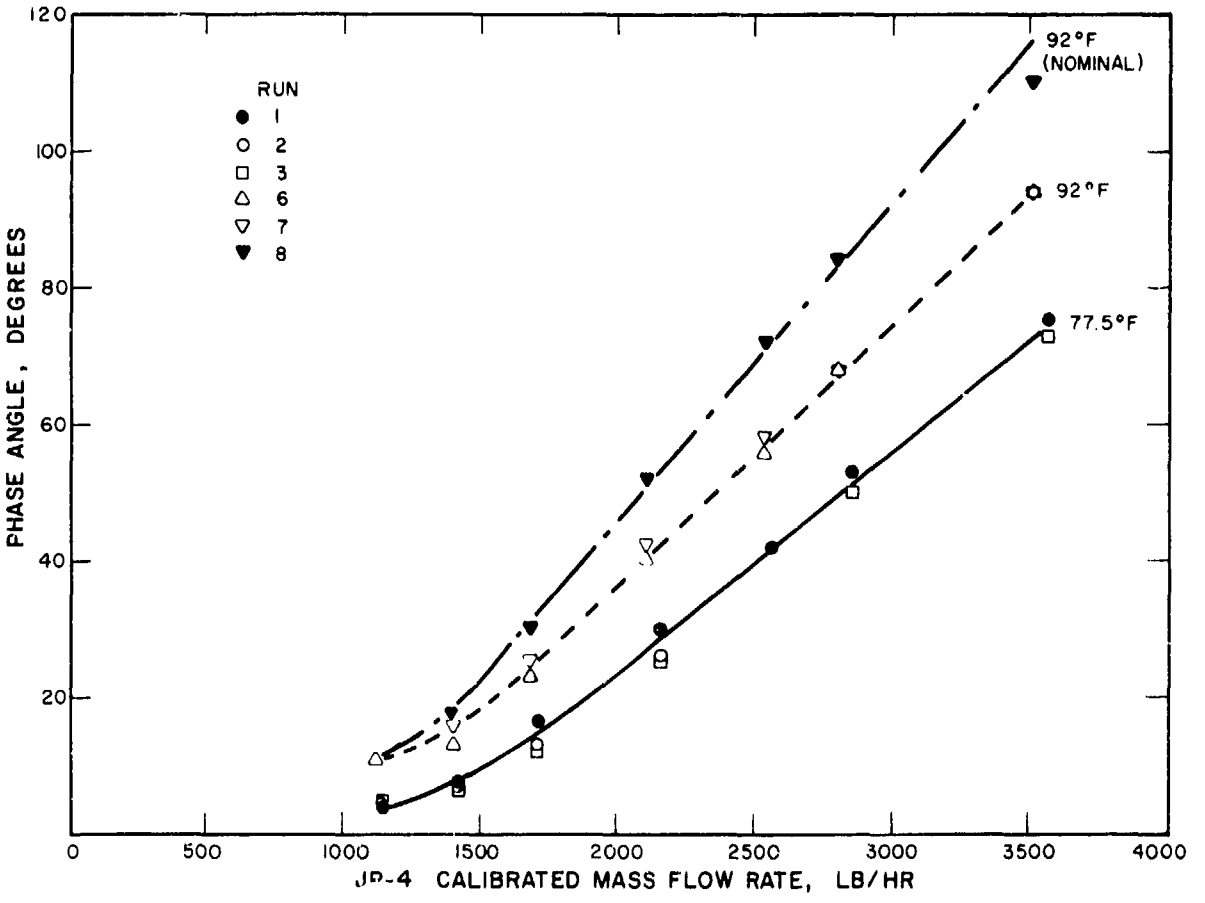

Figure 39. Recalibration Curves for JP-4 at Different Temperatures.

TABLE XIV. RECALIBRATION DATA FOR JP-4 AT 77.5°F

Cox Cal. Pts. (Hz)	Cal. Wt. (lb)	Avg. Flow Time (s)	Computed Mass Flow Rate (lb/hr)	Phase Angle 5 MHz Coded CW Run 1	Run 2	Run 3	Alter. Dir. Run 4	Run 5
				(degrees)				
90	2.25	37.857	214.0	-	-	-	-	-
120	3.0	37.887	285.1	-	-	-	-	-
180	4.5	37.847	428.0	-	-	-	-	-
240	6.0	37.897	570.0	-	-	-	-	-
300	7.5	37.957	711.3	-	-	-	10	-
360	9.0	37.937	854.0	-	-	-	13	14
480	12.0	37.860	1141.0	4	5	5	25	-
600	15.0	37.947	1423.0	8	6	6	38	40
720	18.0	37.940	1708.0	17	13	12	45	-
900	22.5	37.923	2135.9	30	26	25	64	59
1080	27.0	37.923	2563.1	42	42	41	73	78
1200	30.0	37.903	2849.4	53	53	50	-	80
1500	37.5	37.910	3561.1	75	75	73	-	89

TABLE XV. RECALIBRATION DATA FOR JP-4 AT 92°F

Computed Mass Flow Rate (lb/hr)	Phase Angle Run 6	Run 7	Run 8
	(degrees)		
210	-	-	-
280	-	-	-
420	-	-	-
560	-	-	-
698	-	-	-
838	-	-	-
1120	11	11	11
1397	13	16	17
1677	23	25	30
2096	40	41	52
2516	56	58	72
2797	68	68	84
3504	94	94	110

In Figure 39, the three runs of v/c^2 or phase data for 77.5°F show minor hysteresis or drift, which amounts to $\pm$ 3% of the range. For 92°F, runs 6 and 7 show even less spread, generally less than $\pm$ 2%. Run 8 appears anomalous, and is probably due to a fuel temperature increase. Difficulty was encountered in controlling fuel temperature during these tests. In summary, these recalibration data points show that the cell and transducers were able to function after prolonged exposure to a contaminated fluid.

Figure 40 demonstrates that if one does not transmit simultaneously in both directions, scatter of the data increases, since small variations in c influence the v/c^2 readout. These results involved the manual switching or alternating of the propagation direction, with phase being averaged over several seconds for each direction.

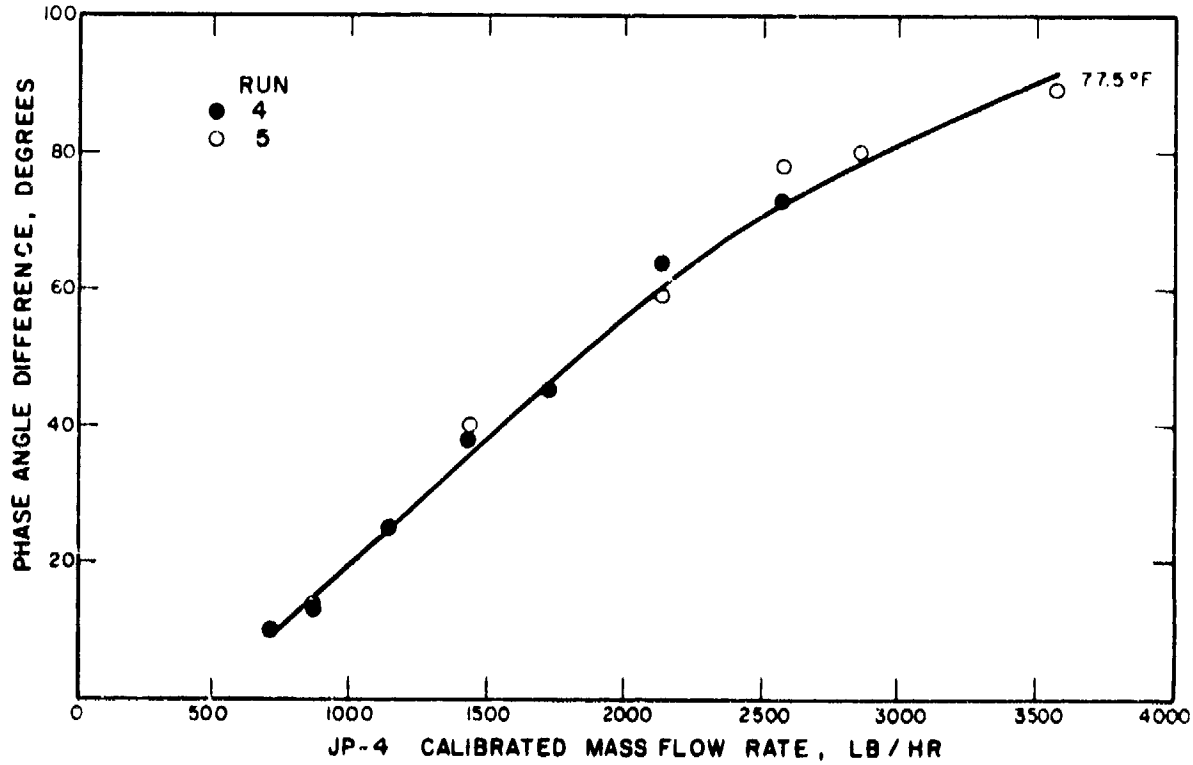

Figure 40. Phase Angle Difference for Alternate Propagation Directions for JP-4.

SUMMARY OF RESULTS

The principal results of the theoretical, experimental and test portions of this program may be summarized as follows:

- The ultrasonic mass flowmeter measuring cell has been demonstrated to operate without clogging, both during and after exposure to a fluid contaminated essentially in conformance to MIL-E-5007C. Exposure included shifts of approximately 8 hours each, totaling 104 hours at approximately 1900 lb/hr, plus overnight and weekend soaking of 428 hours at no-flow. Endurance appears to be far in excess of the two 2.5-hour tests required for instruments in MIL-F-3615.

- A pseudo-random-noise phase coding technique has been demonstrated to provide, for the first time, separation of two continuous waves of the same frequency transmitted upstream and downstream over a common path. This technique provided a flow velocimeter response time of 20 ms, a factor of 25 faster than the contractual objective of 0.5 s, and a range up to 5000 lb/hr. It was found that undesirable circuit unbalances were produced by fluctuations in fuel temperature of a few degrees, or by changes in the acoustic radiation impedance due to changes in impedance of the fuel or transducer backing. To overcome this problem, it will be desirable to choose a transducer with minimal variation in properties due to temperature, and to isolate the transducer from the fuel, using, for example, an attenuating acoustic window as a pad.

- Immunity to uncertainties in Reynolds number or uncertainties in unidirectional flow profiles appears achievable using the square flow channel wherein 100% of the fuel cross section is interrogated by a rectangular plane wave beam of ultrasound. This is the basis for accurate, linear response to flow velocity, independent of fuel composition, temperature, density or viscosity. In the present measuring cell, the observed departures from linearity appear to be due to nonideal inlet conditions, probably correctable with a flow straightener, and to fuel rotation at the measuring region, probably correctable with flush-mounted acoustic windows, wedges, screens or other means.

- Based on the encouraging first results obtained with coded single fixed frequency waves, it appears that the use of two variable frequencies should work too, to measure v independent of c. This is the basis for an improved ultrasonic mass flowmeter, where both v and ρ are each measured independent of c. The product of their outputs is thus proportional to $\dot{M}$.

- Since signal levels in some cases were as small as 20 mV rms, and whereas the accuracy of the Ad-Yu phase meter available for the tests is specified* for signals above 300 mV rms, it is understood that much of the system's present inability to measure $\dot{M}$ with sufficient accuracy, especially below ~ 500 lb/hr, corresponding to relatively small phase angles, is attributable to operating beyond this meter's limitations. Further, the fact that the extrapolated results do not pass through the origin, in Figures 26, 33, 34, 35, 39 and 40, is attributed to the manual "zero" adjustment of the phase meter at a non-zero flow. This adjustment was required in order to match the present circuits to the transducer, whose electrical impedance depends on the acoustic impedance of the adjacent media, and on its own temperature. It is recognized, however, that phase meter requirements such as automatic 0 adjust, 0.3° accuracy on 10 mV signals, faster warmup and 10 ms response can now be met by a new instrument available commercially. Also, use of a different temperature - immune piezoelectric crystal, instead of a ceramic transducer, and acoustical isolation or padding of this crystal from the variable load presented by different fuels, is expected to avoid the other observed deficiencies. Accordingly, range, accuracy, response time and other goals are considered achievable.

* For the Ad-Yu 422A, the relative accuracy is $1/4^{\circ}$ plus a high frequency error of 0.1° per MHz. The absolute error is $\pm 1^{\circ}$ or $\pm 2\%$, whichever is greater. In addition, there is a high frequency error of 0.1° per MHz or 0.1% of the reading per MHz, whichever is greater. For tests at 5 MHz, this amounts to $\pm 0.5\%$, for signals between 300 mV and 20 V rms. A further error source especially at low flow rates (small phase angles) is drift. For example, after one hour warm up, the meter reading will drift less than 1° in ten hours. This drift must be reset manually with the panel zero set control.

CONCLUSIONS

After examining the program's results, five major conclusions may be drawn:

- A new ultrasonic transmission flow velocimeter technique for continuously measuring v/c^2 has been demonstrated. This technique is believed to inherently offer the best accuracy consistent with fast response, 20 ms, of any ultrasonic approach demonstrated so far. Operation up to 5000 lb/hr was demonstrated.

- A new ultrasonic reflection densitometer technique for measuring ρc has been demonstrated on liquids ranging in density from about 0.7 to 1.6 μ/cm^3.

- A new method of interrogating 100% of the flowing liquid's square cross section using a rectangularly collimated plane wave, which potentially offers linearity and accuracy essentially independent of Reynolds number or unidirectional flow profile, has been demonstrated on water, Avgas-100, JP-4, JP-5 and a contaminated solvent.

- Using a cell design containing nonintrusive transducers and no rotating parts, endurance of over 100 hours has been demonstrated using a test fluid flowing at ~1900 lb/hr and contaminated essentially in conformance with military specifications for flow measuring instruments.

- A new ultrasonic mass flowmeter has been built, consisting of a flow velocimeter (v/c^2), a densitometer (ρc) and a time intervalometer ($T \sim 1/c$). The combination of these outputs has been shown to yield an output voltage approximately proportional to the mass flow rate $\dot{M}$ over specified ranges. Departures from linearity are presently mainly attributed to stationary eddies which are partly in the measuring path. It is expected that they can be virtually eliminated using acoustic windows, wedges, screens or other means.

Based on the theoretical, experimental and test results, it is concluded that most of the observed inaccuracy in v/c^2 (about $\pm$ 3% at high flow) and in ρc (about $\pm$ 5%) and therefore nearly $\pm$ 10% in $\dot{M}$ at 2000 lb/hr can be attributed to factors which can be eliminated. For example the inaccuracy of the phase meter available in this program to measure v/c^2 was $\pm 2^{\circ}$. Phase meters now available can reduce this source of inaccuracy to $\pm 0.3^{\circ}$. Further, in the ρc case, the observed drift and/or noise of several mV produces an error in ρ of 2% per mV, yet drift and noise levels of 0.1 mV or less are considered achievable. Thus, ρc imprecision

or errors no larger than 0.2% appear achievable. It is therefore estimated that a (v/c^2) (ρc) $(1/T)$ system could achieve an $\dot{M}$ accuracy of better than 1% at 2000 lb/hr, and as a corollary, a ρv system independent of c should provide even better accuracy, since c errors are eliminated, and other electronic computation error sources would be reduced in number.

Several other conclusions from this work include:

1. Any type of ultrasonic measurement in the far field is subject to serious error due to wavefront curvature under laminar flow.

2. In the near field, time of flight measurements using pulses would require subnanosecond accuracy, and fast response, beyond the limits of present instruments.

3. Doppler measurements could properly weight the profile if insonification were uniform and if scatterers were uniformly distributed. Alternatively, range gating of waves obliquely incident upon axisymmetric flow could weight the profile. Uniformity of scatterers could be enhanced using a Kenics static mixer containing at least 7 sections, which is probably an acceptable number based on length and pressure drop for a 1/2-inch-diameter pipe. The dual-frequency Doppler system would sense v/c in the scattering zone, and would be relatively immune to v/c outside that zone. If a static mixer is used, sensing should be accomplished within ~1 to 3 diameters of the mixer exit. High Doppler S/N obtained on a standard cross section (glass sphere) and on bubbles implied that useful Doppler measurements on fuels contaminated above ~1% of MIL-E-5007C may be achievable, but accuracy and response time may be sacrificed, especially on uncontaminated fuel.

4. If a clamp-on flowmeter is to be installed on a standard all-metal straight tube or pipe, conical waves can provide a measure of v_d independent of Reynolds number or flow profile. Difficulties anticipated in measuring c and ρ for this geometry suggest that a two-frequency technique be employed, to yield v_d (not v_d/c or v_d/c^2). ρ data may be obtained nonacoustically (e.g., from fuel type and temperature inputs) if $\dot{M}$ is the desired final output.

   Analysis of ν versus a density-temperature function, taken with the profile equations, shows that if ρ and T are known to 1%, ν and hence Re can be determined to 20% or better, for which the uncertainty in $K = v_a/v_d$ would be $\leq 0.1\%$, if the profile were fully

developed. On the other hand, determination of K from measurements of v_d alone is generally not possible to better than 1%, since in the present problem the viscosity and Re ranges span over a factor of 10 for different (unknown) fuels even at known temperatures.

5. The Doppler method, while not used in the final flowmeter, might nevertheless be useful to detect contaminants well below 1% of MIL-E-5007C, or to measure v/c (average and/or profile) in fluids in which scatterers such as bubbles or microballoons could be introduced.

The above conclusions may be summarized by observing that a refinement of the new technology demonstrated in this program should result in an ultrasonic mass flowmeter capable of meeting current USAAMRDL requirements for diagnostics and control.

RECOMMENDATIONS

Based on the present work, it appears that the present ultrasonic mass flowmeter system can be refined. This new system, without deleting any of the essential requirements of the present program, could additionally provide a mass flow reading which is substantially a linear function of $\dot{M}$ with a flow velocity response time of 20 ms, and in one arrangement may provide v and ρ measurements each independent of c. To achieve this improved performance, we recommend the following approach:

- Optimize the present ultrasonic mass flowmeter to combine v/c^2, ρc and T with cell improvements such that the output is essentially in direct proportion to $\dot{M}$.

- Determine the limits of a commercially available resonant vane densitometer, particularly with respect to contaminants and vibration.

- Assuming the resonant densitometer (ρ) device operates satisfactorily, add to the v/c^2 equipment a two-frequency capability such that v can be determined independent of c.

- Optimize the combination of ρ and v to provide $\dot{M}$, where ρ and v are each independent of c.

- Conduct preliminary calibration and endurance tests using water and Avgas flowing at rates of up to ~2000 lb/hr, and demonstrate densitometer and transducer operation from -65° to $+160^{\circ}$F, at least under no-flow conditions.

- Conduct calibration tests and contaminant tests as per the latest applicable military specification on instrument endurance. The calibration tests should use one fuel such as JP-4 or JP-5, and a second fluid of substantially higher viscosity, for evaluation over a range of Reynolds numbers of at least two orders of magnitude. Calibration shall be conducted near room temperature and possibly at other temperatures such as 50° and 115°F.

- To the extent that scheduling permits, install and test the ultrasonic mass flowmeter cell on an actual full running engine.

LITERATURE CITED

1. P. M. Morse, Vibration and Sound, 2nd Ed., McGraw-Hill Book Co., Inc., New York (1948), pp. 346-357.

2. R. B. Lindsay, Mechanical Radiation, McGraw-Hill Book Co., Inc. New York (1960), pp. 91-105.

3. F. Noble, Rev. Sci. Instrum. 39 (9) 1327 (Sept. 1968); see also R. E. Fishbacher, Flowmeters, U. S. Patent No. 3,097,526 (July 16, 1963).

4. W. P. Mason, et al., Phys. Rev. 75 (6) 936-946 (1949).

5. F. R. Rollins, Jr., Materials Evaluation 24, 683 (1966); Int'l. J. NDT 1 (2) 127-145 (July 1969).

6. N. S. Ageeva, Soviet Physics-Acoustics 1 (1, 2), 117-127 (1955).

7. H. Schlichting, Boundary Layer Theory, 2nd Ed., Pergamon Press, London (1953), pp. 147, 394-398.

8. J. Kritz, ISA Proc. 10, Part 2, 55-16-3, pp. 1-6 (1955); Instruments and Automation 28, 1912-1913 (Nov. 1955).

9. J. L. McShane, Westinghouse Sci. Paper 71-1C6-FLOME-P1 (Aug. 13, 1971).

10. G. W. Marks, J. Acoust. Soc. Amer. 41 (1) 103-107 (1967).

11. V. F. Nozdrev, The Use of Ultrasonics in Molecular Physics, p. 272, translated by J. A. Cade and E. R. Dobbs, Pergamon Press/MacMillan Co., New York (1965).

12. H. E. Dahlke and W. Welkowitz, ISA Journal 7 (10) 60-63 (Oct. 1960).

13. W. E. Abbotts, U. S. Patent No. 3,648,512 (March 14, 1972); Instrumentation Technology 19 (7), p. 66 (July 1972).

14. L. C. Lynnworth and B. J. Spencer, U. S. Patent No. 3,514,747 (May 26, 1970).

15. A. E. Brown, Rev. Sci. Instr. 37 (9) 1181-1186 (Sept. 1966); U. S. Patent No. 3,184,959; Paper No. 2-10-110, Proc. 1971 Flow Symposium.

16. Herbert Kartluke, Ultrasonic Flowmeter for High Temperature Operation, AEC Report NYO-3622-25 (July 1969).

17. S. Ramo and J. R. Whinnery, Fields and Waves in Modern Radio, 2nd Ed., Wiley & Sons, N. Y., 1953, p. 32.

18. G. J. Rubissow and R. S. Mackay, Ultrasonic Imaging of In Vivo Bubbles in Decompression Sickness, Ultrasonics 9 (4), 225-234 (Oct. 1971).

19. W. P. Mason, Piezoelectric Crystals and Their Applications to Ultrasonics, D. Van Nostrand Co., Inc., Princeton, N. J. (1950), p. 105.

APPENDIX I
SCATTERING COMPUTATIONS

In this appendix, we present the details of the computations which were made relative to the acoustic scattering experiments. The scattering particles are in the quantities given in Table XIII of the text as per MIL-E-5007C. The objective of these calculations is to determine the total scattering cross section of the contaminant concentration within a 1-cm range gate in a 1/2-in.-diameter pipe.

We chose the frequency of the incident wave to be 20 MHz. A significantly higher frequency than this would have given rise to very severe attenuation in the fuel, while a significantly lower frequency would have caused too many of the contaminant particles to be in the Rayleigh region, whose bound is given by

$$d(\min) = \frac{\lambda}{2\pi} \tag{23}$$

where d (min) is that particle diameter for which geometrical (versus Rayleigh) scattering prevails. For a 20 MHz wave and a sound speed of ~1500 m/s (0.06 in./μs, we have a wavelength of 12 microns and minimum particle diameter given by

$$d(\min) = 12 \text{ microns} \tag{24}$$

Thus, from Table XIII, we see that the iron oxide particles are eliminated, as are 0-5 and 5-10 micron Arizona road dust particles. The cotton linters, being of such small volume (0.1 gm/1000 gal.) were not considered. The particles which were considered are listed in Table XVI.

TABLE XVI. CONTAMINANTS CONTRIBUTING TO SCATTERING

No.	Type	Diameter (μm)	Concentration
1	Sharp silica sand	300-420	1.0 gm/1000 gallons
2	Sharp silica sand	150-300	1.0 gm/1000 gallons
3	Road dirt	10-20	14% of 8 gm/1000 gallons
4	Road dirt	20-40	23% of 8 gm/1000 gallons
5	Road dirt	40-80	30% of 8 gm/1000 gallons
6	Road dirt	80-200	9% of 8 gm/1000 gallons

The average diameter of the particles was assumed in each of the above instances, e.g., for first category, we take the diameter as 360 microns.

The following formula was derived for converting the given concentrations (gm/ 1000 gal.) into fractional volume concentrations:

$$F_v = \frac{\text{conc (gm/ 1000 gal.)}}{\rho \text{ (gm/cm}^3\text{)}} \times \frac{10^{-6}}{3.785} \tag{25}$$

where F_v = cm^3 of contaminant per cm^3 of fuel and ρ = mass density of contaminant.

If $\bar{n}_i$ is the average number of particles of the i' th kind per cm^3 of fuel,

$$\bar{n}_i = \frac{F_v}{\frac{4}{3}\pi a_i^3} = \frac{6 F_v}{\pi d_i^3} \tag{26}$$

where d_i = average diameter of the i' th particle type. If d_i is given in microns, and $\bar{n}_i$ has the dimension cm^{-3}, then

$$\bar{n}_i = \frac{6 F_v}{\pi d_i^3} \times 10^{12} \tag{27}$$

In terms of the concentrations listed in Table XVI,

$$\bar{n}_i = \frac{\text{conc (gm/ 1000 gal.)}}{d^3 \text{ (microns cubed)}} \times 2.28 \times 10^5 \tag{28}$$

The scattering cross section per particle, assuming roughly spherical particles, is

$$\sigma_i = \frac{\pi}{4} (d_i)^2 = 0.786 (d_i)^2 \tag{29}$$

and for all particles in the i' th category, the scattering cross section per unit volume of the medium is

$$\text{Scattering per unit volume} = n_i \sigma_i \tag{30}$$

The quantities n_i and σ_i were separately computed for each of the six particle types. Next, the overall scattering per unit volume is simply

the linear sum of the separate contributions:

$$\bar{r}\,\sigma = \sum_i \bar{n}_i \sigma_i \tag{31}$$

and, finally, if V_c = volume of the cell throughout which we measure the scattering, we see that the overall scattering is given by

$$\sigma_{total} = V_c \sum_i \bar{n}_i \sigma_i \tag{32}$$

The detailed results are given in Table XVII.

TABLE XVII. RESULTS OF SCATTERING COMPUTATIONS

Particle Type	Average Diameter (microns)	$\bar{n}_i$ (cm^{-3})	σ_i (cm^2)	$\bar{n}_i \sigma_i$ (cm^{-1})
1	360	4.9×10^{-3}	1.0×10^{-3}	5×10^{-6}
2	175	4.2×10^{-2}	2.4×10^{-4}	1.0×10^{-5}
3	15	74	1.1×10^{-6}	1.3×10^{-4}
4	30	15.5	7.1×10^{-6}	1.1×10^{-4}
5	60	2.5	2.8×10^{-5}	7.1×10^{-5}
6	[illegible]	0.44	1.1×10^{-4}	4.8×10^{-5}

From Table XVII, we find that the overall scattering per unit volume of the fluid is

$$\sum_i \bar{n}_i \sigma_i = 3.3 \times 10^{-4}\ cm^{-1} \tag{33}$$

For a round pipe, the interrogation volume is

$$V_c = \frac{\pi}{4} D^2 X \tag{34}$$

where D = pipe diameter and X = interrogation length. Combining (32), (33) and (34), the total scattering cross section from the interrogation

volume for a 1.27 cm (1/2 in.) diameter pipe and an interrogation length of 1 cm is

$$\sigma_{total} = \frac{\pi}{4} D^2 \times \sum_i \bar{n}_i \sigma_i = 2.86 \times 3.3 \times 10^{-4} \cong 10^{-3} cm^2 \qquad (35)$$

In order to check the sensitivity of the technique to levels of this order, a glass sphere having a backscatter cross section of $4 \times 10^{-4} cm^2$ (diameter= 0.75 mm or 0.030 in.) was lowered into the fluid (water) and the Doppler wave amplitude was measured on an oscilloscope. The resulting signal-to-noise ratio was found to be greater than 30 dB. It was also found that, under flow conditions, when bubbles were not present in the flow, no Dopplers were observed above the noise.

Since the scattering cross section of a particle is proportional to the square of its dimension and the mass of the particle is proportional to the cube of its dimension, it follows from the above measurements that the system would have been able to detect contaminant concentrations of about 1% of those given in MIL-E-5007C. Such levels, however, were not observed - either in the tap water runs or in the uncontaminated aviation gas runs. At this point, it was concluded that, even though the full two frequency system including the coherent signal processor would provide much higher signal-to-noise ratio than that observed in the above preliminary measurements, the overall accuracy requirements of the system are such as to raise serious questions as to whether the dual Doppler technique is the correct one to use in this application. The decision, after consultation with the Contract Monitor, was to redirect the flow velocimeter portion of the program in favor of the phase measurement described in the main text of this report. Time has shown that this decision was (at least) not unwise, since the final technique does in fact work and shows high promise of leading to a flow velocimeter which will accurately measure v independent of c.

It should also be understood, however, that while contaminant levels of about 1% or more of those given in MIL-E-5007C appear necessary in order for one to measure v/c to 1% in 0.5s, with a given Doppler system, the presence of much lower levels could be detected.

APPENDIX II
FAR FIELD ANALYSIS OF PHASE SHIFT UNDER LAMINAR FLOW CONDITIONS

PART I. AXIAL WAVE

Assume that we have a means of generating a plane wave at location x = 0 in a pipe of radius R. The wave is transmitted upstream. At a distance x upstream is located a receiving transducer, which is assumed to be capable of receiving a plane wave. Due to the fact that, under laminar flow conditions, the flow profile is parabolic, rather than uniform, the wave traveling upstream will be transformed from a plane wave to one whose phase front is no longer planar. Therefore, the phase of this wave, as measured at the receiver, will not be a linear function of the fluid velocity. Simultaneous propagation and reception of upstream and downstream waves, and subsequent subtraction of the two measured phase shifts will not correct this problem since the upstream wave undergoes a concave distortion and the downstream undergoes a convex distortion. Thus, the subtraction of the measured phases of the two waves results in $\theta = (\theta_1 + \Delta) - (\theta_2 - \Delta) = (\theta_1 - \theta_2) + 2\Delta$, where θ_1 and θ_2 are the phases of the two waves assuming ideal flow and Δ is the distortion due to the actual (parabolic) flow profile.

If we assume that the wavelength, λ_o, of the acoustic wave is much smaller than the pipe radius R, and that the distance x between transmitter and receiver is large enough so that $x >> R^2/\lambda_o$, we can rather easily obtain the expression for the measured phase at point x. We first divide the cross-sectional area of the pipe into a number N of concentric rings, each with a width of ΔR. The measured phase will be

$$\phi = \tan^{-1}\left\{\frac{\sum_{i=1}^{N} 2\pi R_i \Delta R \sin\theta_i}{\sum_{i=1}^{N} 2\pi R_i \Delta R \cos\theta_i}\right\} \tag{36}$$

where R_i = radius of i'th strip and θ_i = phase of the i'th wave component at point x:

$$\theta = \frac{2\pi x}{\lambda_i} \tag{37}$$

where λ_i = wavelength at the radius R_i.

Equation (36) can be written in integral form by letting $\Delta R \rightarrow dr$:

$$\phi = \tan^{-1}\left\{ \frac{2\pi \int_0^R r \sin\theta\ (r)\, dr}{2\pi \int_0^R r \cos\theta\ (r)\, dr} \right\} \tag{38}$$

where

$$\theta\,(r) = \frac{2\pi x}{\lambda\,(r)} \tag{39}$$

If the flow is laminar, the flow profile will be parabolic, i.e.,

$$v(r) = v(0)\left[\,1 - \left(\frac{r}{R}\right)^2\,\right] \tag{40}$$

where v(0) = flow velocity at r = 0.

Therefore, since

$$\lambda\,(r) = \frac{c - v(r)}{f} \tag{41}$$

where f = transmitter frequency,

$$\lambda\,(r) = \frac{c - v(0)\left[\,1 - \left(\frac{r}{R}\right)^2\,\right]}{f} \tag{42}$$

from which we find $\theta\,(r)$:

$$\theta\,(r) = \frac{\omega x}{c - v(0)\left[\,1 - \left(\frac{r}{R}\right)^2\,\right]} \tag{43}$$

The overall phase of the received wave is, from (38),

$$\phi = \tan^{-1}\left\{ \frac{\int_0^R r \sin\left[\dfrac{\omega x}{c - v(0)\left[\,1 - \left(\frac{r}{R}\right)^2\,\right]}\right] dr}{\int_0^R r \cos\left[\dfrac{\omega x}{c - v(0)\left[\,1 - \left(\frac{r}{R}\right)^2\,\right]}\right] dr} \right\} \tag{44}$$

Note that, when v(0) = 0, the above equation has the solution

$$\theta\,(v(0) = 0) = \frac{\omega x}{c} \tag{45}$$

which is, of course, the correct solution for zero flow.

Equation (44) can be solved by transforming the variable from r to $\theta\,(r)$ as given by Eq. (43).

Abbreviating Eq. (44) as

$$\phi = \tan^{-1}\left\{\frac{I_1}{I_2}\right\} \tag{46}$$

we find that

$$I_1 = -\frac{R^2 \omega x}{2\, v(0)} \int_{\theta(0)}^{\theta(R)} \frac{1}{\theta^2} \sin\theta \; d\theta \tag{47}$$

and

$$I_2 = -\frac{R^2 \omega x}{2\, v(0)} \int_{\theta(0)}^{\theta(R)} \frac{1}{\theta^2} \cos\theta \; d\theta \tag{48}$$

These integrals have the solutions:

$$I_1 = -\frac{R^2 \omega x}{2\, v(0)} \left\{\frac{\sin\theta}{\theta} - \int_{\theta}^{\infty} \frac{\cos\theta}{\theta} \, d\theta\right\}\Bigg|_{\theta(0)}^{\theta(R)} \tag{49}$$

$$I_2 = -\frac{R^2 \omega x}{2\, v(0)} \left\{\frac{\cos\theta}{\theta} - \int_{0}^{\theta} \frac{\sin\theta}{\theta} \, d\theta\right\}\Bigg|_{\theta(0)}^{\theta(R)} \tag{50}$$

Thus, the measured phase at point x along the pipe is

$$\phi = \tan^{-1}\left\{\frac{\dfrac{\sin\theta(R)}{\theta(R)} - \dfrac{\sin\theta(0)}{\theta(0)} + \displaystyle\int_{\theta(0)}^{\theta(R)} \frac{\cos\theta}{\theta} \, d\theta}{\dfrac{\cos\theta(R)}{\theta(R)} - \dfrac{\cos\theta(0)}{\theta(0)} + \displaystyle\int_{\theta(R)}^{\theta(0)} \frac{\sin\theta}{\theta} \, d\theta}\right\} \tag{51}$$

We next note from Eq. (43) that $\theta(R)$ is just the phase under zero flow conditions. Therefore, $\theta(R)$ can be fixed and will remain constant for any (laminar) flow conditions. For convenience, we set

$$\theta(R) = 2n\pi \;, \quad n = 1, 2, 3, \ldots \tag{52}$$

This means that $\theta = 0$ under zero flow conditions.

We now have a simpler, but no less exact, solution for θ:

$$\phi = \tan^{-1}\left\{\frac{\frac{\sin\theta(0)}{\theta(0)} - \int_{\theta(0)}^{\theta(R)} \frac{\cos\theta}{\theta}\,d\theta}{\frac{\cos\theta(0)}{\theta(0)} - \frac{1}{\theta(R)} - \int_{\theta(R)}^{\theta(0)} \frac{\sin\theta}{\theta}\,d\theta}\right\} \tag{53}$$

We next wish to determine whether or not Eq. (53) behaves linearly in the relationship between ϕ and v(0). Although, strictly speaking, numerical methods should be employed, if we restrict our solution to small values of $\theta(0) - \theta(R)$, we can obtain a measure of the range of linearity of ϕ vs v(0).

We first note that $\theta(0)$ is large because the total path contains many wavelengths. But if we restrict the range $\theta(0) - \theta(R)$ so that

$|\theta(0) - \theta(R)| << \frac{\pi}{2}$, we can make the following approximations:

$$\sin\theta(0) \doteq \theta(0) - \theta(R) \tag{54}$$

$$\cos\theta(0) \doteq 1 - \frac{1}{2}\left[\theta(0) - \theta(R)\right]^2 \tag{55}$$

$$\int_{\theta(0)}^{\theta(R)} \frac{\cos\theta}{\theta}\,d\theta \doteq \int_{\theta(0)}^{\theta(R)} \frac{d\theta}{\theta} = \ln\left(\frac{\theta(R)}{\theta(0)}\right) \tag{56}$$

$$\int_{\theta(R)}^{\theta(0)} \frac{\sin\theta}{\theta}\,d\theta \doteq \frac{\cos\theta(0) - \cos\theta(R)}{\frac{1}{2}\left[\theta(0) + \theta(R)\right]} \tag{57}$$

$$= \frac{1 - \frac{1}{2}\left[\theta(0) - \theta(R)\right]^2 - 1}{\frac{1}{2}\left[\theta(0) + \theta(R)\right]} = \frac{\left[\theta(0) - \theta(R)\right]^2}{\left[\theta(0) + \theta(R)\right]} \tag{58}$$

The justification for (56) is that $\theta \gg 2n\pi$ over the integration range. Therefore, $\cos\theta \doteq 1$ over this range. The opposite state of affairs occurs with (57), where we notice that, since $\theta = 2n\pi$ is <u>large</u> (as we originally assumed), and since the integration range is small, we can allow $\sin\theta$ to be the variable, and in the denominator let $\theta \rightarrow (1/2)\left[\theta(0) + \theta(R)\right]$.

Therefore, under the conditions specified,

$$\phi = \tan^{-1}\left\{\frac{\frac{\theta(0)-\theta(R)}{\theta(0)} - \ln\left(\frac{\theta(R)}{\theta(0)}\right)}{\frac{1-\frac{1}{2}\left[\theta(0)-\theta(R)\right]^2}{\theta(0)} - \frac{1}{\theta(R)} + \frac{\left[\theta(0)-\theta(R)\right]^2}{\left[\theta(0)+\theta(R)\right]}}\right\} \tag{59}$$

Since

$$\left|\frac{1}{\theta(0)} - \frac{1}{\theta(R)}\right| >> \left|\left[\theta(0)-\theta(R)\right]^2\left(\frac{1}{2\theta(0)} - \frac{1}{\theta(0)+\theta(R)}\right)\right| \tag{60}$$

Eq. (54) becomes

$$\phi \doteq \tan^{-1}\left\{\frac{\frac{\theta(0)-\theta(R)}{\theta(0)} - \ln\left(\frac{\theta(R)}{\theta(0)}\right)}{\frac{1}{\theta(0)} - \frac{1}{\theta(R)}}\right\} \tag{61}$$

Letting $\beta'(0) = v(0)/c$, and noting that

$$\theta(0) = \frac{\omega x}{c - v(0)} \tag{62}$$

and

$$\theta(R) = \frac{\omega x}{c} \tag{63}$$

we find that

$$\theta(0) - \theta(R) = \beta'(0)$$

$$\ln\left(\frac{\theta(R)}{\theta(0)}\right) = \ln\left(1+\beta'(0)\right) \doteq \beta'(0) - \frac{1}{2}\beta'^2(0) \tag{64}$$

$$\frac{1}{\theta(0)} - \frac{1}{\theta(R)} = \frac{v(0)}{\omega x} \tag{65}$$

Substituting the above three quantities into (61), we finally obtain

$$\phi \doteq \tan^{-1}\left\{\frac{n\pi x}{\lambda_o}\beta'(0)\right\} = \tan^{-1}\left\{\frac{n\pi x}{\lambda_o}\left(\frac{v(0)}{c}\right)\right\} \tag{66}$$

For parabolic flow profile the average velocity, $\bar{v}$ is just half the maximum velocity $v(0)$. Therefore,

$$\phi \doteq \tan^{-1}\left\{\frac{2n\pi x}{\lambda_o}\left(\frac{\bar{v}}{c}\right)\right\} \tag{67}$$

The approximations required to obtain this relationship were accurate to order β'^2. Therefore, we find that (67) is linear in v(0) only insofar as the arc tangent is linear. For example, if inaccuracy of $\pm$ 0.25% were required, the range of ϕ could not exceed 4.8 deg and the measurement precision of ϕ itself would have to be better than $\pm$ 0.12 deg! If inaccuracy of $\pm$ 0.6% were required, the allowed range of ϕ would be 9.2 deg and a measurement precision on ϕ would be $\pm$ 0.06 deg.

To extrapolate the interpretation of (67) further would be to violate the assumptions made in deriving it. However, it is obvious that Eq. (53) (which is the exact solution for the problem formulated) becomes increasingly nonlinear as the range θ (0) - θ (R) is widened. It seems reasonable to conclude that, within the potential range of high accuracy, the instrumental errors in measuring phase angle (to within ~ $\pm$ 0.06 deg) would prevent high accuracy from actually being achieved.

It is clear that instrumental errors prohibit high accuracy for small values of θ, and the nature of the flow itself prohibits high accuracy for large values of θ.

It is precisely because of these limitations on the usual "upstream minus downstream" phase or time difference flowmeter, that we considered a dual-frequency measurement based on scattering.

PART II. OBLIQUE WAVE

We wish to determine if, to first order approximation, the measurement of phase is independent of flow profile in an oblique transmission system. We assume plane wave transmission and reception. The setup is shown in Figure 41. A plane wave is transmitted to a plane wave receiver across a circular pipe of radius R. The beam makes an angle, β, with respect to the normal to the axis of the pipe. If the receiver and transmitter transducer apertures are very small as compared with the radius R, then the phase ϕ of the received wave is given by

$$\phi = \int_0^L \frac{2\pi \, dL}{\lambda} \tag{68}$$

where

$$L = \frac{2R}{\cos \beta} \tag{69}$$

$$dL = \frac{2\,dr}{\cos \beta} \tag{70}$$

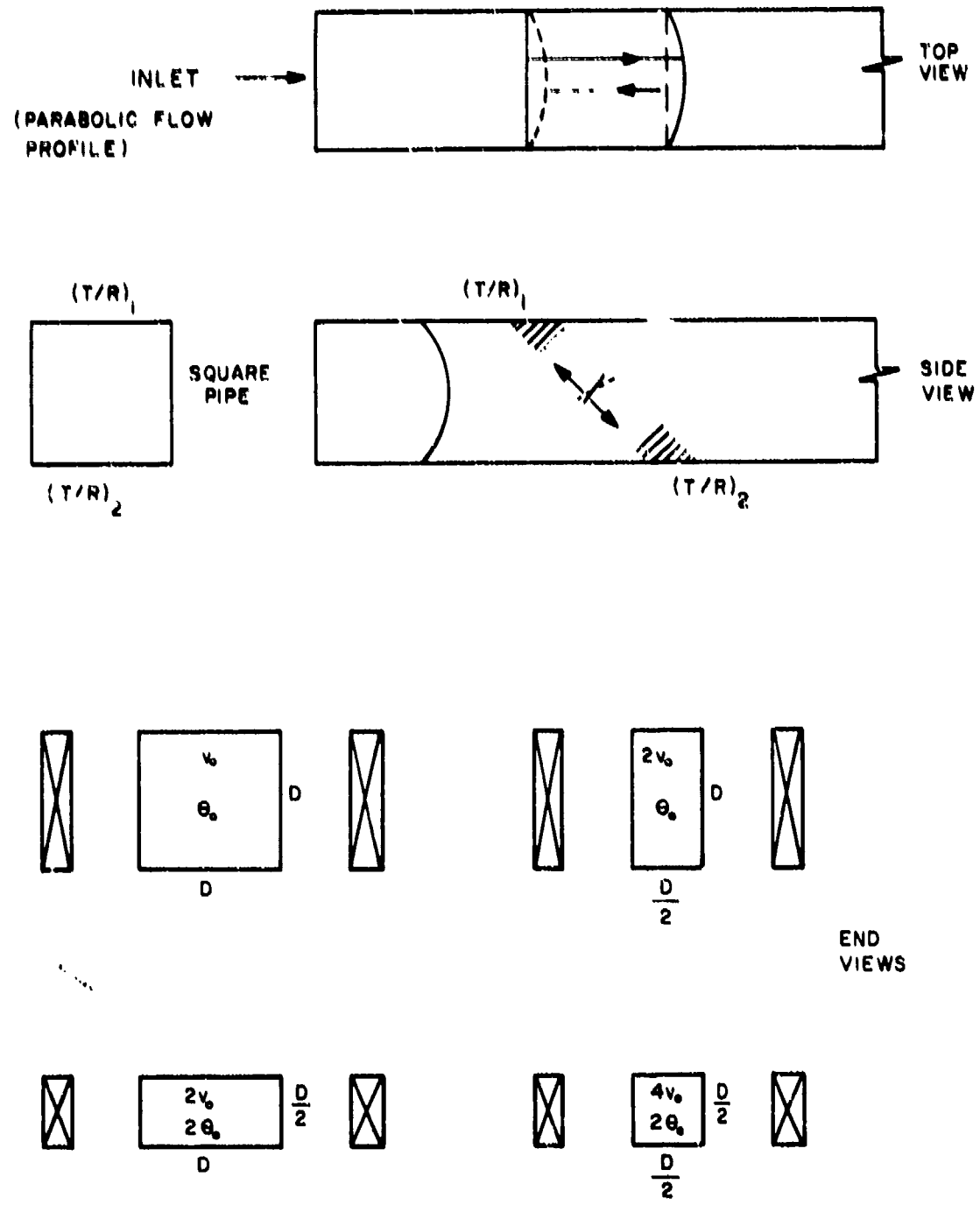

Figure 41. Wavefront Distortions for Oblique Incidence Laminar Flow.

In the case of a parabolic flow profile,

$$\lambda = \lambda(r) = \frac{2\pi (c - v(r))}{\omega} \tag{71}$$

and

$$v(r) = v(0)\left[1 - \left(\frac{r}{R}\right)^2\right] \tag{72}$$

where $v(r)$ = flow velocity, $v(0)$ = axial flow velocity, c = sound speed, and ω = angular frequency.

Substituting (69), (70), and (71) into (68) yields

$$\phi = \frac{2\omega}{c \cos\beta} \int_0^R \frac{dr}{1 - \beta'(0)\left[1 - \left(\frac{r}{R}\right)^2\right]} \tag{73}$$

where

$$\beta'(0) \equiv v(0)/c \tag{74}$$

Assuming that $\beta'(0) << 1$,

$$\phi \doteq \frac{2\omega}{c \cos\beta} \int_0^R \left\{1 + \beta'(0)\left[1 - \left(\frac{r}{R}\right)^2\right]\right\} dr \tag{75}$$

The change in phase due to a change from zero flow to finite flow is

$$\Delta\phi \doteq \frac{2\omega\beta'(0)}{c \cos\beta} \int_0^R \left[1 - \left(\frac{r}{R}\right)^2\right] dr \tag{76}$$

The total mass flow rate in the pipe, $\dot{M}$, is given by

$$\dot{M} = \int_0^R \rho\, v(r)\, dA \tag{77}$$

where ρ = mass density, assumed constant, not a function of r.

From Eq. (72) and noting that $dA = 2\pi\, r\, dr$ we have

$$\dot{M} = 2\pi\rho\, v(0) \int_0^R r\left[1 - \left(\frac{r}{R}\right)^2\right] dr \tag{78}$$

or

$$\dot{M} = 2\pi\rho c\beta'(0) \int_0^R r\left[1 - \left(\frac{r}{R}\right)^2\right] dr$$

Thus, the ratio of phase shift to flow rate is

$$\frac{\Delta\phi}{\dot{M}} = \frac{\dfrac{2\omega\beta'(0)}{c\cos\beta}\displaystyle\int_0^R \left[1 - \left(\frac{r}{R}\right)^2\right] dr}{2\pi\rho c\beta'(0)\displaystyle\int_0^R r\left[1 \quad \left(\frac{r}{R}\right)^2\right] dr} \tag{79}$$

We see in the above equation that the axial flow term $\beta'(0)$ cancels, and that $\Delta\phi/\dot{M}$ is thus independent of (laminar) flow velocity profile $v(r)$. That is to say, the measured phase shift, or time interval, is proportional to mass flow rate $\dot{M}$, for laminar flow, when the stated assumptions are met. Instrumental calibration is required, however, for different pipe sizes because $\Delta\phi/\dot{M}$ is obviously dependent upon R.

It should be understood that although the wavefront is assumed plane at the transmitter and receiver, the wavefront becomes curved and then uncurved as it traverses the fluid, as far as its projection in the plane of incidence is concerned. Actually, however, its projection increasingly curves, in planes orthogonal to the plane of incidence, and parallel to the axis.

The above remarks apply to the far field. In the near field, to the extent that waves remain plane, phase measurements are essentially proportional to the flow velocity. Referring to Figure 41 again, we may note that if one dimension of the square flow channel is modified, giving a rectangular cross section of different area, one can arrange to extend or narrow the flow range, for a given set of fixed electrical parameters such as frequency and range of phase shift.